CREEP UNDER HIGH TEMPERATURE OF STAINLESS STEEL FIBRE REINFORCED REFRACTORY CONCRETE

Karyne Ferreira dos Santos

Dissertação de Mestrado apresentada ao Programa de Pós-graduação em Engenharia Civil, COPPE, da Universidade Federal do Rio de Janeiro, como parte dos requisitos necessários à obtenção do título de Mestre em Engenharia Civil.

Orientadores : Romildo Dias Toledo Filho
Eduardo de Moraes Rego Fairbairn

Rio de Janeiro
Março de 2016

CREEP UNDER HIGH TEMPERATURE OF STAINLESS STEEL FIBRE REINFORCED REFRACTORY CONCRETE

Karyne Ferreira dos Santos

DISSERTAÇÃO SUBMETIDA AO CORPO DOCENTE DO INSTITUTO ALBERTO LUIZ COIMBRA DE PÓS-GRADUAÇÃO E PESQUISA DE ENGENHARIA (COPPE) DA UNIVERSIDADE FEDERAL DO RIO DE JANEIRO COMO PARTE DOS REQUISITOS NECESSÁRIOS PARA A OBTENÇÃO DO GRAU DE MESTRE EM CIÊNCIAS EM ENGENHARIA CIVIL.

Examinada por:

Prof. Romildo Dias Toledo Filho, D.Sc.

Prof. Eduardo de Moraes Rego Fairbairn, Dr.Ing.

Prof. Samir Maghous, D.Sc.

Prof. Luiz Fernando Lomba Rosa, D.Sc.

RIO DE JANEIRO, RJ - BRASIL

MARÇO DE 2016

Santos, Karyne Ferreira dos

Creep under high temperature of stainless steel fibre reinforced refractory concrete / Karyne Ferreira dos Santos - Rio de Janeiro: UFRJ/COPPE, 2016.

XIX, 89p.: il.; 29,7 cm.

Orientadores: Romildo Dias Toledo Filho
Eduardo Moraes de Rego Fairbairn

Dissertação (Mestrado) - UFRJ/COPPE/Programa de Engenharia Civil, 2016.

Referências Bibliográficas: p. 77-79.

1. Creep. 2. Refractory concrete . 3. Steel fibres reinforcement. 4. Burning temperature. 5. Cementing Wells. 6. Mechanical Behavior I. Toledo Filho, Romildo Dias *et al.* II. Universidade Federal do Rio de Janeiro, COPPE , Programa de Engenharia Civil. III. Título.

Acknowledgments

First, I thank God for everything.

I thank my family, Jairo and Enoi, for their love, affection, bearing the distance and for always being there when I needed, supporting, and being the best parents. To my cousin, Leila who always was present during this master course and my niece, Camila, whose sweetness cheered me up when I was feeling down. My sincere gratitude and love, for my fiancée, Javier Andres Forero, for his kindness, encouragement, support, helping me do my tests, staying up just to keep me company and being an amazing person, without him none of this would have been possible.

I would like to express my sincere appreciation to my advisers, Prof. Romildo and Professor Eduardo for their guidance, encouragement and continuous support through the course of this master.

To all my friends. First, I would like to thank a very special group, made up of people who I first became friends with in Rio. This group was made up of students doing different kinds of research. It is still unknown to me what exactly connected us, but true friendship developed and without it I couldn't have done my master degree. Thanks to Erica Carneiro, Rodrigo Costa, Mariane Rita, Alfredo Quiroga, Renato Evangelista, Eudes Marinho, Vinicius Telles, Nelson Santos, William Godoy and Rafaela Sanches, for all the experience exchanged during lunches and breaks. They all were always willing to help me in my studies and to grow as a person, giving me strength when I most needed it. A special thanks to Rodrigo, for being the grumpiest of all and Erica for being the happiest, you both were the reason why I wrote in English, always making me believe that I could do more, teaching me Latex, and pushing me always forward.

I place on record my sincere thanks to all my friends of NUMATS: Alfredo, Tamara, Daniele, Mayara, Caroline, Yassin, Raphael, Iolanda, Thayane, Mostafa, Livia, Aline, Nina, Andrielli, Tina, Adriana, Camila, Carol Sermarini, Clarice, Nathalia, Renata, Anne, Saulo, Fabricio, Otávio, Samantha and Thiago. We made up a great group, and I would like to express my appreciation to you all. Special thanks to, Oscar and Dimas for being the ones that directly helped me during this research. Also to Tamara and Daniele that in the end of this master helped me with new on going tests for the doctorate, making it possible for me to finish my writing. Without your help, it would have been a lot harder.

To all friends and staff of the Structures Laboratory for the collaboration and support provided during all activities. The department's secretaries: Carmen,

Sandra, Luzidelle and Paulinho (*in memorium*). I thank all the laboratory technicians, Marcio, Anderson, Clodoaldo, Adailton, Alessandro, Rosangela and Alex who contributed to the results of the work. In particular, Renan who became a true friend, and who I deeply admire for the amazing person he is and kind soul he has.

I place on record, my thanks to Prof. Leila Motta, for being the person who introduced me to the academic field. Her care towards her students inspired me during this work and will for the rest of my life as an educator.

For financial support, I would like to thank CNPq (National Council for Scientific and Technological Development) that ensured my exclusive dedication to study for mastering.

Karyne Ferreira dos Santos

"Each day we go to our work in the hope of discovering."

Nikola Tesla.

Resumo da Dissertação apresentada à COPPE/UFRJ como parte dos requisitos necessários para a obtenção do grau de Mestre em Ciências (M.Sc.)

FLUÊNCIA SOB ALTAS TEMPERATURAS DE CONCRETOS REFRATÁRIOS REFORÇADOS COM FIBRAS DE AÇO INOX

Karyne Ferreira dos Santos

Março/2016

Orientadores : Romildo Dias Toledo Filho
Eduardo Moraes de Rego Fairbairn

Programa: Engenharia Civil

Este trabalho tem como objetivo estudar a fluência do concreto refratário sob cargas de tração, compressão e flexão. Os ensaios realizados à temperatura ambiente (21°C) foram realizados tanto em amostras submetidas a uma temperatura de 110°C quanto em amostras secas a 110°C e queimadas a 600°C. Os ensaios de fluência ensaiados a quente (600°C) foram realizados com amostras secas em estufa a 110°C e queimadas no próprio forno onde foi realizado o ensaio de fluência. A carga aplicada nos ensaios foi correspondente a 40% da carga máxima de ruptura em ensaios estáticos realizados nas misturas estudadas. Um concreto auto adensável denso com baixo teor de cimento aluminoso (LCC) foi utilizado, com fibras de aço inox de 25 mm de comprimento e 0,51 mm de diâmetro (relação de aspecto de 49). Foi utilizada como reforço uma fração de fibra de 6%. Ensaios micros estruturais (análise termogravimétrica, análise por difração de raios X e composição química) foram realizados para indicar mudanças microestruturas devido a temperatura.

Os resultados na fluência em todos os estados de solicitação estudados indicaram que a fluência no concreto refratário estabiliza no máximo em 30 dias, após isso seu aumento não é significativo. Os resultados dos ensaios de fluência na compressão indicaram que a fluência foi maior nos concretos ensaiados a quente, sendo maior no concreto com reforço fibroso. Os ensaios microestruturas confirmaram ocorrer uma conversão dos hidratos C_3AH_6 e AH_3 em $C_{12}A_7$ e CA, aumentando a porosidade e explicando o aumento da fluência observado nos concretos que foram submetidos a queima de 600°C. A diferente dilatação a 600°C, da fibra em relação ao concreto pode causar micro fissuração explicando o aumento da fluência em concretos com reforço fibroso.

Abstract of Dissertation presented to COPPE/UFRJ as a partial fulfillment of the requirements for the degree of Master of Science (M.Sc.)

CREEP UNDER HIGH TEMPERATURE OF STAINLESS STEEL FIBRE REINFORCED REFRACTORY CONCRETE

Karyne Ferreira dos Santos

March/2016

Advisors : Romildo Dias Toledo Filho
Eduardo Moraes de Rego Fairbairn

Department: Civil Engineering

This work aims to study the creep of refractory concrete under tensile, compression and flexure loads. Tests were carried out at room temperature (21°C), on samples subjected to a temperature of 110°C, as for samples dried at 110°C and burned at 600°C. Creep tests at hot stage (600°C) were carried out with samples dried at 110°C and then burned in a kiln where the creep test was carried out. The load applied in the tests was equivalent to 40% of the maximum strength in static tests performed on the studied mixtures. A dense self compacting refractory concrete of low cement castable (LCC) was used, reinforced by stainless steel fibres of 25 mm length and 0.51 mm diameter (aspect ratio of 49) in a 6%(in mass) fraction. Micro structural tests (thermogravimetric, X-ray diffraction and chemical composition) were performed to indicate micro structure change due to temperature.

Creep results at all states studied indicated that creep of the refractory concrete stabilizes at a maximum of 30 days after which the increase in creep rate is not significant. The results of creep tests in compression indicated that creep deformation was higher for the hot stage test, being highest for the concrete with fibre reinforcement. Micro structures tests confirmed the conversion of the hydrates C $_3$AH$_6$ and AH$_3$ into C$_{12}$A$_7$ and CA, increasing porosity and explaining the increase in creep observed in concretes burned at 600°C. The mismatch of the expansion coefficient at 600°C, between the fibre and the concrete can cause micro cracks, explaining the increase in creep for the concrete with fibre reinforcement.

Contents

List of Figures

List of Tables

Chapter 1

Introduction and Motivation

In the last decades, the petrochemical industry has grown considerably. Such growth has increased concern regarding maintenance and repair of the equipments in petroleum platforms. It is desired to improve the lifespan of the materials and structures in these facilities since a failure in these equipments can cause a decrease in oil refinery and carry huge losses for the companies.

Fluid Cracking Catalytic Units (FCCU), illustrated in Figure 1.1, are subjected to recurrent failures associated with great thermal stress, due to its high operating temperature of around 600°C. The FCCU units are usually composed of two materials: the carbon steel that supports the mechanical and dynamical stresses and the refractory castable concrete used to protect the carbon steel from the high temperature (600°C).

The concrete is used as internal coating reducing the temperature along its thickness to the temperature supported by the carbon steel of around 200°C. To assure the adhesion between the metallic face and the concrete, an anchorage of stainless steel is used, as illustrated in Figure 1.2. As pointed out by KIM (1984), when the interior of the vessel is heated, reversible thermal expansion causes the lining's hot face to expand producing compressive stresses at the hot face and tensile stresses in the remainder of the lining, leading to the collapse of these units, that normally present map cracking, as seen in Figure 1.2. The main reason for this failure is a thermal gradient problem, basically related to imposed deformations, for which creep can be very important for the stresses relaxation.

Figure 1.1: Converter set and ducts of the fluid catalytic cracking units. Source: MEDEIROS (2012).

(a) (b) (c)

Figure 1.2: Inside the Riser: a) Riser, with concrete covering the steel; b) Crack propagation in the concrete thickness; c) Map crack inside the riser. Source: Personal archive of Professor Eduardo Fairbairn.

Creep can relieve the tensions imposed by the thermal gradient and could avoid the cracking of the concrete. This occurs because creep increases the plastic deformation of a material, when submitted to a constant stress with time. This deformation causes relaxation stress that could interfere in the state of tensions of this structure. Although it is known that creep increases with temperature, not enough studies have been carried out on the subject until now

To comprehend the reason of this failure and avoid it in future, it is fundamental to study the creep behaviour of concrete at high temperatures. According to BAZANT and KAPLAN (1996), materials that are usually

submitted to high temperatures and static mechanical stress for long periods of time are susceptible to changes in mechanical behaviour. This occurs mainly because of: the atoms diffusion process, disagreement movements, the grain boundary sliding and recrystallization process.

There is another aggravating aspect of this refractory concrete, that needs to be studied in combination with creep. As reported by HEWLETT (2003), normally this kind of concrete works at temperatures higher than 900°C developing ceramic bonding, that is more stable and resistant. Usually, at around 500°C this kind of material presents a loss of mechanical strength which is linked to a higher creep deformation, provoked by porosity and crack propagation in the concrete. Despite the importance of this phenomenon not many investigations are concerned with creep of refractory concretes at 600°C or similar temperature, especially with fibre reinforcement.

1.1 Main Objectives

The main objectives of this work are:

- To study the creep behaviour of refractory concrete under compression, tensile and flexure loads at both room temperature and high temperature (however only possible at compression).
- To study the effect of the reinforcement of 6%(in mass) of stainless steel fibres on the creep behaviour.
- To understand the creep behaviour of dense self compacting refractory concrete of low cement castable (LCC), submitted to two thermal conditions: dried at 110°C and dried at 110°C and then burned at 600°C.
- To study micro structural changes in dense self compacting refractory concrete of low cement castable (LCC), submitted to two thermal conditions: dried at 110°C and dried at 110°C then burned at 600°C.

1.2 Text organization

In order to cover the pre-requisite topics and present the contributions of this research, the present dissertation is divided into 7 chapters including this one.

Chapter 2 is an introduction to the basic creep concepts. It brings out the importance and effects of creep, the main parameters, typical creep curves and classifications obtained by these curves. At the end a review of the creep studies in refractory concrete is presented.

In Chapter 3 a complete review is given of the materials used, focusing on the aluminous cement and its transformation that could affect creep. Also the material characterization, the techniques and results for the refractory concrete are given.

In Chapter 4 all the experimental procedures are described, from the specimen production to how creep tests were carried out, throughout the progress, the drying and burning processes. The mechanical tests in compression, tensile and flexural were also described.

Chapter 5 presents all the results of the mechanical characterization and results of creep tests. This chapter seeks to compare those results and the results of the material characterization to understand the creep behaviour.

Chapter 6 offers the main contributions of the studied subject, as well as proposed topics for future research.

Finally, Chapter 7 lists the bibliographic references used in this work, and the Appendix presents all creep curves plotted in this work.

Chapter 2

Creep

Creep is a time-dependent strain observed during a constant stress through time. There are three main factors that affect directly creep: the load applied, temperature and time. The higher these parameters are, the higher creep deformation will occur in most materials. The combination of these three factors determine whether creep is relevant for a particular application.

In the application on UFCC, all those main parameters are involved, the temperature of work is high (600°C), the time of the load applied is desired to be as high as possible, so it can increase the lifespan of the units. In addition, there is a constant load applied due to the own weight of the structure, making this study relevant for such application.

Creep deformation will produce stress relaxation that will affect the state of tensions and needs to be taken into account as the engineer wants to meet his aim of the structure strength being adequate, but not wastefully excessive, the long durability under exposure conditions, and whose serviceability should fit its purpose.

A review of the main properties of creep will be presented in further sections. In the most general form, the strain-time curve for material subjected to creep is of the form shown in Figure 2.1. According to SHAMES (1997) and NEVILLE *et al.* (1983), there are four main stages in creep tests:

- Elastic strain: The strain at zero time is primarily elastic but may include a non-elastic component. Immediately upon loading at the test temperature, an elastic strain ε_e, occurs. If the applied stress exceeds the yield stress at the test temperature, a plastic strain, ε_p, also follows. The elastic strain occurs in a very short time interval. Although the plastic strain occurs over a greater time interval than the elastic strain, the plastic strain time interval is still short when compared with the time scale of a creep test. Thus, for practical, purposes, both ε_e, and ε_p can be considered instantaneous responses.

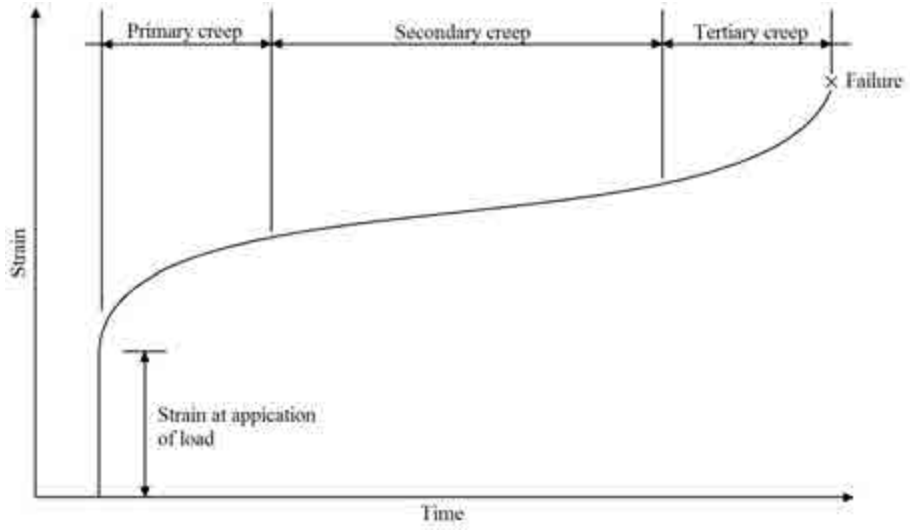

Figure 2.1: General form of the strain-time curve for a material subjected to creep.

- Primary creep region: This is an internal section of the creep curve in which the strain rate, $\dot{\varepsilon}$, decreases continuously. If one is concerned mainly with creep over very long periods of time at constant stress, the strain accumulated during the primary creep region may be small compared with the strain accumulated in the subsequent intervals. However, primary creep is important if the load duration is short. Furthermore, if the stress is not constant in time, the mechanism, active during the primary creep interval of a constant stress, will be active during the entire load history.

- Secondary creep region: Sometimes called stationary creep, the creep rate ($\dot{\varepsilon}$) is essentially constant in this region. In many instances it is actually decreasing slowly during this interval, but the data are frequently approximated nicely by a straight line. The secondary creep region is usually the dominant interval of a creep curve.

- Tertiary creep region: It may or may not exist, depending on whether or not there is an increase in stress. In this region $\dot{\varepsilon}$ increases until creep rupture finally occurs. For instance, in concrete this may arise from an increase in creep due to microcracking at high stresses, i.e. at stresses greater than the typical range of working stresses, which is generally 25 to 40 per cent of the short-term strength.

Creep tests are frequently conducted at constant load rather than at constant stress, since it is not an easy matter to adjust the load continually in proportion to the change in cross-section area due to the creep's Poisson effect. However, the tertiary creep region is greatly exaggerated during a constant load test, since the actual stress is in fact increasing.

For the normal working levels of stress in concrete, primary creep cannot be distinguished from secondary creep and tertiary creep is not considered. The strain-time curve is of the form shown in Figure 2.2 and creep is simply defined as the gradual increase in strain with time under a sustained stress according to NEVILLE *et al.* (1983).

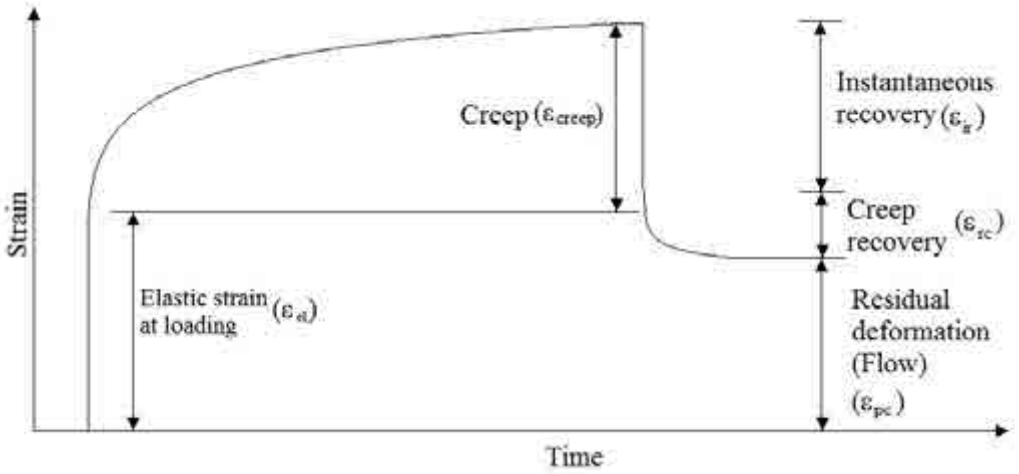

Figure 2.2: General form of the strain-time curve for concrete subjected to normal levels of sustained load.

It is clear from the comments above that the total strain at any time t is given by Equation 2.1

$$\varepsilon(t) = \varepsilon_{el} + \varepsilon_{creep}(t) \tag{2.1}$$

where $\varepsilon_{creep}(t)$ is the total amount of creep strain in time t.

If the load is removed at time $t = t_1$, all of the elastic strain should be recovered instantaneously plus some of the creep strain over an interval of time. Hence it is clear that the creep strain at time t_1 may be divided into recoverable and non recoverable types, and the Equation 2.2 may written as.

$$\varepsilon_{creep}(t_1) = \varepsilon_{rc} + \varepsilon_{pc} \tag{2.2}$$

where ε_{rc} designates recoverable creep, and ε_{pc} designates permanent nonrecoverable creep.

As reported by NEVILLE *et al.* (1983), creep and shrinkage can be additive phenomena. Essentially, there are two types of creep, depending on the humidity of surroundings, *basic creep* i.e creep occurring under conditions of no moisture

exchange with the ambient medium (hygral equilibrium) and *total creep* i.e creep occurring under drying conditions in which there is an additional component termed *drying creep* which is induced even after allowing for free shrinkage as measured on an unstressed specimen.

Shrinkage, elastic deformation and creep are expressed as strain (millimetre per millimetre), i.e as dimensionless quantities. However, sometimes it is convenient to give the magnitudes of elastic deformation and creep not for the actual stress applied (usually expressed as a proportion of the short-term strength) but per unit of stress. Such values are specific elastic strain and specific creep, if σ = stress acting, we denote specific elastic strain (ε_{sp}) by Equation 2.3.

$$\varepsilon_{sp} = \frac{\varepsilon_{el}(t_0)}{\sigma} = \frac{1}{E_c(t_0)} \tag{2.3}$$

where c = creep;ε_{el} = elastic strain; σ = stress applied and $E_c(t_0)$ = modulus of elasticity at the age t_0.

We denote specific creep c_{sp} by

$$c_{sp} = C(t, t_0) = \frac{c(t, t_0)}{\sigma} \tag{2.4}$$

where $c(t, t_0)$ = creep at age t due to a stress applied at age t_0.

In addition, the sum of the specific elastic strain the time of load application or at the time when creep is determined and of the specific creep at time t is termed the creep function ϕ, i.e.

$$J(t, t_0) = \frac{1}{\sigma}[\varepsilon_{el}(t_0) + c(t, t_0)] = \frac{1}{E_c(t_0)} + C(t, t_0) \tag{2.5}$$

The ratio of creep to the elastic strain is termed the creep coefficient

$$\phi(t, t_0) = \frac{c(t, t_0)}{\varepsilon_{el}(t_0)} \tag{2.6}$$

When stress is removed, concrete undergoes instantaneous recovery, already denoted by $\varepsilon_{el}(t_1)$. Generally $\varepsilon_{el}(t_1) < \varepsilon_{el}(t_0)$, the instantaneous recovery is followed by a time-dependent recovery, referred to as creep recovery. The situation is illustrated in Figure 2.2, which shows that the creep recovery tends to a finite value.

NEVILLE *et al.* (1983) explained that the magnitude of the creep and the creep recovery are such that $\varepsilon_{rc} < \varepsilon_{creep}$, except in concrete subjected to the sustained stress at a very advanced age when it is possible that $\varepsilon_{rc} = \varepsilon_{creep}$. Thus, concrete subjected to a sustained stress and subsequently unloaded exhibits an irrecoverable or residual strain, sometimes referred to as permanent set, residual deformation or flow.

The compliance function or specific creep for compression and tensile applications are calculated by the deformation obtained in the creep test divided by the strength applied in the creep test.

However, for flexure such a calculation does not work, since compression and tension are working in combination. To obtain the compliance function for this solicitation, the first and second correspondence theorems need to be used, as described below.

Thus the first theorem of correspondence is established: the structure is subject to constant static load over time, with null imposed displacements at connections. σ_0, ε_0 and δ_0 are the stress fields, strains and displacements are given by the Theory of Elasticity. Elastic modulus (E_0) and Poisson's ratio ν in the time t, the respective stress fields σ, strains ε and displacements δ are given by Equations 2.7 to 2.9:

$$\sigma = \sigma_0 \tag{2.7}$$

$$\varepsilon = \varepsilon_0(1 + \phi(t)) \tag{2.8}$$

$$\delta = \delta_0(1 + \phi(t)) \tag{2.9}$$

The second theorem of correspondence is established: the structure is free of loads, subjected to imposed displacements in the connections.σ_0, ε_0 and δ_0 are the stress fields, strains and displacements given by the Theory of Elasticity. Elastic modulus (E_0) and Poisson's ratio ν in the time t, the respective stress fields σ, strains ε and displacements δ are given by Equations 2.10 to 2.12.

$$\sigma = \sigma_0(1 - \Psi(t)) \tag{2.10}$$

$$\varepsilon = \varepsilon_0 \tag{2.11}$$

$$\delta = \delta_0 \tag{2.12}$$

where $\phi(t)$ designates creep function and $\Psi(t)$ the relaxation function.

2.1 Creep in refractory concrete

According to NEVILLE *et al.* (1983), creep behaviour of the high alumina cement differs from that of ordinary Portland cement due to the structural changes which take place in hydrated high alumina with time. This conversion will be better explained in Chapter 3, but it is basically the change in hydrated high-alumina cement paste from the conversion of the metastable calcium aluminate hydrates, CAH_{10} and C_2AH_8 from hexagonal to cubic form, the reactions being the type:

$3CAH_{10} \rightarrow C_3AH_6 + 2AH_3 + 18\ H$

$C_3AH_6 + 2AH_3 \rightarrow C_{12}A_7 + H$

The change results in a lowering of strength, probably owing to an increase in the porosity of the hydrated paste. The conversion is encouraged by a temperature higher than normal and by the presence of moisture. In practice most high-alumina cement concrete mixes contain at the end of an initial period of curing enough moisture for conversion to take place. Creep rate must increase when conversion takes place. As shown in NEVILLE and KENINGTON (1960 apud NEVILLE, 1983) investigation, shown in Figure 2.3

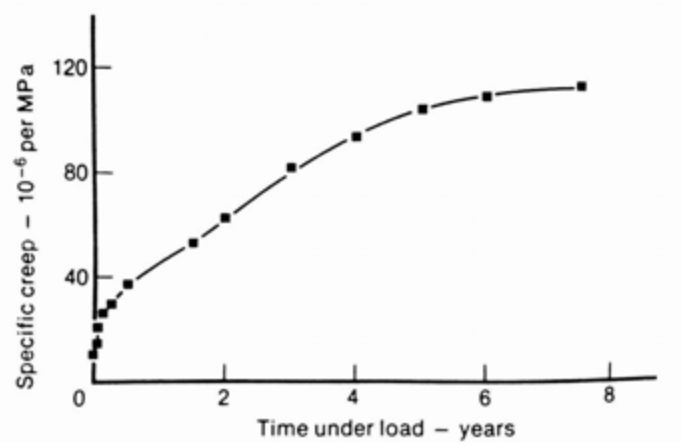

Figure 2.3: Specific creep of high-alumina cement concrete: 1:2:4 mix with a water/cement ratio of 0.7; age at application of load = 1 month. Font: NEVILLE and KENINGTON (1960 apud NEVILLE, 1983).

The increase in creep due to the conversion has also been confirmed by MISHIMA (1968 apud NEVILLE, 1983) who compared the behaviour of high alumina cement

concretes under accelerated and under normal curing conditions. For accelerated curing, specimens were cured at 20°C for seven days and then stored at 40°C so that conversion was taking place under load, but conversion had almost ceased for 28-day loading. The results are shown in Figure 2.4.

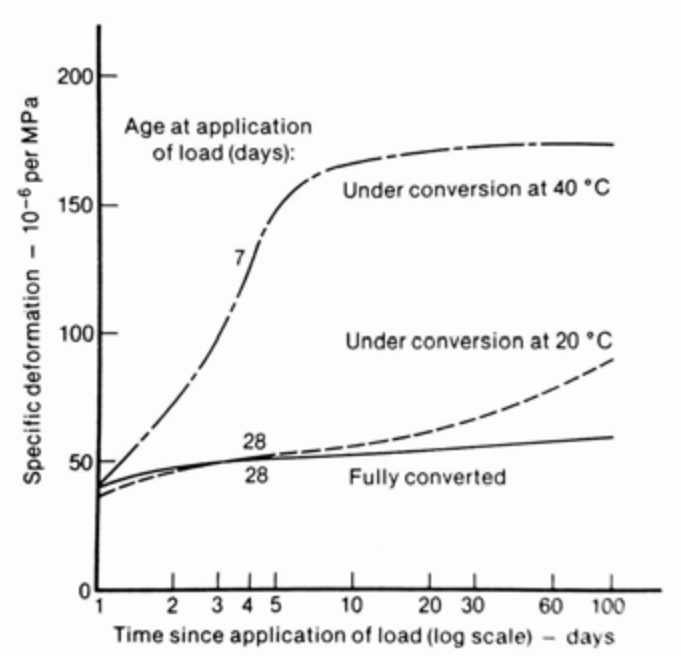

Figure 2.4: Effect of conversion of high-alumina cement concrete on creep. Font: MISHIMA (1968 apud NEVILLE, 1983).

More recent studies were carried out to clarify the effects on creep at high temperatures as seen in BRAULIO *et al.* (2011), KUMAR *et al.* (2003), DÍAZ and TORRECILLAS (2007), MARTINEZ *et al.* (2012) and TERZIĆ and PAVLOVIĆ (2009). However all these studies were carried out at temperatures of above 1000°C, and the longest test under such high temperatures lasted 30 hours. They all presented similar conclusions: creep in the refractory concrete is influenced mostly by the cement; the conversion of CA to C_2 is a fundamental reaction that controls the creep behaviour; the creep behaviour above 1000°C can be controlled by the concrete dosage influenced by the cement type and the alumina content. This conclusions showed that further investigations are necessary to study the alumina cement and understand the conversions that occur at 600°C.

Only one study was found of refractory concrete at a similar temperature KIM (1984), who studied different temperatures from 516°C to 1150°C. Two series of concrete were studied containing 25% calcium aluminate cements: a generic 90% Al_20_3 refractory concrete in the first series and, a 50% Al_20_3 refractory concrete composed of calcined kaolin in the second series. The study concluded that the cement played a dominant role in the refractory concrete, creeping more than the

aggregate. It was also found that grain boundary sliding is the dominant mechanism in creep. X-ray and SEM data showed that dehydration of the cement phase occur, and that CA converts to C_2A with increasing temperature. The research shows that the amount and quantity of cement, the grain size and water-to-cement ratio can be controlled to obtain desired creep properties within certain limits.

As seen in this literature review there are some studies about creep in the refractory concrete at temperatures above 1000°C, however none was found on low cement castable (LCC) at a temperature of 600°C. The main reason for that, is that refractory concrete usually develops ceramic bonding above 1000°C. It was also observed that the dominant effect in creep was the convertion of CA, CA+A→CA2, that changes microstructure and this conversion only happens in temperatures higher than 1000°C. However, as seen in BRAULIO *et al.* (2011), KUMAR *et al.* (2003), DÍAZ and TORRECILLAS (2007), MARTINEZ *et al.* (2012) and TERZIĆ and PAVLOVIĆ (2009), it is important to understand the micro structure of the cement, and the conversions of the calcium aluminate cement since the cement that will play this main role in creep deformation.

Chapter 3

Materials

This research is part of a on going project of refractory concretes designed for petroleum platforms, based on the work of research colleagues. The refractory concrete chosen for the present work is used in real world applications. Its matrix was already designed to fulfil its mechanical appliance in petroleum platforms in UFCC. The main purpose of this work was to investigate creep behaviour and not to design a better or more resistant creep matrix.

MEDEIROS (2012) studies about this concrete concluded that the reinforcement of 6% of corrugated stainless steel fibre of 0.51 mm diameter and 25 mm length (aspect ratio of 49), improved the mechanical properties of the matrix. Based on this, the influence of creep was investigated in the matrix with and without this percentage of reinforcement.

The working temperature for the refractory concrete was of 600°C. Further two different temperature treatments were considered in order to simulate the usage of this matrix in its natural state. In the first treatment, the matrices were cured at 21°C, dried at 110°C and then burned at 600°C. For the second one, the matrices were cured at 21°C and only dried at 110°C. In this way, it was possible to identify the burning effects at 600°C. The overall procedure is fully described in Chapter 4.

For a real understanding of creep behaviour, an empirical knowledge must be combined with a molecular knowledge of the particular behaviour of the material. For example, the use of cure temperature at 21°C with the drying process carried out at 110°C is adequate for the calcium aluminate hydration process.

Once this matrix and fibres are commercial materials, the need to investigate its composition arises. Initially, a complete literature review of the dense refractory castable was done, focusing on the calcium aluminate cement and the aggregates

that were supposedly present in this matrix. Then follows a review of the stainless steel fibres.

Based on this review, a series of material characterization tests in the matrix were carried out. Chemical composition, thermogravimetric, X-ray diffraction and scanning electron microscopy were performed. These tests, combined with previous tests by MEDEIROS (2012) of porosity and density, led to the determination and estimation of the composition phase of the calcium aluminate cement and the effect of temperature increase on the overall material. Granulometry tests to determine the size of the aggregates were also performed.

Although the differentiation of the cement from the aggregate could not be determined, the changes in the material, due to temperature variance were successfully recorded. The final material matrix was more porous and developed the conversion of the hydrates from metastable to stable state.

3.1 Dense refractory castable

The matrix chosen was a dense refractory concrete. It is commercialized as Brasilcast 560 by Brazilian company IBAR and has a low content of aluminous cement. This matrix comes already dosed and it needs only water addition. The ratio used for this study was of 7,6% (in mass). The matrix is illustrated in Figure 3.1 without the water addition.

Figure 3.1: Dense refractory concrete, Brasilcast 560, without water addition.

The properties of this concrete provided by the company IBAR, are presented in Tables 3.1 and 3.2.

Table 3.1: Chemical properties of the refractory concrete Brasilcast 560. Font: Report of the company IBAR, IBAR (2010).

Chemical composition	Weight percentage (%)
Al_2O_3	67.0 %
SiO_2	25.0 %
CaO	2.5 %
TiO_2	- %
Fe_2O_3	1.4 %
Properties	**Nominal**
Maximum working temperature T_{Max} (°C)	1500
Bulk density at 110°C ρ_{110} (kg/m^3)	2350
Bulk density at 815°Cρ_{815} (kg/m^3)	2350
Compression strength after exposing the concrete at 110°C for 24h (MPa)	50.0
Compression strength after exposing the concrete at 815°C for 5h (MPa)	80.0
Amount of water used in the mixture (%)	7.0
Setting time (min)	240

Table 3.2: Thermal expansion coefficients of refractory concrete Brasilcast 560. Font: Report of the company IBAR, IBAR (2010).

Temperature (°C)	Linear thermal expansion coefficient - α_L (mm/m)
21.1	0.000
100.0	0.300
200.0	0.500
300.0	0.900
400.0	1.400
500.0	1.900
600.0	2.500
700.0	3.400
800.0	4.000
900.0	4.900

Refractory concretes, usually called castable refractory, are ceramic materials consisting of complex formulations. Composed by precision-sized graded refractory aggregates, modifying fillers and additives, they are most of the time bound with aluminous hydraulic cements. Portland cement is still used but in smaller applications.

Castable concretes can be classified according to the Brazilian Standart NTP-1728 (2005), presented in Figure 3.2. This classification helps to associate the concrete with the type of application, therefore it is usually used in the Petroleum Industry in Brazil. Using this and comparing to the data provided by the company IBAR it is possible to classify the concrete as dense, anti-erosive class C. This type of concrete according to the NTP-1910 (2008), can be used for Risers, with thickness of 125 mm, which is in accordance with its application.

Characteristics	Dense/ Plastic (Grade 4)					Unit	Brazilian's Standard
	Anti Erosion			Regular			
	Class A	Class B	Class C	Class A	Class B		
Chemical analysis:						%	ABNT NBR 8826 ABNT NBR 9644 ABNT NBR 11308 ABNT NR 11303
- Al_2O_3 (minimum);	80,0	60,0	-	70,0	-		
- SiO_2 (maximum);	8,0	(Grade 3)	-	-	-		
- CaO (maximum);	5,0	5,0	-	10,0	7,0		
- Fe_2O_3 (maximum);	1,0	1,0	1,5	1,5	3,0		
Maximum Temperature of Use	1650	1650	1400	1600	1400	°C	-
Apparent specific weight: Dried at 110 °C	≥ 2600	≥ 2600	≥ 2400	> 2300	≥ 2500	kg/m³	ABNT NBR 6115 ABNT NBR 11221 ou ASTM C 134
Minimum compression strenght:						Mpa (kgf/cm²)	ABNT NBR 6224 ABNT NBR 10965 ABNT NBR 11222 ou ASTM C133
- Dried at 110 °C;	49,1 (500)	44,3 (450)	34,3 (350)	39,2 (400)	19,6 (200)		
- Burned at 815 °C.	49,1 (500)	39,2 (400)	29,4 (300)	54,5 (550)	11,7 (120)		
Linear maximum dimensional variation - Burned at 815 °C.	0,5	0,5	0,5	0,5	0,5	%	ABNT NBR 8385 ou ASTM C 113
Thermal Conductivity at Average temperature:						W/m.K (kcal/ m.h.°C)	ASTM C 201
200 °C;	-	-	1,29 (1,11)	-	-		
400 °C;	-	-	1,27 (1,09)	-	-		
600 °C.	-	-	1,24 (1,07)	-	-		
Maximum loss by erosion: - Burned at 815 ° C.	8	12	20	-	-	cm³	ABNT NBR 13185 ou ASTM C 704

Figure 3.2: Classification of refractory concretes. Font: NTP-1728 (2005).

As reported by LEE *et al.* (2001), conventional castable concrete usually contains 15-30% of calcium aluminate cement and 8-15% of water. The 6-10% water percentage is used to develop the cement bond, 2-6% is added to make the concrete flow and a relatively large amount of water 0-5% is often taken up by porosity of the aggregate and does not contribute to the hydraulic bond.

Because of that, LEE *et al.* (2001) described a major disadvantage of conventional castable presents, as usually porous and open textured, which greatly reduces the strength. This occurs mostly because of the excess of water in the drying and firing processes. When the concrete is exposed to 110°C, the conversion destroys the dehydration process. During this modification, the pore size distribution changes

and porosity grows significantly. Porosity grows even higher when the castable is fired at 1000°C and can vary from 22 to 26%.

In order to improve the performance of conventional castable, the low cement castable (LCC) and ultra-low cement castable (ULCC) were developed. The main idea was to reduce the water requirement for placement while maintaining strength. This was achieved by improving the packing density of the material. More efficient particle packing reduces the maximum size of the interstice between particles. This was done by the addition of superfine or colloidal particles, such as silica fume and alumina, deflocculants, and setting control additives. That helped to reduce the water requirement for placement and improve the ceramic bond.

The matrix used is already classified as LCC. Granulometry tests were performed to confirm the grain size distribution and results are presented further in a follow up section. The presence of microsilica in the matrix confirmed by the chemical composition improved the packing and density.

The main advantages of the LCC cited by LEE *et al.* (2001) are the physical properties, such as the high density, low porosity and high cold and hot strengths. LCC also has high abrasion and corrosion resistance and usually higher rupture modulus and lower creep values than conventional castable cement.

According to PARR *et al.* (2005), the calcium aluminate cement is also deeply linked to the mixing, placing, consolidating, curing and drying processes as well as the applications of the castable and therefore linked to creep properties.

In order to understand the role of calcium aluminate cement, it is first necessary to consider the reactions that take place within CAC during the hydration process and then to link these reactions to the physical aspects of the castable properties. Hence, a brief description of the structure of the hydrated aluminous cement is given in the following.

3.2 Calcium Aluminate Cement

Calcium aluminate cement (CAC) is defined by SCRIVENER *et al.* (1999) as a special kind of cement that in reaction with water, instead of calcium silicate hydrate (C-S-H) and crystalline calcium hydroxide (CH) as their principal hydrates, produces hydrates and reactive phases of calcium aluminate. CACs contains CaO and Al_2O_3 as principal oxides, with little or no silica. These two combined give monocalciumaluminate (CA) as the principal active phase in the cement, which reacts with water to give calcium aluminate hydrates.

SCRIVENER *et al.* (1999) also stated, that the main properties of the CACs are: rapid strength development, even at low temperatures; high temperature resistance/refractory performance resistance to a wide range of chemically aggressive conditions.

3.2.1 Raw material of calcium aluminate cement

Calcium aluminate cements are obtained by fusing or sintering a mixture of suitable proportions of lime and alumina and grinding the resulting product to a fine powder. Its color ranges from black to white, depending on the impurities present and on the iron oxide quantity and oxidation state, while high purity cements are white.

Uncombined lime and alumina begin to react with the high lime products and form lower lime or higher alumina compounds. These reactions continue in the kiln until the mix is completely combined as follows.

$C+A \rightarrow C_3A \rightarrow C_{12}A_7 \rightarrow CA \rightarrow CA_2 \rightarrow CA_6$

3.2.2 Hydration of calcium aluminate cement

The hydration of calcium aluminate cement is dependant on time, temperature and humidity. It is believed that the hydration process of CAC affects creep significantly, since creep in most materials is affected by temperature and is a time dependant deformation. The formation of hydrates and its effects on porosity, can lead to microcracking and enhancement of creep deformation. The hydration process is illustrated in Figure 3.3 and the conversions are described in Table 3.3.

Table 3.3 shows that the hydration of CAC below 10°C leads to the formation of CAH_{10} (that is dominating) and continues up to around 27°C. Studies have shown that for w/c ratios between 0.3 and 0.7, hydration at 20 °C leads to a dense microstructure, with low porosity.

Table 3.3: Hydration scheme for mono calcium aluminate PARR *et al.* (2005)

Temperature	Hydration		Reaction
< 10 °C	$CA + 10H$	$\rightarrow$	CAH_{10}
10 - 27 °C	$2CA + 11H$	$\rightarrow$	$C_2AH_8 + AH_3$
	$CA + 10H$	$\rightarrow$	CAH_{10}
>27 °C	$3CA + 12H$	$\rightarrow$	$C_3AH_6 + 2AH_3$
F(t °C + time)	$2CAH_{10}$	$\rightarrow$	$C_2AH_8 + AH_3 + 9H$
	$3C_2AH_8$	$\rightarrow$	$2C_3AH_6 + AH_3 + 9H$

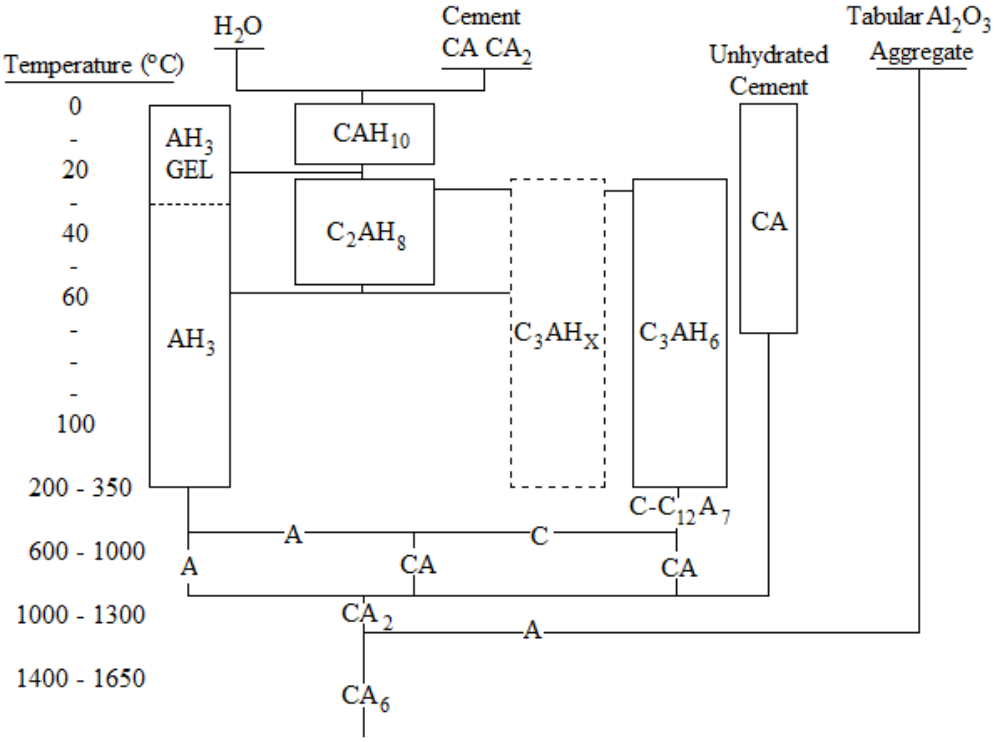

Figure 3.3: Conversion of calcium aluminate cement. Font: KIM (1984)

PARR *et al.* (2005), SCRIVENER *et al.* (1999) and ANTONOVIČ *et al.* (2013) confirmed that the stable hydration products, formed from the initial sintered mineralogical phases and their crystalline structures, generally develop within 3-6 months under ambient conditions, or within the first 24h if curing reactions take place when CAC and water are combined. The morphology and some key properties of each of the main hydrates are shown in Table 3.4.

It is believed that the formation of C_3AH_6 often passes through a transient C_2AH_8 phase. The other two important reactions are the conversion of the metastable hydrates CAH_{10} and C_2AH_8 to the stable C_3AH_6 hydrates. The stable phases are C_3AH_6 and AH_3, and the other phases will inevitably convert to these at a rate depending on temperature and moisture. C_3AH_6 has the highest density of the calcium aluminate hydrates, resulting in a higher porosity at a given degree of hydration.

Table 3.4: The characteristics of the crystalline state CAC hydrates ANTONOVIČ *et al.* (2013).

Hydrates	CaO (%)	Al_2O_3 (%)	H_2O (%)	Structure	Density (g/cm^3)
CAH_{10}	16.6	30.1	53.3	metastable hexagonal	1.743
C_2AH_8	31,3	28.4	40.3	metastable hexagonal	1.950
C_3AH_6	44.4	27.0	28.6	stable cubic	2.527
AH_3	-	65.4	34.8	stable hexagonal or gel	2.420

C_3AH_6 hydrate

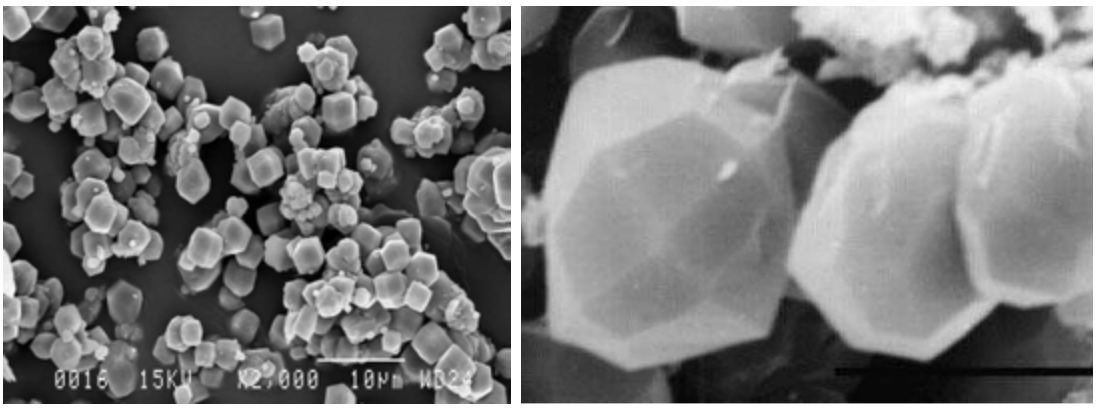

a) b)

Figure 3.4: a) C_3AH_6 hydrate. Font: PARR *et al.* (2005); b) C_3AH_6 hydrate. Font: LEE *et al.* (2001).

AH_3 hydrate

The morphology of the AH_3, that is formed, also changes with temperature. At lower temperatures it exists in gel form and becomes increasingly crystalline as the temperature increases.

3.2.3 Drying process

Conforming to ANTONOVIČ *et al.* (2013), the drying process consists of first heating the concrete to a lower temperature of around 110°C, when the water is removed to avoid undesirable strength loss, spalling or explosion. Up to 24 hours after casting, the hydration process is still incomplete and continues to occur.

During the drying process, residual CA as well as a large part of the CA_2 is hydrated. At this point the strength reaches its maximum, reflecting the degree of hydration development. AH_3 appears as a crystalline phase of gibbsite.

The hydrate development can be different according to the mineralogy of the CAC affecting the mechanical properties during the drying process. PARR *et al.* (2005) cited that in the case of the 50% alumina cement, on heating transfer from ambient temperature to 100°C, the cement hydrates that are initially formed, are converted to the stable hydrates AH_3, and C_3AH_6. With the release of free water, the density of the hydrates and porosity increase and a reduction in the measured mechanical strength takes place.

However according to PARR *et al.* (2005), in the case of the 70% alumina cement, which contains appreciable quantities of CA_2, an increase in strength is observed after drying. In addition, the excess water used for casting is also liberated as steam. Some of the water released by the conversion of metastable to stable hydrates leads to further hydration of the CA_2 resulting in an increase in strength.

3.2.4 Dehydration and firing

ANTONOVIČ *et al.* (2013) in agreement with PARR *et al.* (2005) reported that all CAC hydrates in the bond phase decompose to the calcium aluminates ($C_{12}A_7$, CA, and CA_2) and eventually, if enough free alumina is present, turn into CA_6. When CAC is heated, free and physically and chemically bound water is removed from it. Dehydration by heating follows the scheme described by ANTONOVIČ *et al.* (2013) and PARR *et al.* (2005).

$CAH_{10} \rightarrow C_2AH_8 + AH_3$

$C_2AH_8 + AH_3 \rightarrow C_3AH_6 + 2AH_3$

$C_3AH_6 + 2AH_3 \rightarrow C_{12}A_7 + CA + H$

$C_3AH_6 + 2AH_3 + A \rightarrow CA + H$

According to PARR *et al.* (2005) and confirmed by (ANTONOVIČ *et al.*, 2013), temperatures at which the dehydration occurs and the modifications are :

- Between 100 and 400°C: AH_3 and C_3AH_6 gradually decompose to give amorphous anhydrous relics and water vapour. This water vapour has to escape from the concrete. The porosity increases from 13 to 17% and consequently the mechanical strength decreases. This two stage release of

water is an advantage of the CAC based systems as it helps to reduce a build-up of vapour pressure compared to other bond systems where the water release takes place in a narrow temperature range;

- 400-900°C: During this subsequent dehydration phase the previously stable hydrates C_3AH_6 continue to dehydrate progressively to $C_{12}A_7H$ and at the same time gibbsite (AH_3) is transformed to alumina hydrate relics. The measurable mineralogy does not change significantly during this period. Porosity continues to increase to around 23% and strength declines relative to the strength at 110°C;

An interesting fact observed by LEE *et al.* (2001), is that compounds formed during hydration of CACs dehydrate at temperatures of up to 550°C. The process of hydration, followed by dehydration, creates an anhydrous material which is extremely fine and active. Lime and alumina reappear and recombine in a way similar to that of the original raw materials in the kiln. This was observed further in the scanning micrograph after subjecting the concrete to a temperature of 600°C.

3.3 Steel Fibres

The steel fibre reinforcement enhanced the concrete performance such as by increasing the ability to absorb energy ("tenacity") and improving post cracking strength material, impact strength, fatigue strength, bending strength, strength to thermal fragmentation (thermal spalling) of concrete. Also the addition of metallic fibres positively contributed to inhibit the linear shrinkage and cracks in the concrete.

In this study corrugated stainless steel fibres of 0.51 diameter and 25 mm length, is shown in Figure 3.5 were used. The fibres were obtained from Di Martino Indústrias Metalúrgicas and were the same as used in the study of MEDEIROS (2012).

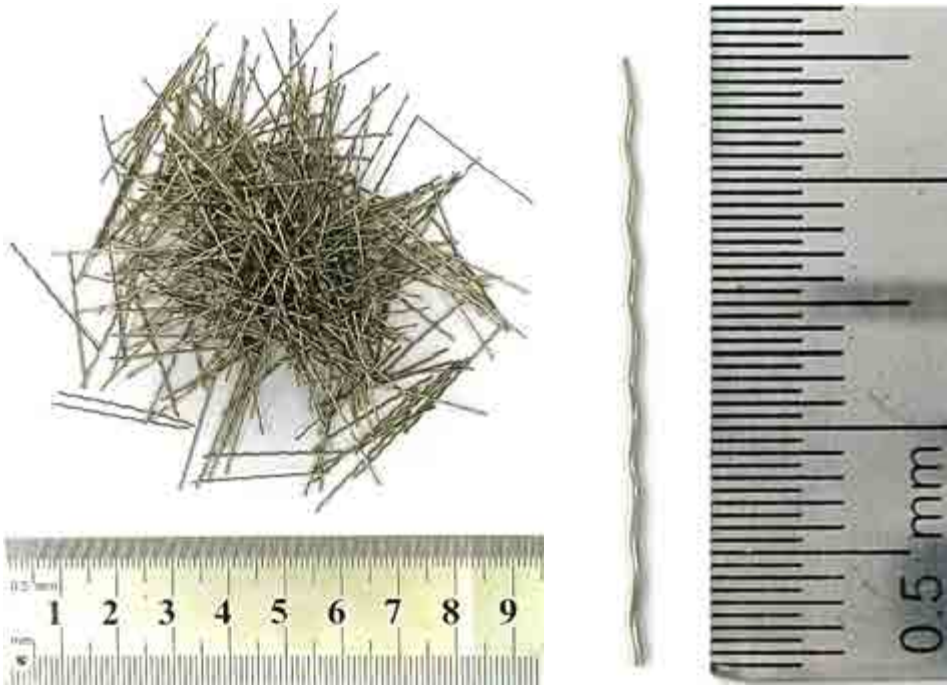

(a) (b)

Figure 3.5: a) Corrugated stainless steel fibres used as reinforcement; b) Single corrugated stainless steel fibres used as reinforcement, showing the size of a single fibre.

The steel was of type AISI 310, and its chemical composition is presented in Table 3.5. According to the manufacturer, it can resist a maximum temperature of 900°C. The Cr in the chemical composition improves corrosion resistance and the Ni stabilizes austenite as found by PLAUT *et al.* (2007).

Table 3.5: Chemical composition of austenitic stainless steel 310

Substances	Content
Chromium (range)	24 to 26
Nickel (range)	19 to 22
External diameter (mm)	0.04 to 0.10
Manganese (maximum)	2
Phosphorus (maximum)	0.045
Sulfur (maximum)	0.03
Silicon (maximum)	1

The mechanical properties of this steel is presented on Table 3.6. Further it is important to know the thermal expansion of the stainless steel AI 310 given in Table 3.7, which need to be compatible with that of the concrete, otherwise, when exposed to high temperature, the steel will expand more and cause micro cracks in the matrix.

Table 3.6: Physical and mechanical properties of the austenitic stainless steel 310. Font: ASME SEC. II (2010) and MEDEIROS (2012).

Properties of AI 310	English System	International System
σ_U (psi, MPa)	70000	482.6
σ_Y (psi, MPa)	30000	206.8
E_{AIC} (psi, GPa)	$28.3\times\ 10^6$	195.1
ρ_{AI} (lb/in^3, g/cm^3)	0.290	8,027
ρ MEDEIROS (2012) (g/cm^3)	-	7,852

Plotting the temperatures in function of the linear thermal expansion coefficients, and adjusting a polynomial tendency line, Equation 3.1 was obtained, with a determination coefficient (R^2) of 1.

$$\alpha_L = 0,0000037082 \cdot T^2 + 0,0165995007 \cdot T - 0,4046101958 \tag{3.1}$$

where: α_L is the linear thermal expansion coefficient and T is the temperature.

Using Equation 3.1, it was possible to obtain the coefficients for the temperatures of 110°C and 600°C, which were 1.466 mm/m and 10.890 mm/m respectively.

3.4 Methods for materials characterization

3.4.1 Granulometry

A coarse granulometry, was carried out to separate the larger particles. The result is given in Figure 3.6. This result indicates that 100% of the particles are smaller than 9 mm, and 90% of the mass is composed of grains smaller than 5 mm.

Table 3.7: Thermal expansion coefficients of stainless steel AI 310. Font: ASME SEC. II (2010)

Temperature (°C)	Average thermal expansion coefficient - α_m (mm/mm/°C)	Linear thermal expansion coefficient - α_L (mm/m)
21.1	1.53E-05	0.000
37.8	1.55E-05	0.250
65.6	1.58E-05	0.667
93.3	1.60E-05	1.167
121.1	1.64E-05	1.667
148.9	1.66E-05	2.083
176.7	1.69E-05	2.583
204.4	1.71E-05	3.167
232.2	1.73E-05	3.667
260.0	1.75E-05	4.167
287.8	1.76E-05	4.667
315.6	1.78E-05	5.250
343.3	1.78E-05	5.750
371.1	1.80E-05	6.250
398.9	1.80E-05	6.833
426.7	1.82E-05	7.333
454.4	1.84E-05	7.917
482.2	1.84E-05	8.500
510.0	1.85E-05	9.000
537.8	1.85E-05	9.583
565.6	1.87E-05	10.167
593.3	1.87E-05	10.750
621.1	1.89E-05	11.333
648.9	1.91E-05	11.917
676.7	1.91E-05	12.500
704.4	1.93E-05	13.167
732.2	1.93E-05	13.750
760.0	1.94E-05	14.333

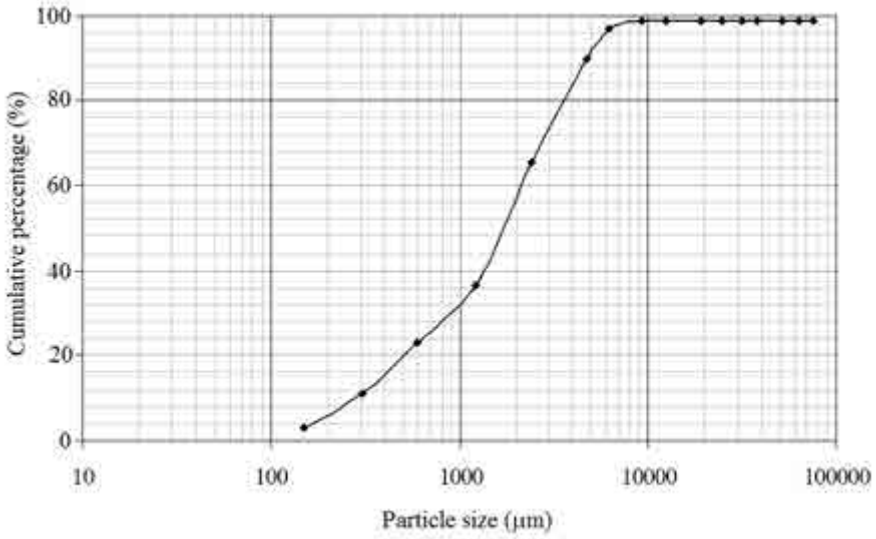

Figure 3.6: Coarse granulometry curve of the refractory castable.

Then a laser granulometry was carried out, using alcohol as a dispersant and as particle sizing instrument, Mastersizer 2000. The result was plotted by the instrument and is presented in Figure 3.7. The result showed that 50% of the volume of particles is inferior of 25μm.

Both results showed that in this concrete there is a high percentage of fine grains and fillers that is characteristic of the LCC.

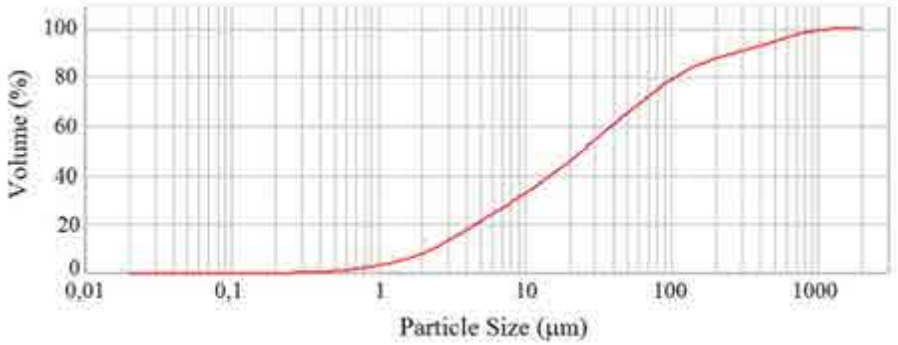

Figure 3.7: Fine granulometry curve of the refractory castable.

3.4.2 Chemical composition

The instrument EDX-720 was used to determine the chemical composition of the matrix. This equipment allows an increased detection of low atomic number elements as elements from C to U are detectable. The results of chemical composition are presented in Table 3.8

By comparing the chemical compositions provided by the manufacturer and those given by MEDEIROS (2012), one can conclude that the concrete presented similar results, and that the batch of concrete is in compliance and can thus produce consistent mechanical results that can be correlated to the mechanical results obtained by MEDEIROS (2012) and the manufacturer (IBAR).

Table 3.8: Results of the chemical composition.

Composition	Weight percentage (%)	Values obtained by MEDEIROS (2012) (%)	Values provided by the manufacture - IBAR (%)
Al_2O_3	61.945	62.470	67.0
SiO_2	27.229	28.324	25.0
CaO	4.959	5.641	2.5
TiO_2	1.734	0.735	-
SO_3	1.628	0.700	-
Fe_2O_3	1.074	0.455	1.4
P_2O_5	0.998	0.901	-
K_2O	0.194	0.274	0.3
ZrO_2	0.118	0.089	-
V_2O_5	0.049	-	-
Ta_2O_5	0.028	-	-
MnO	0.015	0.018	-
Ga_2O_3	0.013	0.009	-
NbO	0.008	-	-
SrO	0.005	0.016	-
Y_2O_3	0.004	0.005	-

3.4.3 Density and Porosity

Density and porosity of the refractory concrete were studied previously by MEDEIROS (2012) and tests were carried out following the Brazilian standard NBR 9778. The concrete samples were dried at 110°C in a kiln for 72h shown in Figure 3.8. The mass was registered and denominated dried mass (m_d).

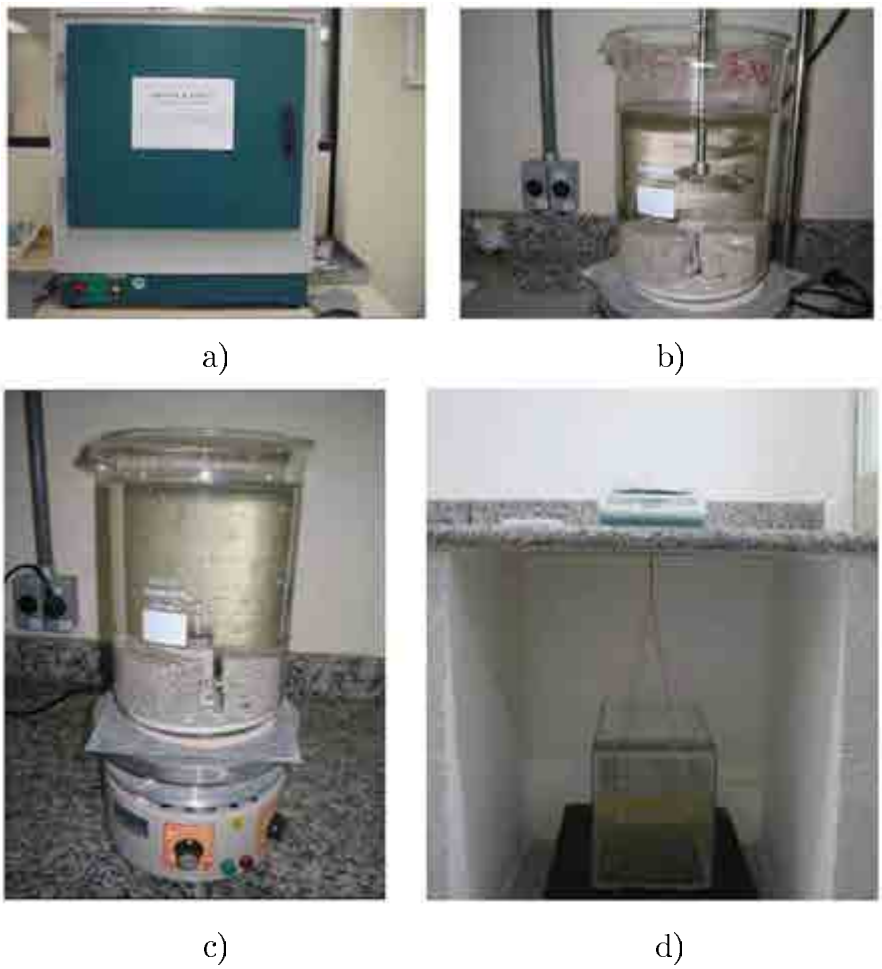

Figure 3.8: a)Kiln for drying samples, determination of the dry mass (m_d); b) Water heating; c) Sample saturation; d) Hydrostatic balance and determination of the immerse mass (m_i).

Then the samples were submerged in water with a temperature of 23±2 and soaked for 72h. After that, the samples were placed in a container full of water, that was gradually brought to boiling point and maintained there for a period of 5 hours. The volume of water was maintained approximately constant. The water was then let to cool naturally to the temperature of 21 ± 2°C. The masses were recorded with a hydrostatic balance and called immersed mass (m_i).

The saturated mass (m_{sat}) was determined by removing the samples from the water and drying them with a damp cloth.

Absorption (A) calculated by Equation 3.2, is the process that water is conducted and tends to occupy the pores of a porous permeable solid body. It is also the mass increase of a porous solid body due to water penetration in its permeable pores in relation to its mass in the dry state.

$$A = \frac{m_{sat} - m_d}{m_d} \cdot 100 \tag{3.2}$$

where: A is the absorption; m_{sat} is the saturated mass; and m_d is the dried mass.

The void ratio (I_V), obtained by Equation 3.3, which is the ratio of permeable pore volume to the total volume of the sample.

$$I_V = \frac{m_{sat} - m_d}{m_{sat} - m_i} \cdot 100 \tag{3.3}$$

where: I_V is the void ratio; m_{sat} is the saturated mass; m_d is the dried mass; and m_i is the immersed mass.

The specific mass of the dry sample (ρ_d) is the ratio of the dry mass of material and the total sample volume, including pores permeable and waterproof. It is determined by the Equation 3.4.

$$\rho_d = \frac{m_d}{m_{sat} - m_i} \tag{3.4}$$

where: ρ_d is the specific mass; m_{sat} is the saturated mass; m_d is the dried mass; and m_i is the immersed mass.

Another property obtained by this test is the specific mass of the saturated sample (ρ_{sat}), that is the ratio between the mass of saturated materials and the total sample volume, including pores permeable and waterproof. It is calculated by the Equation 3.5.

$$\rho_{sat} = \frac{m_{sat}}{m_{sat} - m_i} \tag{3.5}$$

where: ρ_{sat} is the specific mass of the saturated sample; m_{sat} is the saturated mass; and m_i is the immersed mass.

The results of density and porosity are presented in Table 3.9. It was observed that the density increased when metallic fibres were added. When compared to the matrix dried at 110°C, the density increased approximately by 5.5%, when adding 6% mass of fibres. The increase in density with the fibre content is related to the substitution of the matrix with a specific weight of 2.350kg/m^3 and 7.800kg/m^3 respectively by metallic fibre. When compared to the same matrix burned at 600°C the increase is of 4.0%, therefore slightly smaller (but of the same order of magnitude) than the increases for dry matrix 110°C. This is because, a reduction occurs in the density of the matrix, when subjected to the firing temperature, which does not occur with the metal fibre reinforcement.

Table 3.9: Results of density and porosity.

Matrix	Density (kg/m^3)	SD	CV	Porosity	SD	CV
B110-0%F	2.337	92.33	3.95	14.33	0.86	5.98
B600-0%F	2.302	69.59	3.02	17.83	0.68	3.83
B110-6%F	2.463	37.03	1.50	14.38	0.30	2.06
B600-6%F	2.393	32.85	1.37	19.19	0.37	1.95

* Standart Deviation (SD) ** Coefficient of variation (CV)

The tests showed an increase in porosity with fibre reinforcement content of 6% in mass for refractory cement burned at 600°C. This was not observed for the refractory which was only dried at 110°C. The increased porosity of the matrix burned at 600°C is 24.5% compared to that of the matrix dried at 110°C. This is due to dehydration concrete. The reinforcement of 6% by weight of steel fibres increased the porosity by 7.6% in relation to the burned matrix without reinforcement.

3.4.4 Thermogravimetric analysis

Thermogravimetric analysis of the calcium alumina cement was carried out by MEDEIROS (2012), and in this study a themogravimetric analysis of the ground concrete was performed.

The results of MEDEIROS (2012) are presented in Figure 3.9. It was concluded, that for the cement at room temperature the peaks observed in the curve until a temperature of 250°C indicate a loss of the combined water in the: gibbsite gel (AH_3 - at $\sim$ 96°C); the CA_{10} (at $\sim$ 184°C); and "hydrogarnet" C_2AH_6 (at $\sim$ 220°C). At approximately 300°C a small peak was observed probably from one type of gibbsite yAH_3.

Figure 3.9 also presents results by MEDEIROS (2012) of the thermogravimetric tests for the cement exposed to drying temperature of up to 110°C. The results indicate a strong reduction in the gel gibbsite peak and CA_{10}. Only the hydrogarnet peak C_2AH_6 (at $\sim$ 220°C)remained intense. For temperatures above 300°C some small intensity peaks were observed. For the sample submitted to a temperature of 600°C only small peaks were observed but were difficult to identify.

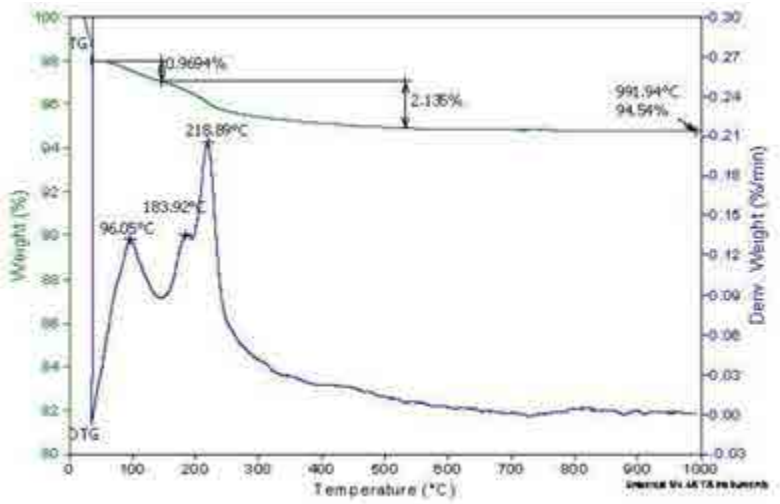

(a)

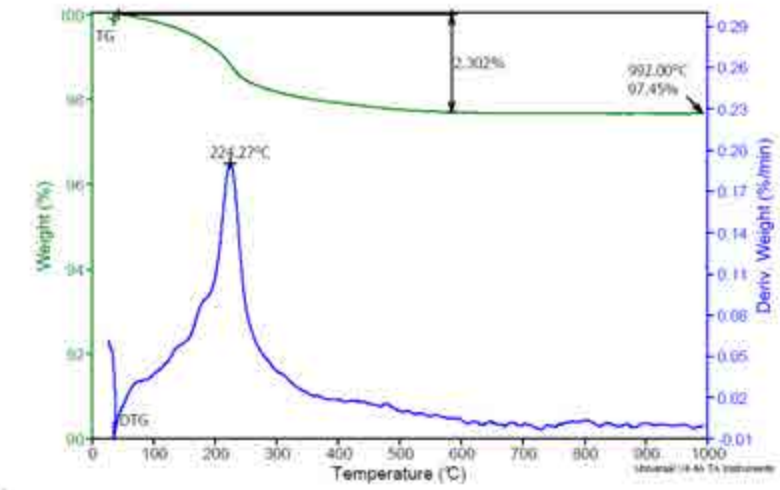

(b)

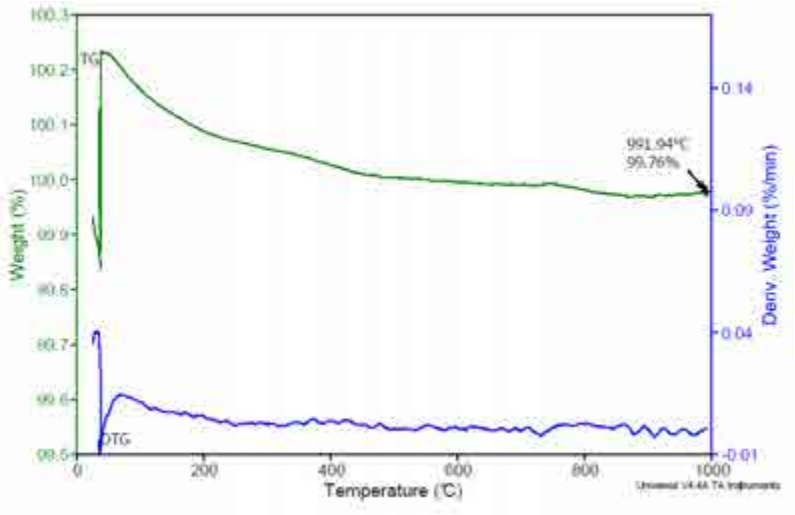

(c)

Figure 3.9: Termogravimetric analysis of the calcium alumina cement: a) at room temperature (21°C); b) dried at 110°C; c) burned at 600°C as performed by MEDEIROS (2012).

Thermal analysis techniques were used to detect the dehydration process of the CAC in the ground concrete. The equipment used was the SDT Q600 of TA Instruments. This is a horizontal balance and furnace, with a dual beam balance design (grown compensated), sample capacity of 200 mg and balance sensitivity of 0.1 μg. The conditions of the analysis were: the sample was heated to ambient temperature of up to 1000°C; heating rate of 10°C per minute; a platinum sample pan was used, with mass of around 10 mg; inert atmosphere (N_2) with maximum flow of 100 ml/min.

The tests were performed on samples dried at 110°C and then burned at 600°C, denominated B600-0F and on samples only dried at 110°C, denominated B110-0F.

For B110-0F, it was possible to see a mass loss of around 2.9% at 241°C, that according to the literature review, was due to the transformations of the: hydrogarnet (C_2AH_6); C_3AH_6 and $2AH_3$, that dehydrate and form $C_{12}A_7$ + CA. For temperatures above 550°C a small intensity peak is observed , seen at 598°C.

For the sample submitted to a temperature of 600°C only a small peak formed at 598°C, presenting a mass loss of around 1% which is not significant. This peak is probably due to carbonation.

Comparing the results obtained with the ones obtained by MEDEIROS (2012), it was possible to see that the cement and the ground concrete thermal gravimetric analysis presented similar results.

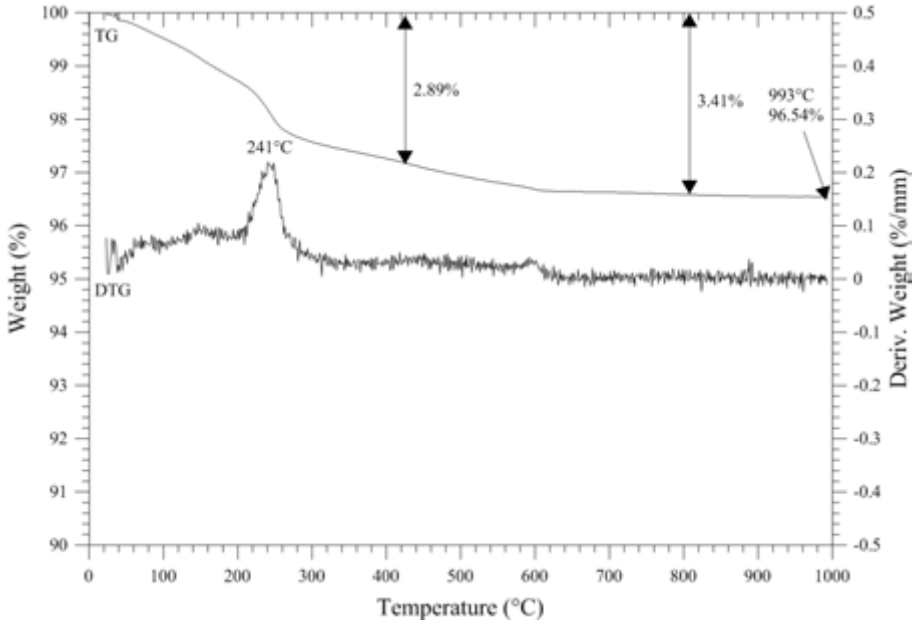

(a)

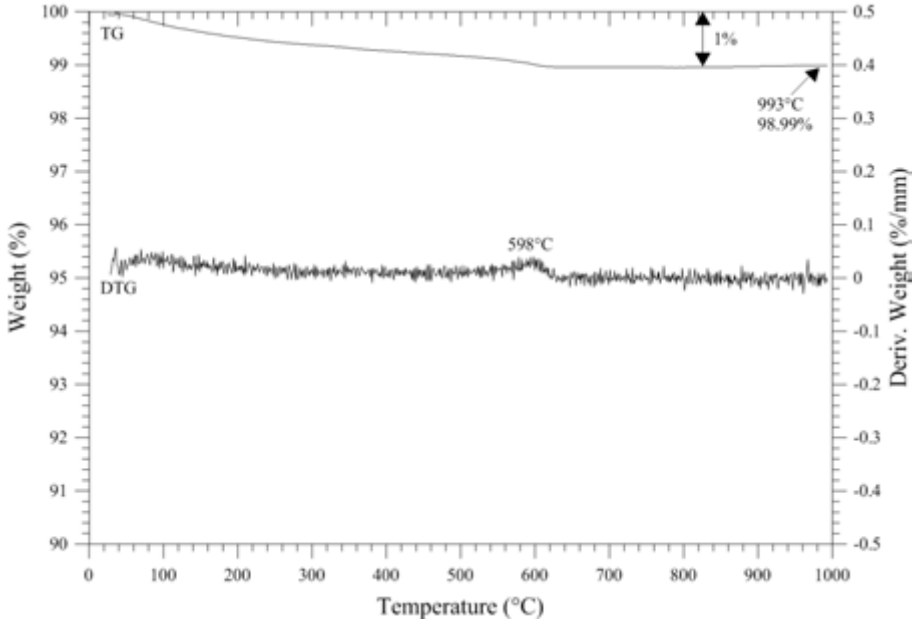

(b)

Figure 3.10: Termogravimetric analysis of the refractory concrete: a) dried at 110°b) burned at 600°C.

3.4.5 X-ray diffraction analysis

The X-ray diffractometer used was the model D8 FOCUS, of the Brucker company. Results are presented in Figures 3.11.

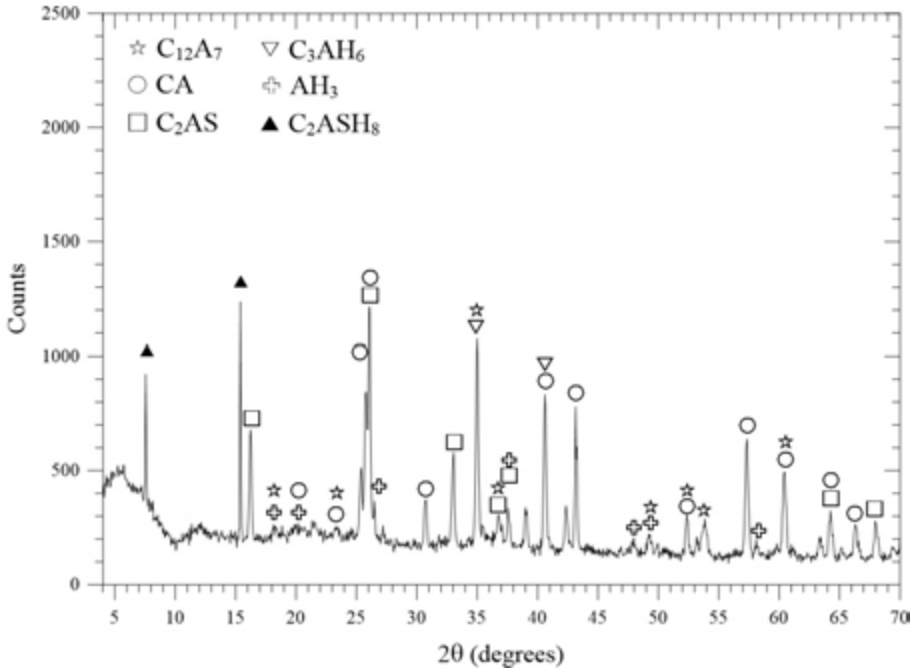

(a)

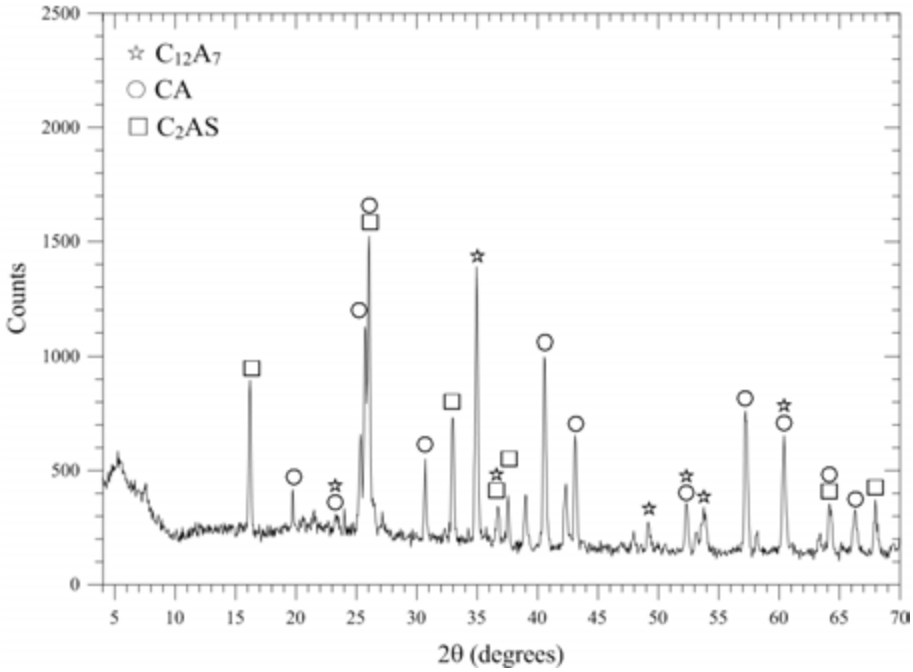

(b)

Figure 3.11: Graphic of the diffractometer analysis of the sample: a) only dried at 110°C; b) dried at 110°C and burned at 600°C.

For the sample dried only at 110°C, the X-ray diffraction analysis was able to identify the calcium alumina products: $C_{10}AH_6$, AH_3, $C_{12}A_7$, CA, C_2AS and C_2ASH_8. After burning, only the products $C_{12}A_7$, CA and C_2AS were identified.

The thermalgravimetric analysis showed that the sample dried at 110°C, presented C_3AH_6 and $2AH_3$, and after burning at 600°C this peak did not show

up. The same can be seen in X-ray diffraction analysis where the products C_3AH_6 and AH_3 ceased to exist.

This confirmed the thermalgravimetric analysis results, showing that the conversion occurred as:

$C_3AH_6 + 2AH_3 \rightarrow C_{12}A_7 + CA + H$

$C_3AH_6 + 2AH_3 + A \rightarrow CA + H$

Also confirming this conversion the peaks of the products $C_{12}A_7$ and CA presented a higher intensity in the sample that was burned, showing that there is a higher percentage of this compounds.

In addition in the sample dried only at 110°C, the C_2AS, shown in the peak of around 8°C and 15°C, but disappeared in the sample burned at 600°C. This indicated that the C_2ASH_8 dehydrates and forms the C_2AS, that appears in the peaks, with a higher intensity than in the sample burned at 600°C.

3.4.6 Scanning electron microscopy

The scanning electron microscopy was performed with two microscopes. One was the Hitachi tabletop microscope TM 3030, and the other one the FEI Quanta 400 located at the Mineral Technology Center (CETEM) of Federal University of Rio de Janeiro (UFRJ). The images are presented in Figures 3.12 and 3.13.

These pictures only visualise the differences between the matrices, indicating that the matrix after burning was finer. However this is only an indicator and further conclusions cannot be drawn from then.

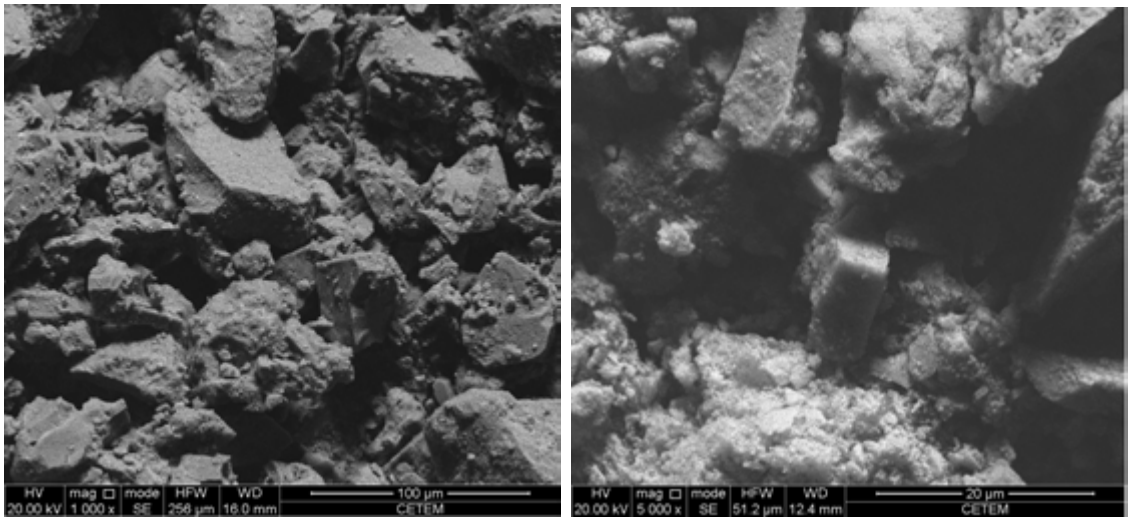

a) b)

Figure 3.12: a) View of the concrete only dried at 110°C; b) Zoom at C_3AH_6 appearing as a cube.

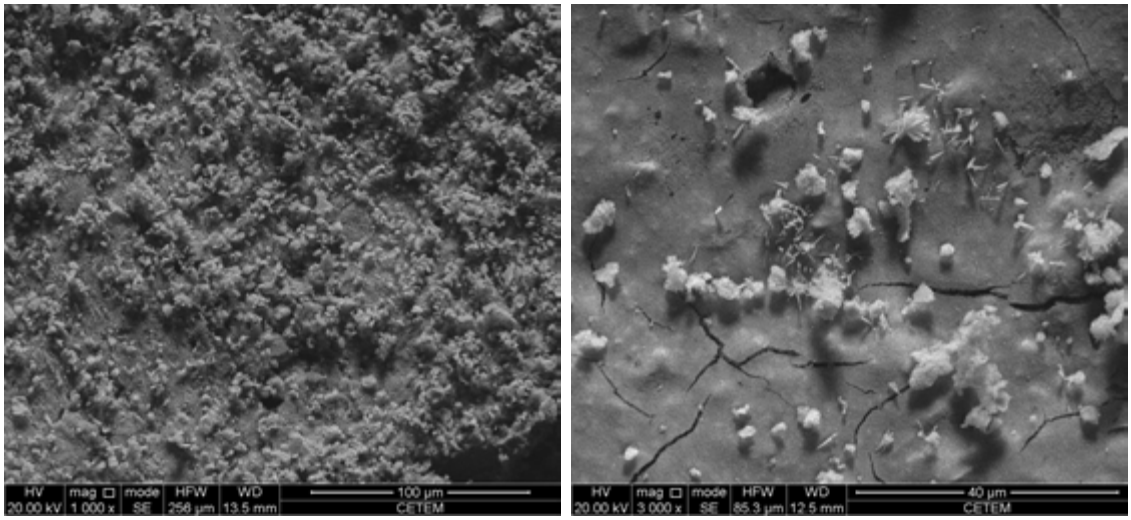

a) b)

Figure 3.13: a)View of the concrete dried at 110 °C and then burned at 600°C; b) Closer look at the matrix shows needles of the C_2AH_8.

Chapter 4

Experimental Procedure

The aim of this study is to better understand the creep behaviour for the application of refractory concrete in UFCC. For this, it was proposed to perform creep tests in compression, tension and flexure. For technical reasons, only compression creep tests at 600°C were carried out. Figure 4.1 presents a resume of the methodology of this work.

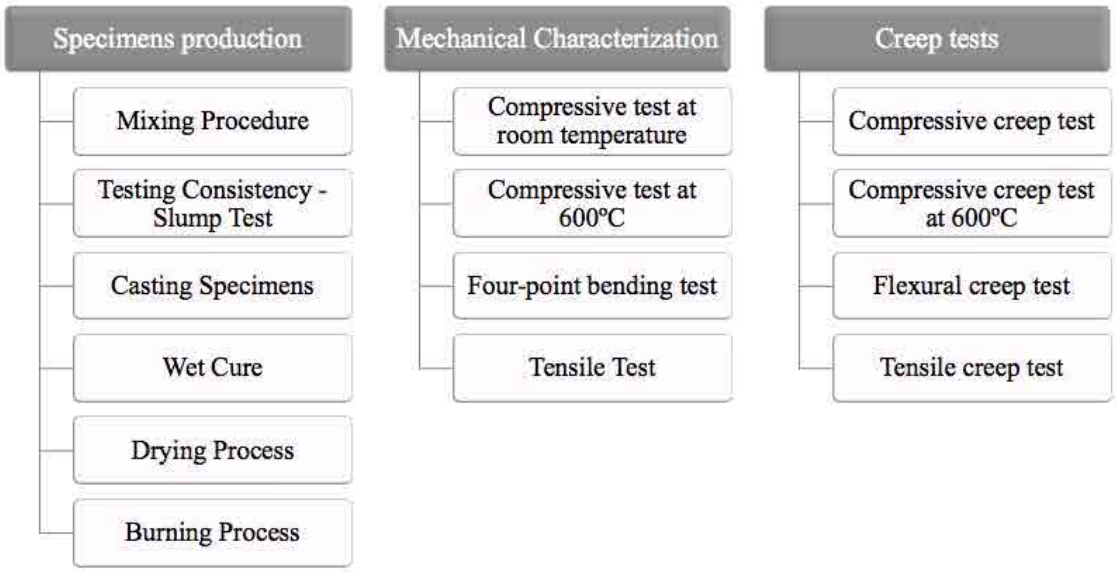

Figure 4.1: Resume of all mechanical tests and preparation of the specimens.

Table 4.1 presents the combinations according to the temperature treatment, concrete constitution and mechanical solicitation. These combinations were used in creep tests and in mechanical test. In order to perform creep tests it was necessary to define the load to be applied and maintained for a certain time. The name BCAST refers to the refractory matrix used together with a percentage of 6% in mass of stainless corrugated steel fibre reinforcement when appropriate. The term

dried refers to the drying process carried out at 110°C, which will be explained in further sections.

Table 4.1: Resume of the creep tests carried out and conditions of each test.

Creep tests	Conditions and type of the concrete	
Compression at room temperature	BCAST 0% of steel fibres dried at 110°C	B110-0F
	BCAST 0% of steel fibres dried at 110°and burned at 600°C	B600-0F
	BCAST 6% of steel fibres dried at 110°C	B110-6F
	BCAST 6% of steel fibres dried at 110°and burned at 600°C	B600-6F
Compression at high temperature	BCAST 0% of steel fibres dried at 110°C with creep test performed at 600°C	BQ600-0F
	BCAST 6% of steel fibres dried at 110°C with creep test performed at 600°C	BQ600-6F
Flexure	BCAST 0% of steel fibres dried at 110°C	B110-0F
	BCAST 0% of steel fibres dried at 110°and burned at 600°C	B600-0F
	BCAST 6% of steel dried at 110°C	B110-6F
	BCAST 6% of steel fibres dried at 110°and burned at 600°C	B600-6F
Tensile	BCAST 0% of steel fibres dried at 110°and burned at 600°C	B600-0F
	BCAST 6% of steel fibres dried at 110°C	B110-6F
	BCAST 6% of steel fibres dried at 110°and burned at 600°C	B600-6F

4.1 Specimen production

The specimens' shapes chosen for this research are illustrated in Figure 4.2. For compressive tests a cylinder shape was used (Figure 4.2 a), for tensile tests a dog bone shape was chosen(Figure 4.2 b) and for flexure tests a prismatic shape with a square cross section was used(Figure 4.2 c).

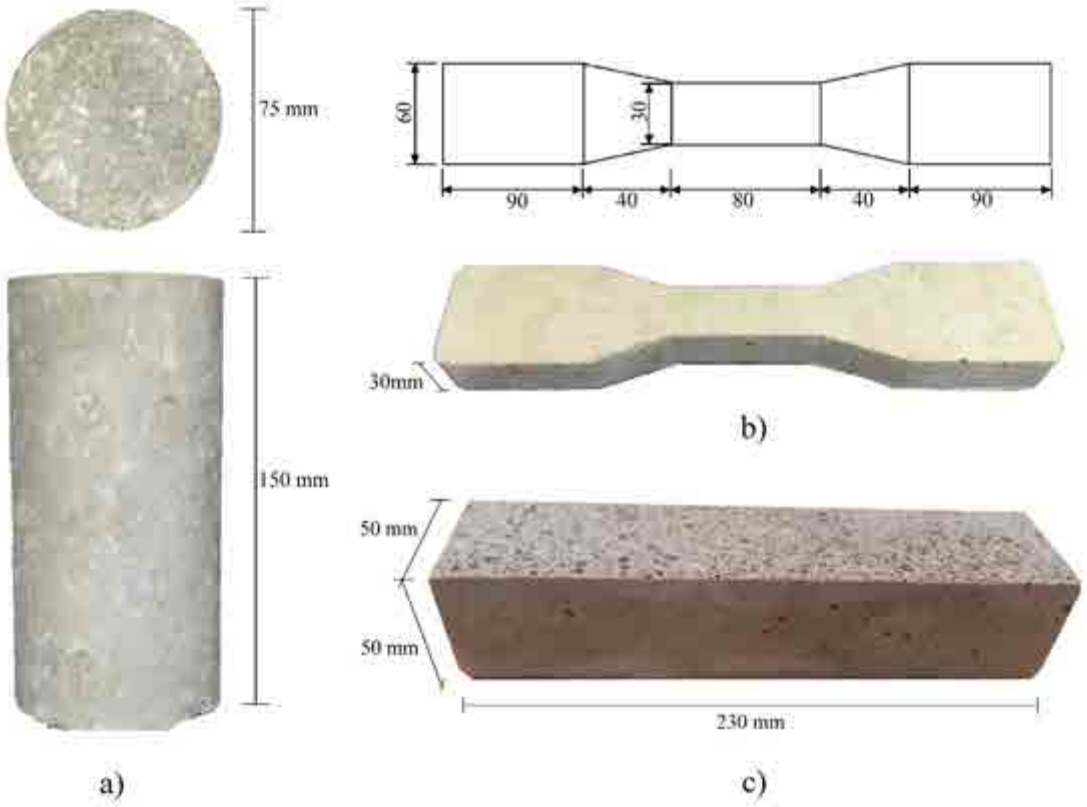

Figure 4.2: a) Compression specimen; b) Tensile specimen c) Flexure specimen.

4.1.1 Mixing Procedure

The concrete was produced at room temperature of 21°C ± 1°C, in a vertical planetary mixer, shown in Figure 4.3 a and b, with a capacity of 100 litre. To homogenize the concrete water was added with a percentage of 7.6%. For matrices without reinforcement the concrete was stirred without water for 1 minute, then water was added during 1 minute, and then the concrete was mixed for 10 minutes more. For matrices with fibre reinforcement the concrete was stirred for 1 minute then water was added for 1 minute. After adding the fibre for 1 min, the content was mixed for 9 minutes more. After the concrete was mixed, the slump test (described bellow) was carried out, and then the concrete was poured into the moulds, shown in Figure 4.3 c, vibrated with a frequency of 68 Hz for concrete consolidation for a brief period of 20 seconds as the matrix was of self-consolidating concrete not needing a long vibration time.

(a) (b) (c)

Figure 4.3: a) Concrete being mixed; b) Vertical planetary mixer; c) Moulds on the vibration table, before pouring the concrete.

4.1.2 Slump test

After mixing the concrete, the slump test was carried out. In this test, the concrete was placed in the inverted Abram's cone in three layers, each layer is compacted with 25 hits with a steel bar. After, the cone was removed and the concrete was allowed to spread on a metallic plate. The maximum diameters of the concrete after spreading were measured. Two measurements were evaluated, orthogonal to each other, as illustrated in Figure 4.4. The main reasons for performing this test on self compacting concrete are: to analyse the capacity of the concrete to flow without separating and to observe the homogeneity and exudation of the material.

Figure 4.4: Inverted slump test procedure.

4.1.3 Wet Cure

Posterior to the mixing procedure, the specimens inside the moulds, were placed in an environment with high humidity of around 100%, allowing the concrete to

set. After setting, the wet cure was carried out, by removing the specimens from the moulds then placing them in a moist chamber for 24 hours, at temperature of around 21°C, and humidity of around 100%. Before being subjected to the drying process, compression and flexure specimens had their surface smoothed by means of a lathe and mechanical saw respectively to avoid stress concentration that could lead to a premature rupture and produce poor results.

4.1.4 Drying Process

After the wet cure, the specimens were moved to the kiln shown in Figure 4.5 a, and then subjected to a low heating rate, shown in Figure 4.5 b, of 18°C/h, until temperature of 110°C was reached. The specimens stayed in the kiln for 24 hours. Some specimens were moved to another kiln for another burning process, explained in the further section. The rest of the specimens were left in a sealed plastic box, without humidity, at room temperature of around 21°C, to cool until it was possible to handle them, which took about 3 to 4 hours.

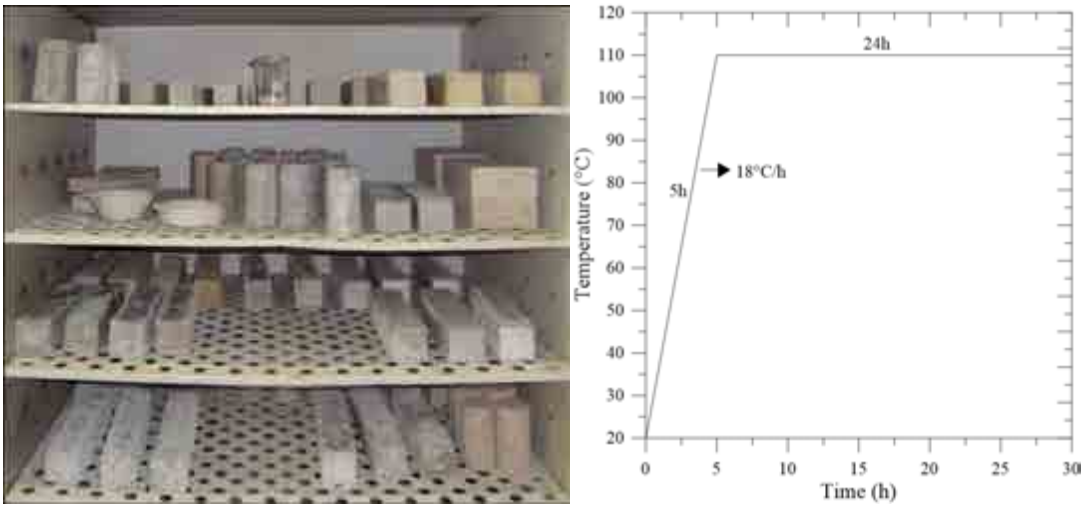

(a) (b)

Figure 4.5: a) Kiln used in the drying process; b) Heating rate for the drying process.

4.1.5 Burning Process

The burning process was carried out in a kiln shown in Figure 4.6 a, and consisted of elevating the temperature of the concrete specimens at a rate of 40°C/h until it reached 600°C, at which they were kept for 6 hours. This heating ramp is illustrated in Figure 4.6 b. After the process, the kiln was turned off and the specimens were kept there to cool. The kiln, fitted with a thermocouple stayed sealed until the

temperature inside reached 100°C. When the specimens were taken out of the kiln, they were placed in an plastic box without humidity and left there to cool until they reached room temperature and could be handled.

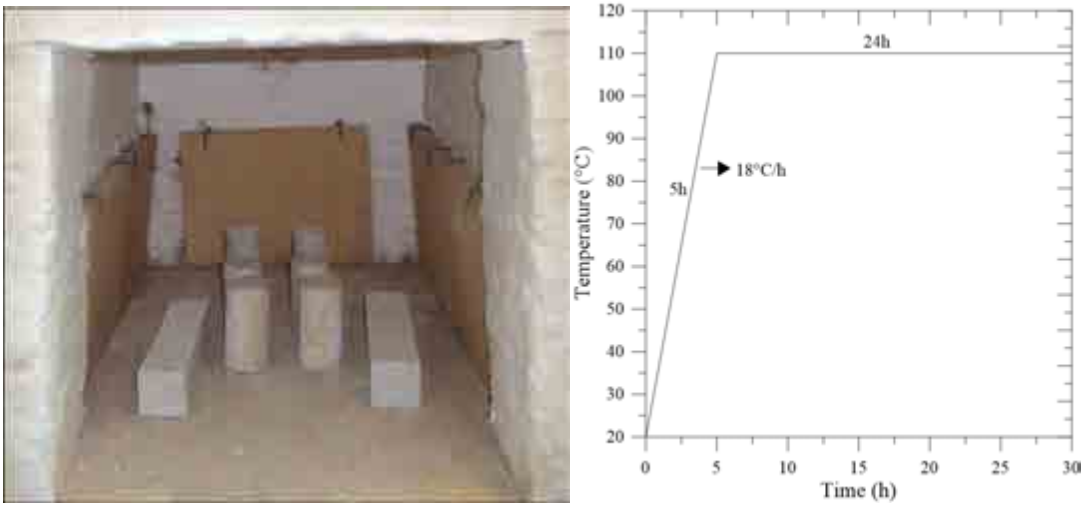

(a) (b)

Figure 4.6: a) Kiln for the burning process; b) Heating rate for the burning process.

4.2 Compressive test at room temperature (22°C)

Compressive tests at room temperature were carried out following the Brazilian Standard NBR-11222 (2010). Using a computerized servo-hydraulic press, of the model *SHIMADZU UH-F*, with the load capacity of 1000kN, and with a load speed of 0.1 mm/min.

Coupled with this machine, was a data acquisition system, ADS 2000 of the brand *Lynx*. This system was connected to two linear variable differential transformers (LVDTs) of the model DTH-A 5mm, made by the company Kyowa, that can capture with $< \pm 1\%$ F.S. accuracy the deformations of each test. This transformers were positioned in a way that the length l_0 was of 100 mm. The system is shown in Figure 4.7.

Figure 4.7: Compression test with LVDT attached.

4.3 Compressive test at 600°C

Compressive tests at 600°C were carried out in the hydraulic press *SHIMADZU EH-FM300K1-070-0A*, with a load capacity of 300kN. This press had a kiln attached, shown in Figure 4.8, together with a temperature controller that adjusted the temperature and heating rate. The data acquisition system ADS 2000 of the brand *Lynx* was used in combination with linear variable differential transducers (LVDT) made by the company RDPE, model LIN 56, resistant to high temperature. According to the manufacturer its working temperature can vary from -220°C to 600°C. Before starting the tests the LVDT were calibrated at 600°C, to calculate the constant that converts voltage to displacement. The load speed used in the tests was of 0.1 mm/min.

4.4 Four-point bending test

The tests were carried out in the *SHIMADZU EH-FM300K1-070-0A*, following the Brazilian Standard NBR-11222 (2010). The lower span used was of 180 mm, and upper span 60 mm, respecting the relation of 1/3 of higher and lower span recommended by the Brazilian Standard NBR-2142 (2012). The load velocity was of 0.1 mm/min. The acquisition system ADS 2000 of brand *Lynx* was used with one LVDT attached to measure the displacement in the center of the sample. The test set up is shown in Figure 4.9.

The modulus of rupture (MOR), also known as flexural strength, was measured by the equation 4.1 used for the four point bending condition.

Figure 4.8: Press *SHIMADZU EH-FM300K1-070-0A*, showing the kiln and the test set up apparatus.

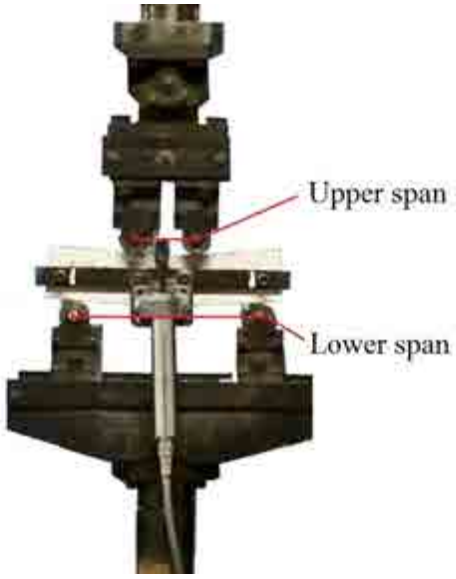

Figure 4.9: *SHIMADZU EH-FM300K1-070-0A*, with four-point bending test.

$$MOR(MPa) = \frac{3 \cdot P_{max} \cdot a}{b \cdot h^2} \tag{4.1}$$

where P represents the load (N); a the distance between the upper span, in this case 60 mm; b is the width of the cross section and h is the height of the cross section. A square section was used so b and h were equal to 50 mm.

4.5 Tensile test

The tensile test was performed in the press *SHUMADZU* model AG-X, with a load capacity of 100 kN and load speed of 0.1 mm/min. Coupled with this machine, was a data acquisition system, ADS 2000 of the brand *Lynx* with two LVDTs. This transformers were positioned in a way that the length l_0 was 100 mm. The set up is illustrated in Figure 4.10.

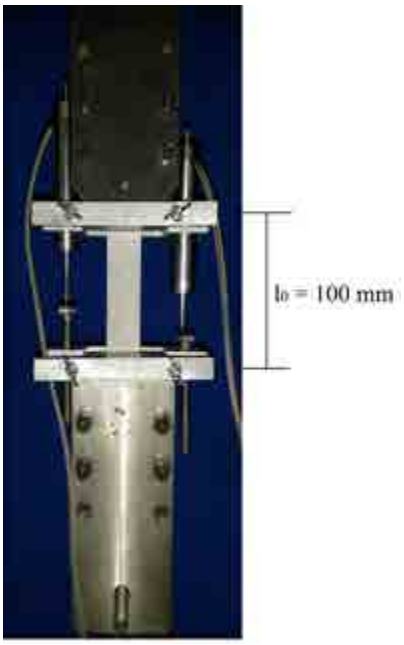

Figure 4.10: *SHUMADZU* model AG-X, with tensile test.

4.6 Creep tests

The creep tests at room temperature were carried out in a controlled environment with a constant temperature of 21°C ± 2°. The ambient temperature was recorded by two thermocouples linked to the acquisition system. Two specimens were tested for each combination described above in Table 4.1.

According to BAZANT and KAPLAN (1996), refractory concrete after exposed to a high temperature and than cooled to room temperature presents no significant shrinkage, due to the permanent deformation that had already occurred during the heating process. For this reason, shrinkage was not measured in this work.

The creep displacements were recorded by a data acquisition system, which consisted of an electrical supply, linear variable differential transducers (LVDTs), data acquisition machinery and software, shown in Figure4.11 a. The electrical

supply from the company *Minipa* model MPL-3305M, that supplied the linear variable differential transducers (LVDTs) with electricity (Figures 4.11 b and 4.11 c). The voltage varied linearly as the linear transducers modified the cursor with displacement. The data acquisition machinery, made by the company Agilent, model LXI 34972A (Figure 4.11 d), registered voltage and kept recording it through time. This machine came with a software of the same company (Figure 4.11 e), that allowed to set the rate of data acquisition and save the data. It was possible to record the voltage for a considerable time. However, the data was still measured as voltage and to convert it into displacement, a calibration was performed to convert volts into millimetre.

The transducers used for all creep tests at room temperature were of model DTH-A-5, *Kyowa*, with a range of 5 mm, shown in Figure 4.11 b. For tests at high temperature, LVDTs that could resist to temperatures varying from -220°C to 600°C, of model LIN 56, company RDPE were used shown in Figure4.11 b. The calibration of this LVDT was done at 600°C since the constant between voltage and displacement varied with temperature. The scheme used in data acquisition is illustrated in Figure4.11.

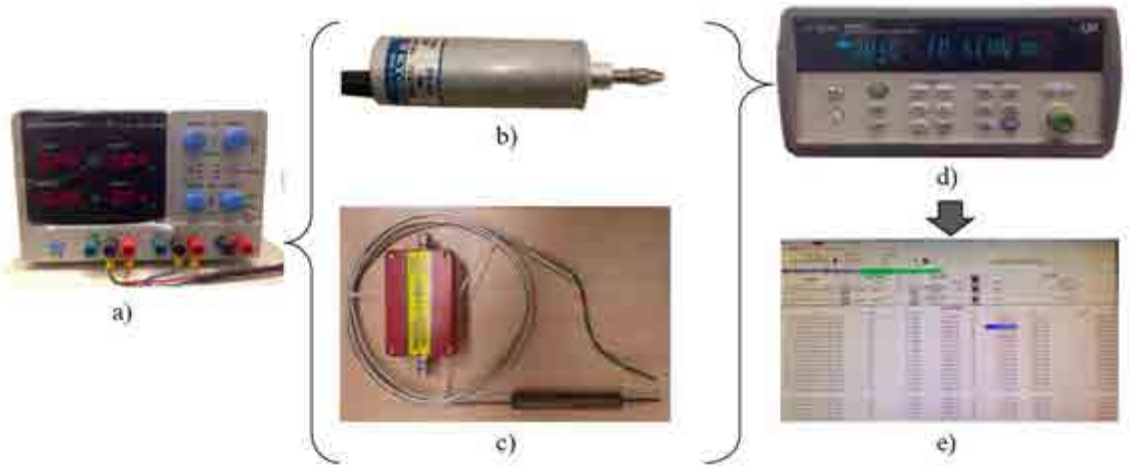

Figure 4.11: a) Font Minipa MPL-3305M; b) LVDT Kyowa DTH-A-5 used for room temperature tests; c) LVDT LIN56 of RDPE, used in high temperature tests; d) Agilent equipment aquisitor LXI 34972A; e) Acquisition software.

For all creep tests the data was measured, with the rate of:

- 10 seconds during loading;
- 1 minute for the first week;
- 5 minutes for the rest of the 3 months.

4.6.1 Compressive creep test at room temperature

The creep rig for the compression creep test is illustrated in Figure 4.12. For this test, the samples were subjected to the thermal processes, and then cooled as described before, until they could be handled.

After cooling the samples were taken out of the box and first sealed with three layers of cling film (PVC) and then additionally covered with two layers of conductive aluminium foil tape. This procedure was indicated by SILVA (2007) to prevent the exchange of water with the ambient.

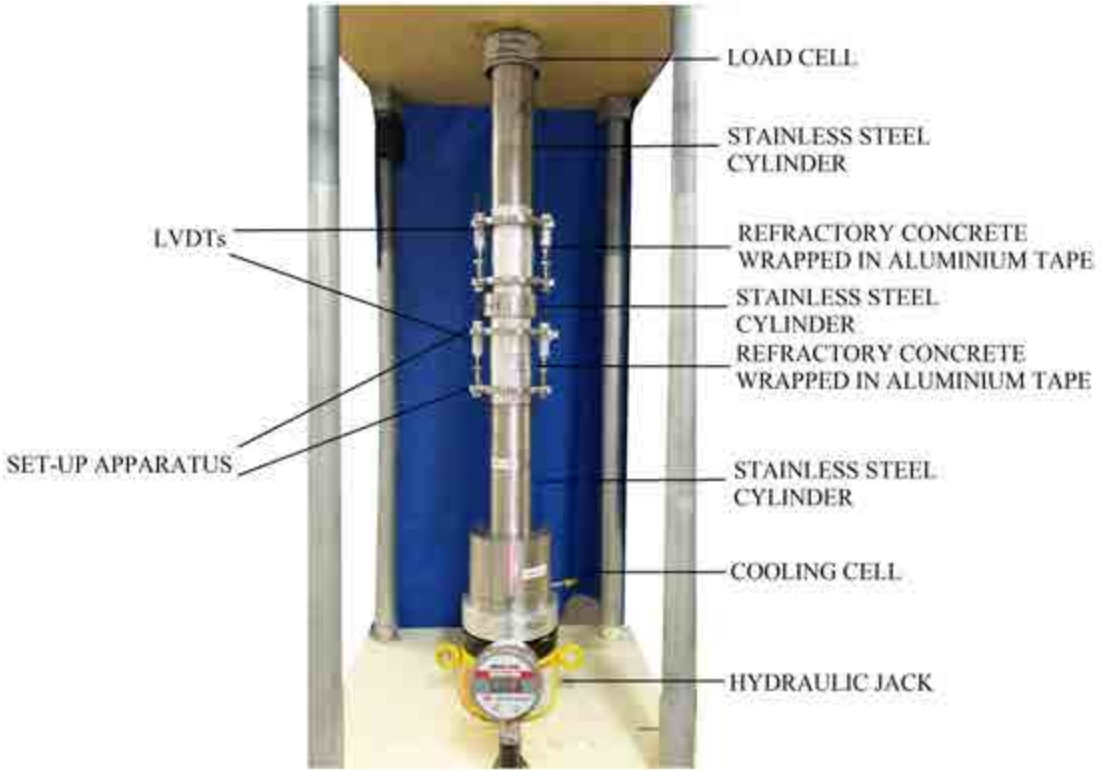

Figure 4.12: Compressive creep test at room temperature.

When all specimens were sealed, a stainless steel set-up apparatus was placed around each specimen, so that the LVDTs could be attached at a later stage to measure the displacement.

Components shown in Figure 4.12 were positioned one by one. And aligned with laser beam and bubble level in two directions, in a way that all pieces were centred and there was no eccentricity. After the creep rig was set up, the linear variable transducers were placed into the stainless steel set up apparatus.

The 40% of the maximum load obtained in the mechanical test was applied by a hydraulic system, for each combination. The hydraulic jack in the Figure 4.12 pushed the creep rig and applied pressure onto the system. The pressure was

measured by a manometer. The correlation between load and pressure was obtained before by a calibration using a load cell and the creep rig.

4.6.2 Compressive creep test at 600°C

The equipment, especially designed used for compressive creep at 600°C is shown in Figure 4.13. It consists of: cooling cells; a kiln; hydraulic system and stainless steel cylinder.

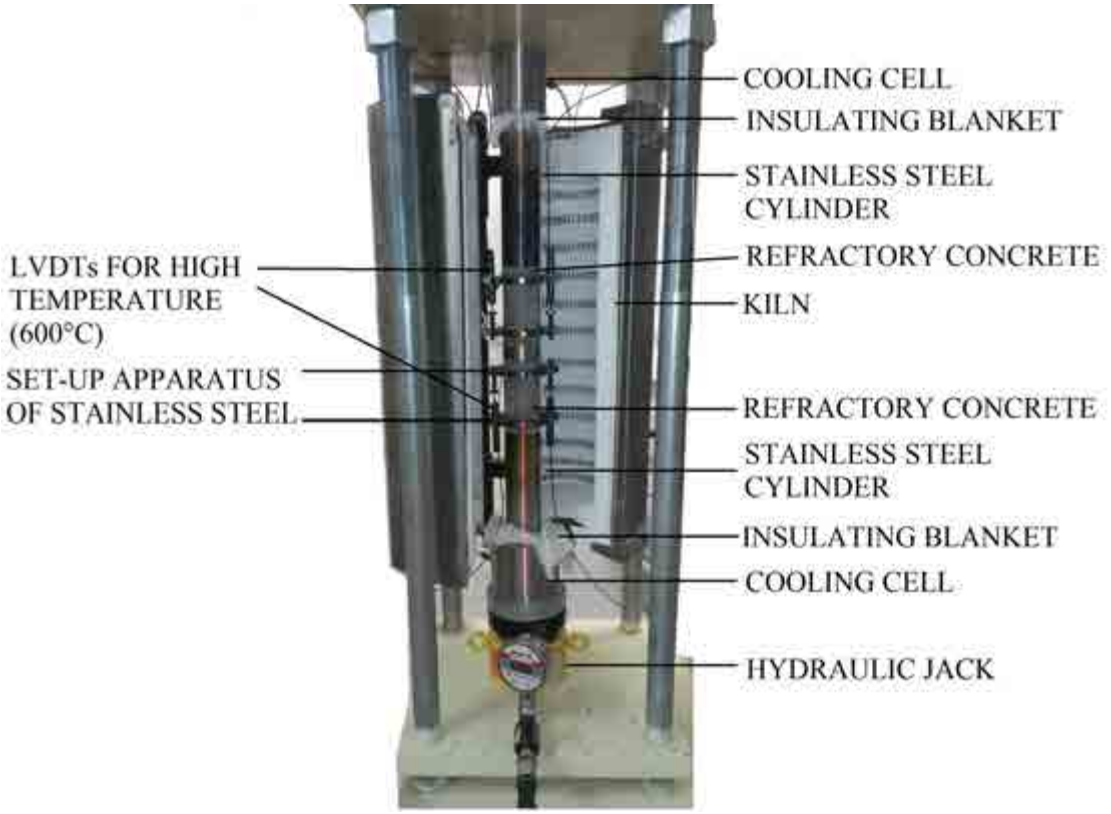

Figure 4.13: Compressive creep test at 600°C apparatus.

The specimens were subjected to the drying process and allowed to cool in a plastic box at room temperature, that isolated them from humidity. They were kept there until it was possible to handle them at around 40°C. In the mean while, the hydraulic jack, the first cooling cell, a layer of insulating membrane and a stainless steel cylinder were positioned in the center of the portico. The pieces were centralised using bubble level and laser beam.

When cool enough each concrete specimen was fitted with a set up apparatus to fix later the LVDTs, of which 2 were used for each specimen. After that, the other pieces of the system were placed and centred, following the order: the first concrete specimen, a second and smaller stainless steel cylinder, the second concrete specimen, a stainless steel cylinder, a layer of insulating blanket and cooling cell.

Both cooling cells were placed next to the kiln, and constantly refrigerated by water, which circulated inside them and which in turn was cooled by another equipment. The insulating blanket was placed to reduce the heat exchange between cooling cell and kiln.

When all pieces were centred and aligned, the LVDTs were placed into position, the data acquisition system was turned on, the kiln was closed and turned on. The kiln was made of glass wool with electrical resistances attached. The glass wool is an excellent isolation material, so that no excessive heat was released into the ambient. The same heat rate as for the burning process was used as already shown in Figure 4.6 b). Heating increased at the rate of 40°C, until it reached 600°C. It remained at this temperature for six hours. In this process a gap left on top of the appliance allowed all pieces to dilate.

There were thermocouples inside the kiln that measured the temperature close to the specimens and a controller panel activated the resistance when temperature decreased with time. Only after six hour at temperature of 600°C, 40% of the maximum load, calculated in the compression mechanical tests, was applied by a hydraulic jack. This load and the temperature of 600°C were kept constant for 15 days.

The period of this test was shorter than that of the other creep tests, because it was observed in the other tests that creep deformation for this refractory concrete reaches a secondary state within 10 to 20 days, at most. Since this tests were expensive and difficult to carry out, they were observed day by day, and when the concrete stabilized the creep deformation the tests were stopped and unloaded. The recovery was measured also until stabilization.

4.6.3 Flexural creep test

For flexural creep tests, the equipment shown in Figure 4.14 was used. A four point bending test configuration was carried out, where the upper span was of 6 centimetres and the lower span of 18 centimetres.

First, all specimens were subjected to temperature treatments and allowed to cool down in a plastic box. When temperature reached around 40°C, the specimens were wrapped first with three layers of plastic film and then with two layers of metallic tape. After that, the positions were marked where the cylindrical bearings and set up apparatus would be placed.

Then, the set-up apparatus and the LVDTs were fixed to the specimens. Two linear transducers were attached to each specimen in order to measure the maximum

(a) (b)

Figure 4.14: a) Flexural creep tests; b) Flexure creep rig.

deflection, as shown in Figure 4.14 b. After all specimens were placed and centred in each creep rig, load was applied to each one in form of a metallic dead weight. 40% of the first crack load was placed relative to each mechanical bending test done previously.

During loading, the displacement and the time during application of the load was measured. The time of each type of concrete is presented in Table 4.2. The creep curves during loading are plotted in Figure 4.15. The displacement measured after placing the load was the one considered in the calculation of the elastic deformation.

Table 4.2: Time while loading each type of concrete in flexure.

Type of concrete	Time loading
B110-0F	11 min
B600-0F	10 min 20 sec
B110-6F	6 min 50 sec
B600-6F	7 min 30 sec

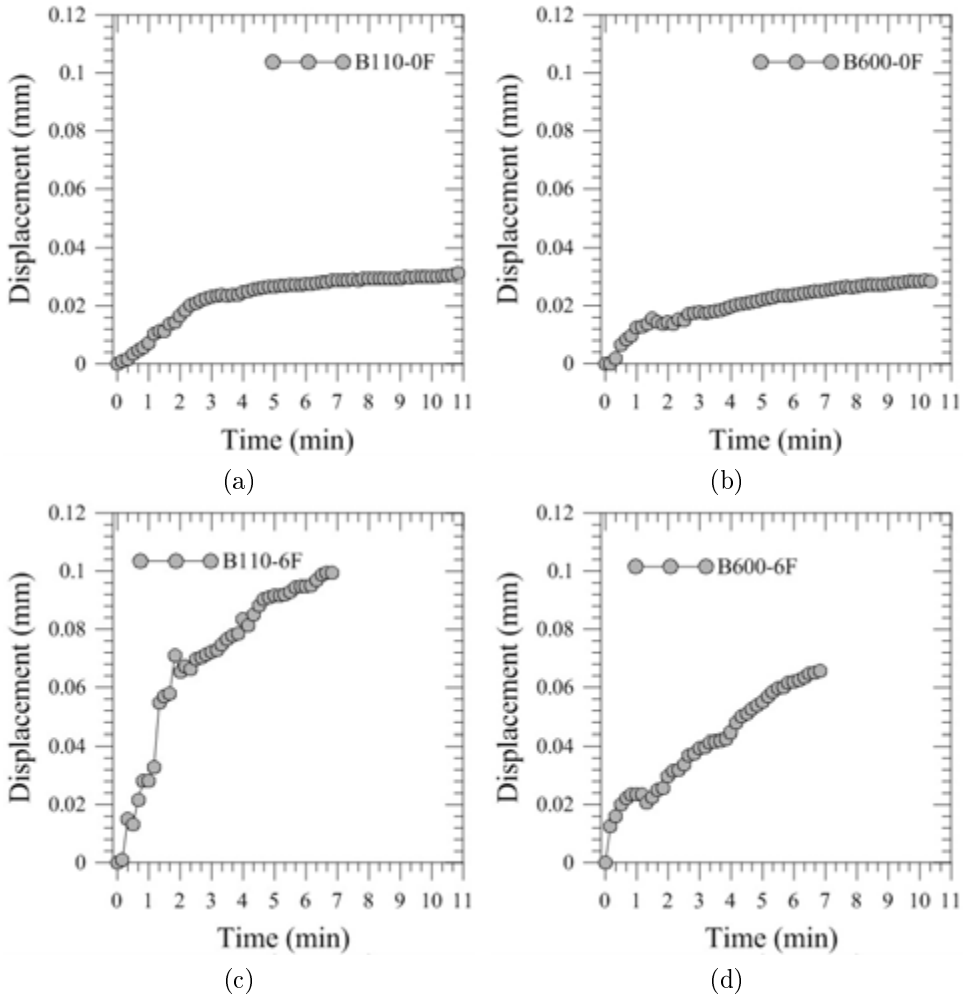

Figure 4.15: Flexure creep curves during loading for matrix type: a) subjected only to the drying process; b) subjected to the burning process at 600°C; c) with fibre reinforcement subjected only to the drying process; d) with fibre reinforcement subjected to the burning process at 600°C.

4.6.4 Tensile creep test

For tensile creep tests, the equipment shown in Figure 4.16 a was used. This leaver apparatus was calibrated before the creep tests in order to determine the real load applied.

(a)

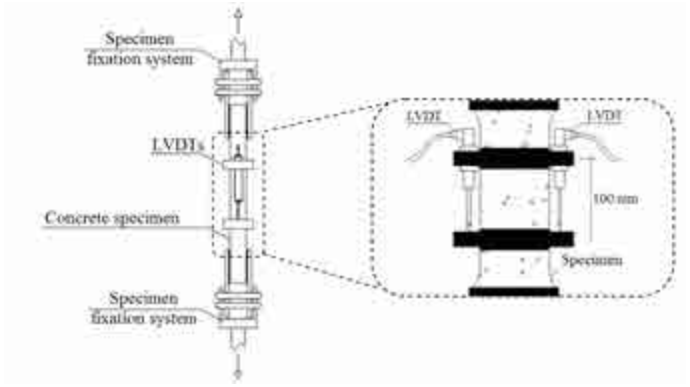

(b)

Figure 4.16: a) Tensile creep test; b) Scheme of the tensile creep test. Font: RAMBO (2012).

First, all the specimens were subjected to temperature treatments and allowed to cool down in a plastic box. When temperature reached around 40°C, the specimens were wrapped with three layers of plastic film and also with two layers of metallic tape. After that, the positions were marked where the set up apparatus was to be attached as illustrated in Figure 4.16 b. When all specimens were positioned in the tensile creep rig, the LVDTs were fixed to the specimens. Two linear transducers were attached to each specimen in order to measure the displacements, as shown in Figure 4.16 b. The data acquisition system was started and each one was loaded with metallic dead weight. 40% of the first crack load was placed relative to each

mechanical tensile test done previously. The time of each load specimen is presented in Table 4.3.

During loading, the displacement and the time during application of the load was measured. The time of each type of concrete is presented in Table 4.2. The creep curves during loading are plotted in Figure 4.17. The strain measured after placing the load was considered as elastic deformation.

Table 4.3: Time while loading each type of concrete for tensile tests.

Type of concrete	Time loading
B600-0F	3 min 40 sec
B110-6F	4 min 10 sec
B600-6F	10 min 20 sec

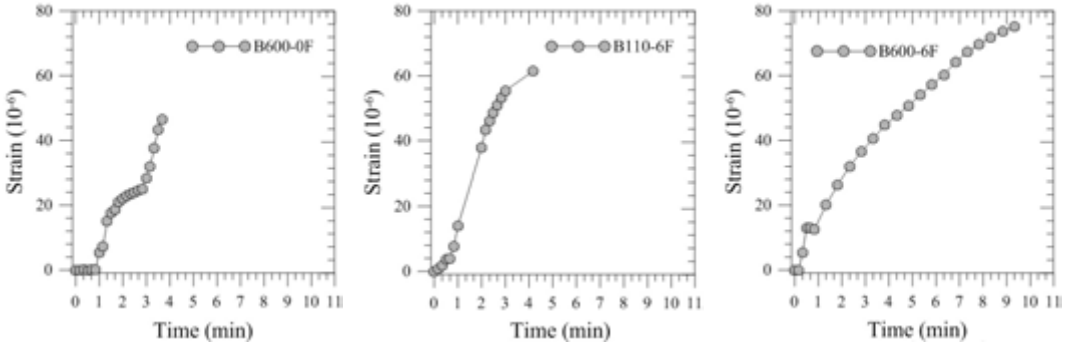

Figure 4.17: Tensile creep curves during loading for matrix type: a) subjected to the burning process at 600°C; b) with fibre reinforcement subjected only to the drying process; c) with fibre reinforcement subjected to the burning process at 600°C.

Chapter 5

Results and Discussions

5.1 Compressive tests

The compression stress x strain curves for concretes without reinforcement are presented in Figure 5.1. Along with the compression stress x strain curves for the concrete with 6% of fibre reinforcement are presented in Figure 5.2.

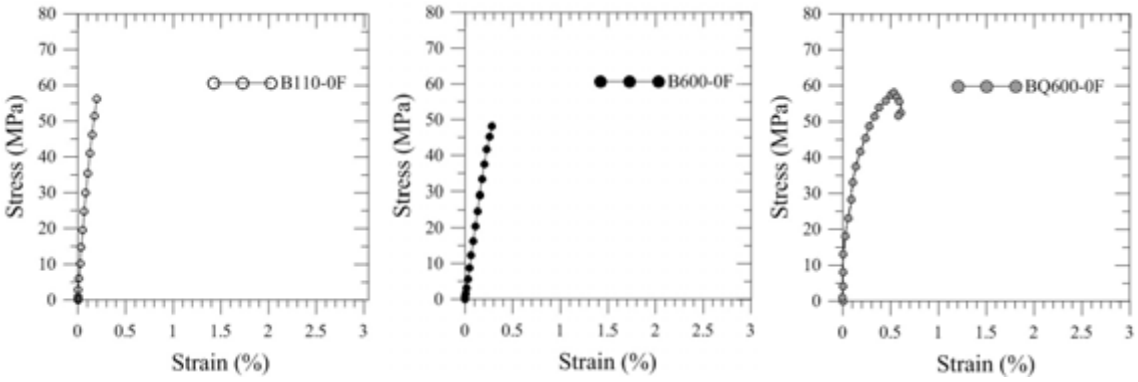

(a) (b) (c)

Figure 5.1: Compression stress x strain curves of the matrix: a) subjected only to the drying process; b) subjecting to the burning process at 600°C and then tested at room temperature; c) tested at hot stage (600°C).

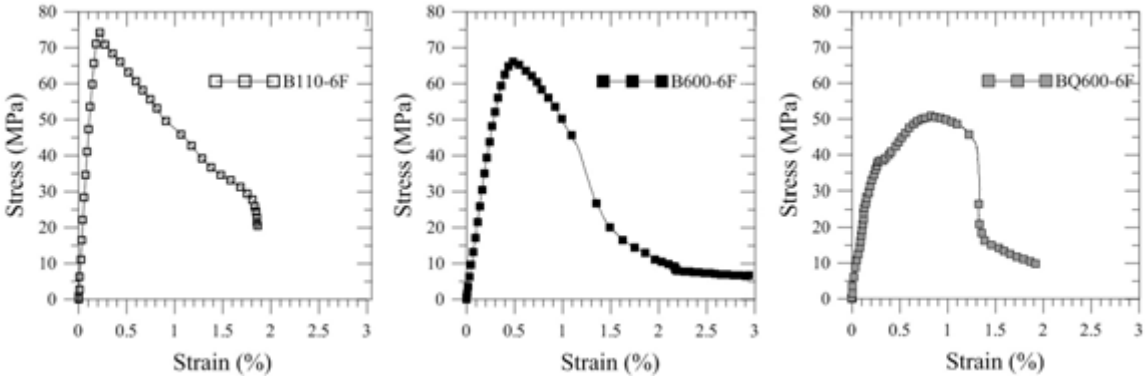

(a) (b) (c)

Figure 5.2: Compression stress x strain curves of the matrix with reinforcement: a) subjected only to the drying process; b) subjecting to the burning process at 600°C and then tested at room temperature; c) tested at hot stage (600°C).

From the compressive stress x strain curves the compressive strength and Young's modulus were obtained for each type of concrete. This properties are presented in Figure 5.3. For all modulus calculated in this report, 40% of the maximum strength in the elastic stage was used and the same strength was applied in creep tests for each combination.

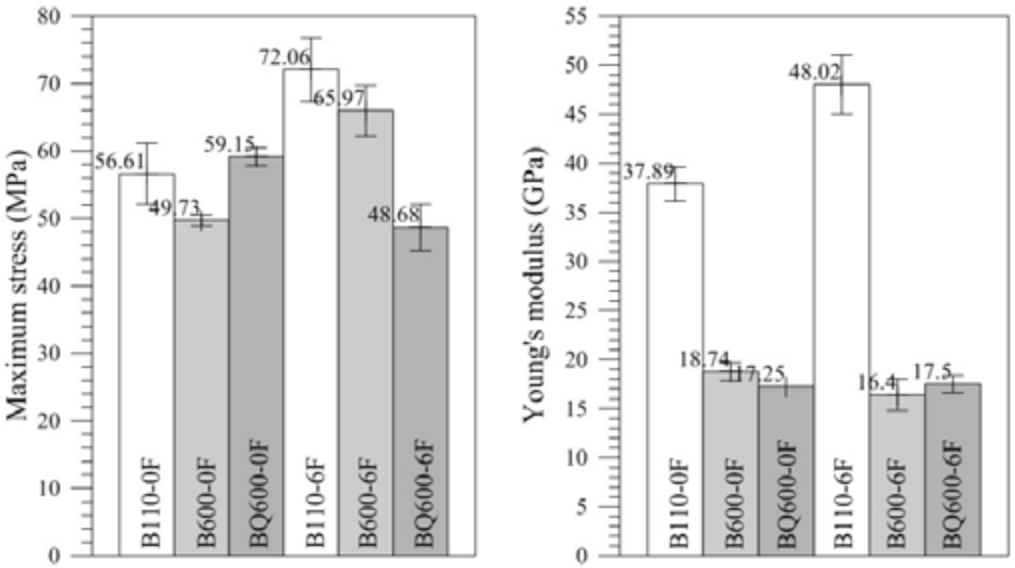

(a) (b)

Figure 5.3: a) Compression maximum strength for each type of concrete (standard deviation is shown in the bars); b) Compression Young's modulus (standard deviation is shown in the bars).

Through the results presented in Figures 5.3 and 5.1, one could observe that 12% of strength was lost when the matrix was burned up to 600°C and cooled to room

temperature. When the specimens were tested at 600°C a small strength increase of 5% was observed.

The Young's Modulus presented a more pronounced reduction when exposed to 600°C. Comparing the results obtained for matrix the loss of stiffness was about 50%. When comparing B110-0F to B600-0F the reduction was slightly higher (55%). Similar results were obtained by MEDEIROS (2012). This might occur due to the alumina cement conversion that increased the porosity of the concrete as seen in the thermogravimetric and X-ray diffraction analysis. The conversion of C_3AH_6 and AH_3, increased the porosity by about 25%.

A loss of 8% of mechanical strength was observed when the concrete with fibre reinforcement was subjected to 600°C. When comparing B110-6F to the test done at hot stage with fibre reinforcement the loss was more significant (32%).

It is important to notice that this loss was not detected in concretes without reinforcement. An hypothesis for this loss of strength can be sustained by a mismatch of the thermal expansion between the two materials. The linear thermal expansion coefficient of the steel fibre at 600°C is of 10.9 mm/m while for the refractory concrete is of 2.5 mm/m, data presented in Chapter 3. In this way, at a temperature of 600°C stainless steel dilates 4 times more than the refractory concrete, producing more pores in the matrix and therefore losing compressive strength.

The Young's Modulus for the matrix with reinforcement presented a considerable loss when exposed to 600°C. Comparing B110-6F to B600-6F and BQ600-6F, the loss was in both cases around 65%.

It was possible to notice that fibre reinforcement increased the strength of the concrete for tests performed at room temperature. When the specimens were dried and then tested the fibre reinforcement increased the compressive strength by 35%. For the matrices burned and then tested at room temperature the increase was 33% of the compressive strength. The exception was when concrete was tested at 600°C. There was a loss of strength of 16%, which could be attributed to the hypothesis previously described regarding the mismatch of the thermal expansion of the concrete and steel.

5.2 Flexural tests

Flexural tests were only carried out at room temperature for which load x displacement curves were obtained as presented in Figure 5.4.

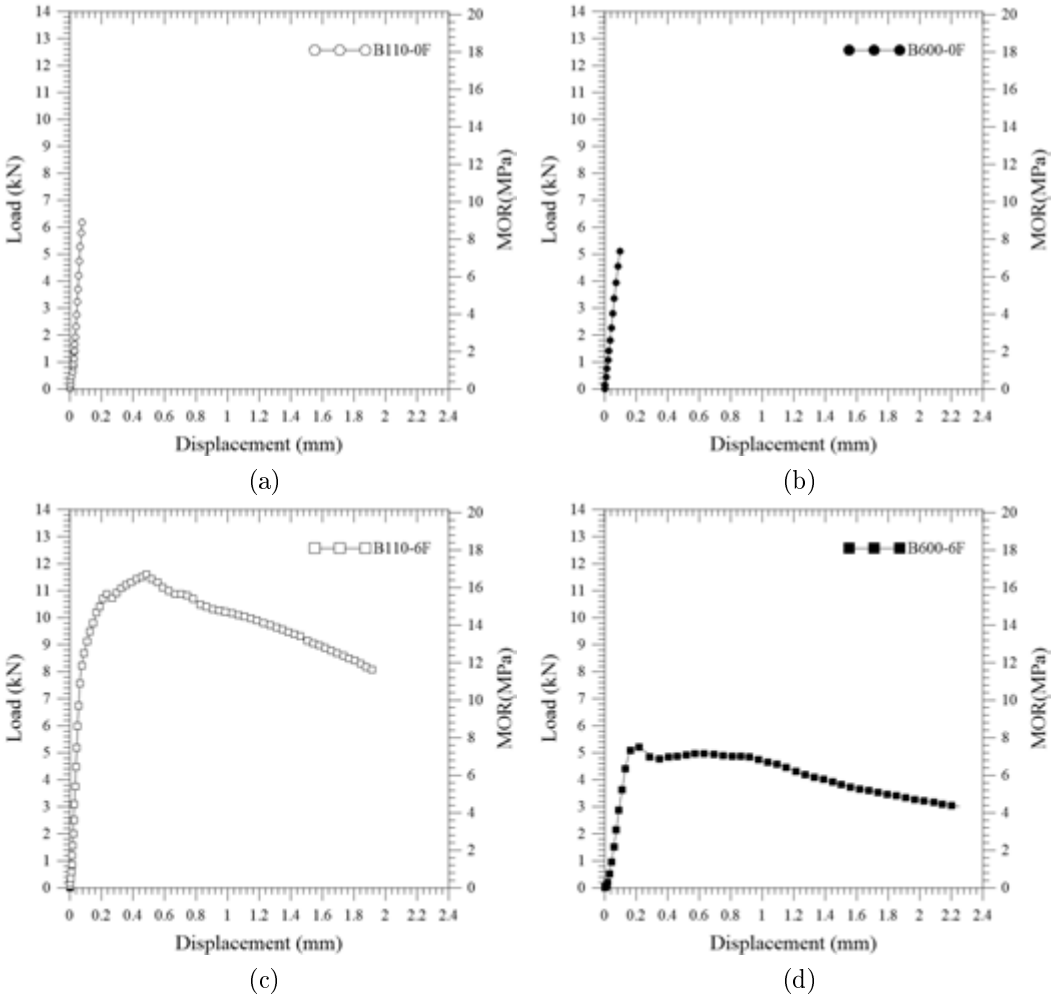

Figure 5.4: Flexure load x displacement curves of the matrix: a) subjected only to the drying process without reinforcement; b) subjected to the burning process at 600°C without reinforcement; c) subjected only to the drying process with 6% of reinforcement; d) subjected to the burning process at 600°C with 6% of reinforcement

The results of the first crack strength and Modulus of Rupture (MOR) are illustrated in Figure 5.5.

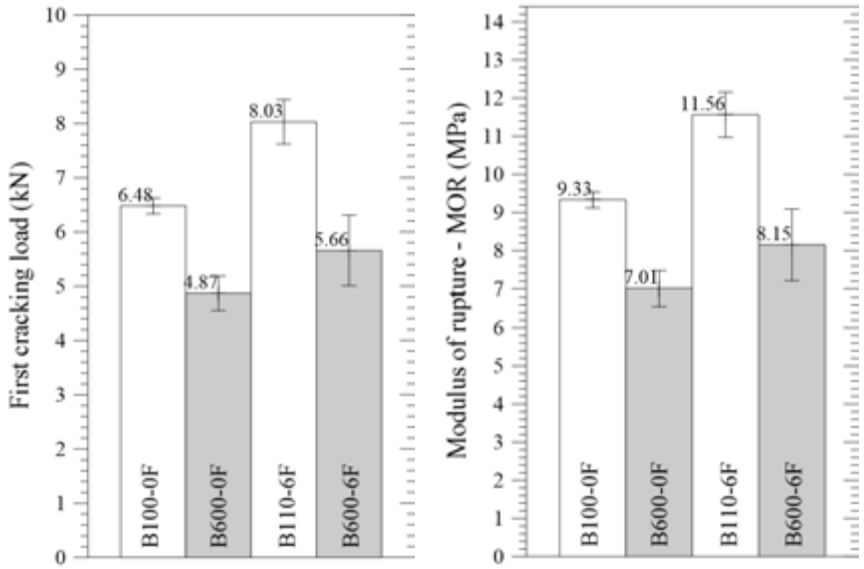

(a) (b)

Figure 5.5: a) First crack load for each type of concrete (standard deviation is shown in the bars); b) It is presented the modulus of elasticity (the standard deviation is shown in the bars).

The burning of the matrix reduced the first crack load by 24.8% and also decreased 29.8% of the modulus of elasticity. When the matrix is reinforced with steel fibre the burning process reduced by 29.5% the first cracking load. There was also a pronounced loss of stiffness of 65.8% in the modulus of elasticity.

The concretes with fibre reinforcement showed a strain hardening behaviour, enhancing the first crack load. When the only dried matrix was reinforced with steel fibre the increase of the maximum load was of 23.91%. In this case, there was also an increase in stiffness of 78.7%.

When the matrix, reinforced with fibres, was subjected to the burning process, it improved the load capacity by 16.22%. However, there was 12.9% loss of stiffness.

5.2.1 Results of tensile tests

The tensile mechanical tests were performed only at room temperature and not performed at 600°C due to limitations of the test set-up and availability of equipment. The tests at high temperatures could be suggested for further studies as additional knowledge of this subject is wanted.

For these tests tensile stress x strain curves were obtained as presented in Figure 5.6.

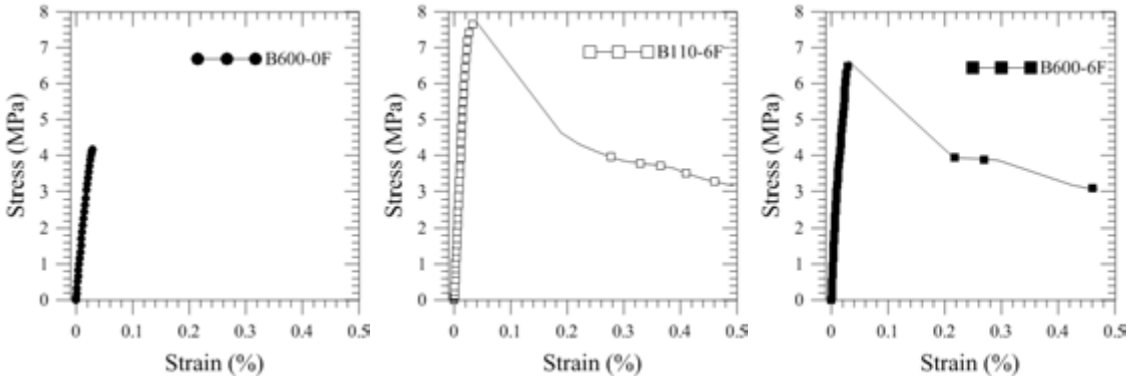

(a) (b) (c)

Figure 5.6: Tensile stress x strain curves of the matrix: a) subjected only to the drying process with 6% of reinforcement; b) subjected to the burning process at 600°C without reinforcement; c) subjected to the burning process at 600°C with 6% of reinforcement

The results of the first crack stress and Young's Modulus are illustrated in 5.7.

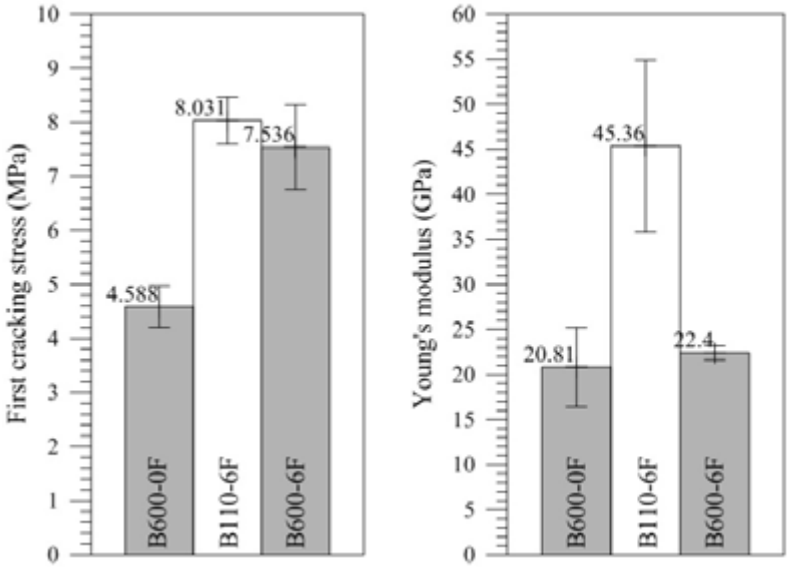

(a) (b)

Figure 5.7: a) Tensile strength for each type of concrete (standard deviation is shown in the bars); b) Tensile Young's modulus (standard deviation shown in the bars).

The curves with fibre reinforcement presented a strain softening behaviour. By observing the curves with fibre reinforcement, it is possible to notice that burning decreased the tensile strength by 6%.

Fibre reinforcement enhanced the first crack strength. When comparing B600-0F to B600-6F the increase was of 40%. However, it was not possible to make more correlations regarding the matrix without reinforcement due to the lack of

information for type B110-0F. Initially, the tensile test of the type B110-0F was performed, but the results were inconclusive for this type of concrete.

The burning decreased the Young's modulus. Correlating the matrices with fibre reinforcement the burning decreased the stiffness by about 51%. With regards to burned concretes it was noted that the fibre reinforcement had no significant effect on the Youngs modulus.

5.3 Conclusions of Mechanical Tests

It was observed for the compression, tensile and bending that:

- In tests performed at room temperature all strength was reduced after the burning process.
- The Young's modulus also decreased with the burning process.
- For the compressive tests performed at 600°C, strength and modulus were similar to the ones subjected to the burning and then cooled to room temperature.
- Young's modulus presented similar results in compression and tensile.

5.4 Compressive creep test

Creep curves obtained by the average of two samples for each combination are presented in Figures 5.15 and 5.9. Creep properties regarding these curves are presented in Table A.1 of the Appendix.

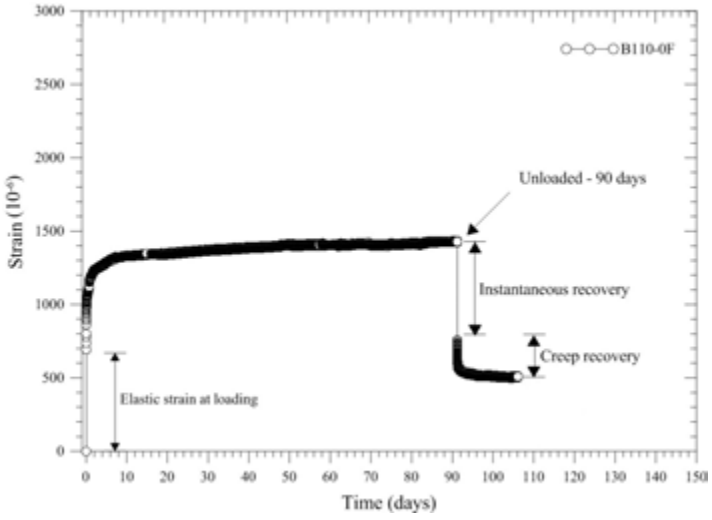

(a)

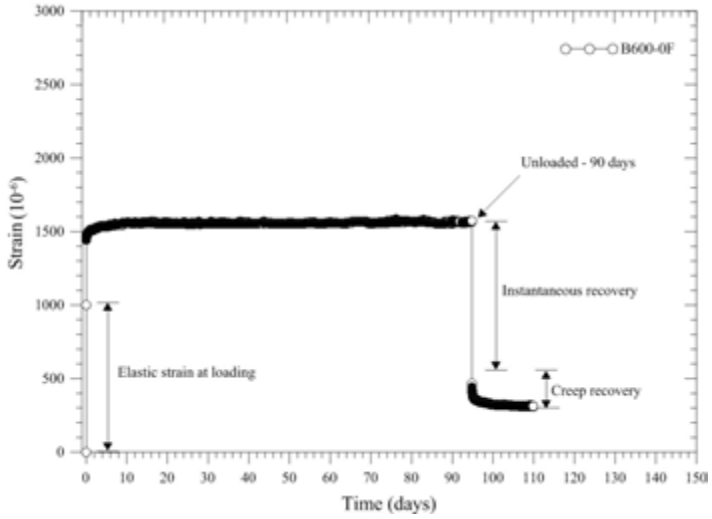

(b)

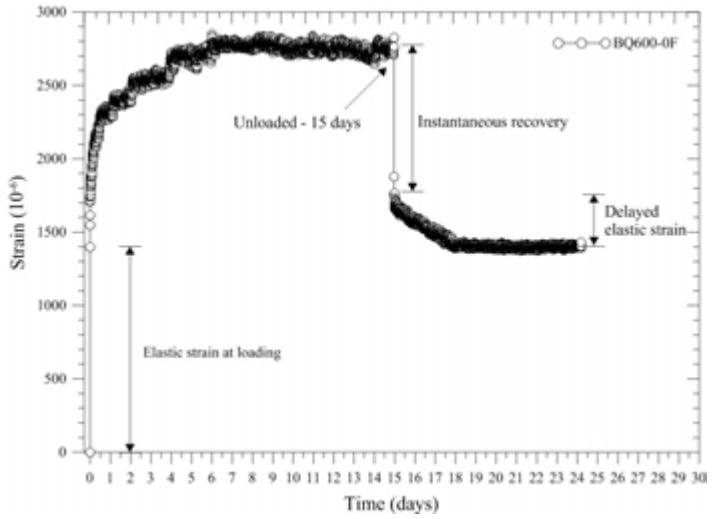

(c)

Figure 5.8: Creep curves with elastic strain for matrix: a) subjected only to the drying process; b) subjected to the burning process at 600°C and then tested at room temperature; c) tested at hot stage (600°C).

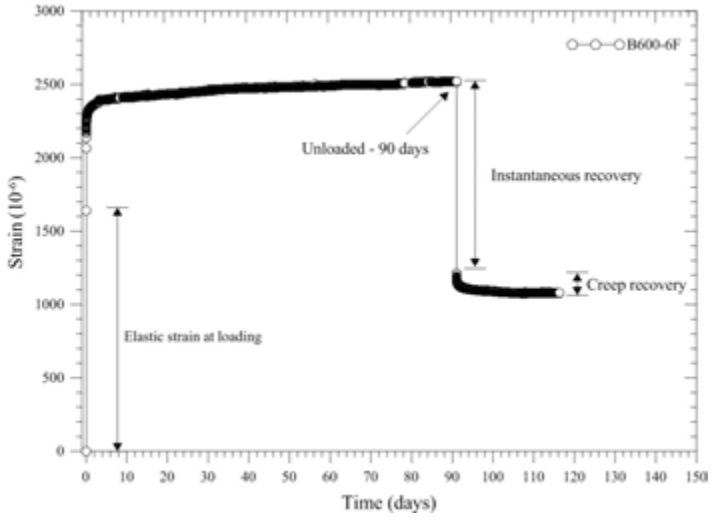

(a)

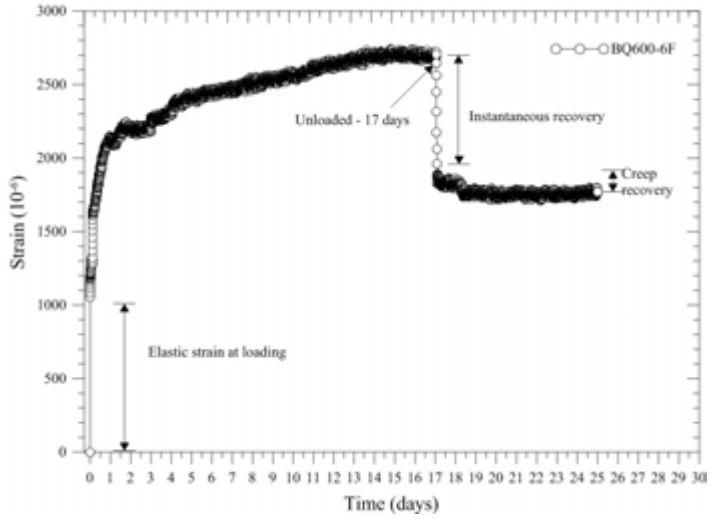

(b)

Figure 5.9: Creep curves with elastic strain for matrix with 6% of fibre reinforcement: a) subjected to the burning process at 600°C and then tested at room temperature; b) tested at hot stage (600°C).

The curves obtained presented similar results, as seen in Figures 5.15 and 5.9 where the majority of creep was obtained in the first few days. The creep deformation was more pronounced in the first hours of the test. After 24 hours there was only a modest increase in the creep slope.

The concrete reinforced with fibre and subjected only to the drying process (B110-6F) presented inconclusive results. Therefore, it was not considered in this analysis.

As shown in Figure 5.15, creep curves reached a steady state in 10, 4 and 6 days for concretes B110-0F, B600-0F and BQ600-0F respectively. Showing that after 10 days creep deformation for the matrix without reinforcement was stable and had no significant increase.

Figure 5.9 showed that creep curves reached a steady state in 2, 6 and 14 days for concretes B110-6F, B600-6F and BQ600-6F. Except for the test performed at high temperature, after 6 days, the creep deformation for the matrix with reinforcement was stable and suffered no significant increase. For the test carried out at high temperature the creep rate stabilized after 14 days. However, the increase for this concrete is still considerable.

It could be concluded, that compression creep tests for this refractory concrete could be carried out for the period of only 14 days instead of 90 days.

Because of that and in order to compare results, specific creep curves were plotted for the first 24 hours. Specific creep curves were obtained using each creep curve divided by the respective strength applied in each test. They are presented in Figure 5.10, for the plain matrix and in Figure 5.11, for the matrix with reinforcement.

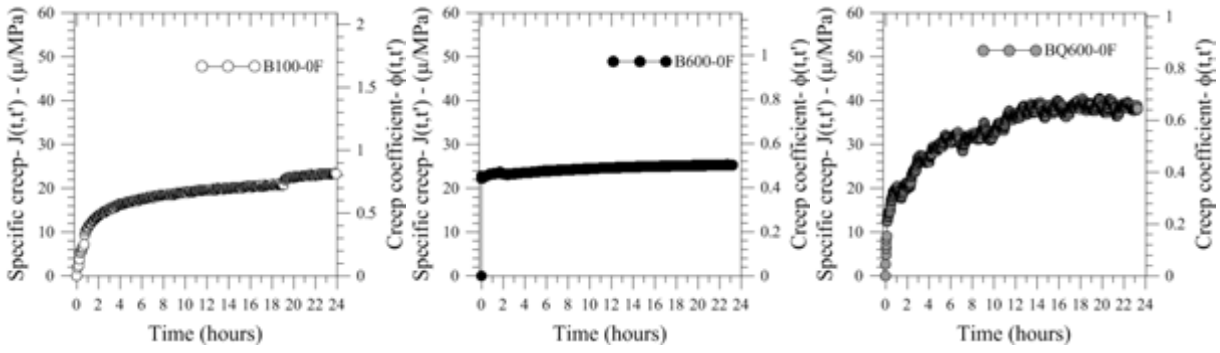

Figure 5.10: Specific creep curves without elastic strain for matrix: a) subjected only to the drying process; b) subjected to the burning process at 600°C and then tested at room temperature; c) tested at hot stage (600°C).

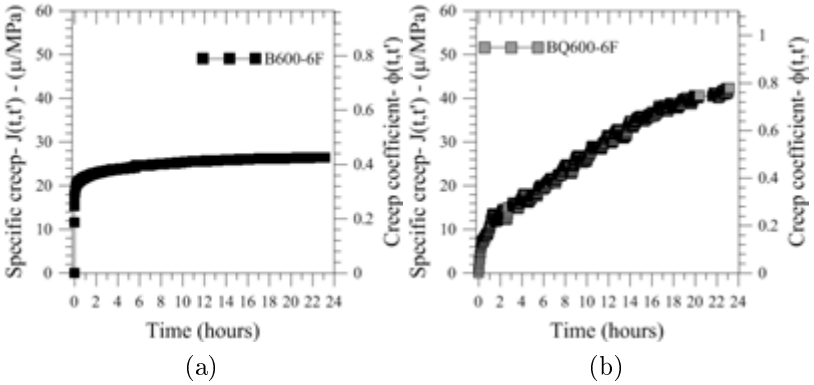

Figure 5.11: Specific creep curves without elastic strain for matrix with reinforcement: a) subjected to the burning process at 600°C and then tested at room temperature; b) tested at hot stage (600°C).

The specific elastic strain at loading, specific elastic strain at unloading, specific basic creep, specific elastic delay deformation and specific flow were obtained from the specific creep curves and presented in Table 5.1.

Table 5.1: Compression specific creep main properties: specific elastic strain in loading, specific instantaneous recovery, specific creep, specific creep recovery and specific flow, after 90 days.

Type of concrete	Specific elastic strain at loading (μ/MPa)	Specific instantaneous recovery (μ/MPa)	Specific creep (μ/MPa)	Specific creep recovery (μ/MPa)	Specific flow (μ/MPa)	Creep coefficient
B110-0F	28.7	28.5	34.5	11.8	22.8	1.2
B600-0F	50.4	49.6	28.6	13.8	15.6	0.6
BQ600-0F	59,2	38.3	60.3	21.5	59.7	1.0
B600-6F	63.2	49.9	33.7	5.9	41.1	0.5
BQ600-6F	54.4	45.4	76.8	3.4	82.4	1.4

The plain matrix, only dried, had shown in 24 hours 80% of the total specific creep obtained after 90 days. As for the plain matrix burned 90% of the total creep was obtained in the first 90 days. However, for the matrix tested at hot stage, the matrix continued to creep for more days. By the end of the first day only 66% of the total creep had occurred. For this test it was observed that the concrete reached a stable creep rate at 15 days, when the creep rate was no longer significant the test was stopped and unloaded.

The plain matrices tested at room temperature presented similar results for specific creep after one day of around 24μ/MPa. They also presented similar results after 90 days of creep tests of around 30μ/MPa. For the matrix tested at hot stage creep was more pronounced, almost twice the creep deformation of the matrix tested at room temperature reaching 60 μ/MPa after 15 days. This might be linked to the fact that the test carried out at hot stage and that the concrete specimen was not sealed and subjected to hot air draft during the test, thus modifying the behaviour.

The fibre reinforcement for the matrix, burned and tested at room temperature, did not affect creep deformation, as specific creep at 24 hours presented similar results of the plain matrix only dried and the matrix burned. Also after 90 days, the results between B110-0F, B600-0F and B600-6F were similar of around 30μ/MPa.

The matrix with reinforcement tested at 600°C, presented the highest creep deformation and continued to creep until 20 days when creep rate was no longer increasing.

The fibre reinforcement increased the creep at hot stage by 30% in the first day, and increased as well the specific creep deformation by 20% after 20 days. This expressive increase in creep could be attributed to the mismatch between the steel and concrete at 600°C as steel linearly dilates 5 times more than the refractory concrete producing micro-cracking in the matrix.

In both cases, with and without reinforcement the test carried out at hot stage increased around twice the specific creep deformation of the ones performed at room temperature.

The concretes tested at hot stage presented a high creep coefficient in relation to the ones tested at room temperature, except for the concrete dried without reinforcement that presented 1.2 of creep coefficient. The highest creep coefficient was of the concrete tested at high temperature with fibre reinforcement.

For compression it is expected that the specific elastic strain at loading is similar to the specific instantaneous recovery. The results obtained showed that for the concretes without reinforcement and tested at room temperature, the specific elastic strain at loading presented similar results compared to those of specific instantaneous recovery.

However for concretes tested at hot stage the specific instantaneous recovery were lower than the specific elastic strain at loading, by about 35% and 16% for the concretes without and with reinforcement respectively. Also for concretes with reinforcement tested at room temperature, the specific instantaneous recovery were lower than the specific elastic strain at loading of around 15% for the concrete only dried and 21% for the concrete with reinforcement. This result can indicate that there was a rearrangement of particles or molecules in the concrete.

The specific creep recovery was 34%, 48% and 36% of the specific creep for the concretes without reinforcement when subjected to the drying process at 110°C, subjected to the burning and tested at room temperature, and tested at hot stage respectively. As for the concretes with reinforcement the percentage was of 29%, 17% and 4% of the specific creep for the concretes when subjected to the drying process at 110°C, subjected to the burning and tested at room temperature and tested at hot stage, respectively.

Indicating that creep of the refractory does not recover fully, the higher percentage of recovery was of 48% in the case of the concrete burned and tested at room temperature without reinforcement.

The concretes that presented the highest flow or residual deformation were the ones tested at high temperature and they also presented the highest creep deformation.

5.5 Flexural creep test

Flexure creep curve obtained by the average of two samples for each combination are presented in Figures 5.12 and 5.13. Creep properties regarding these curves are listed in Table A.2 of Appendix.

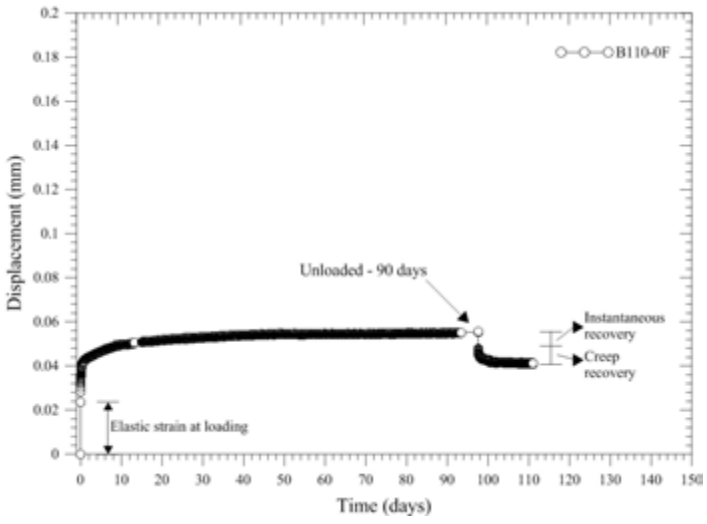

(a)

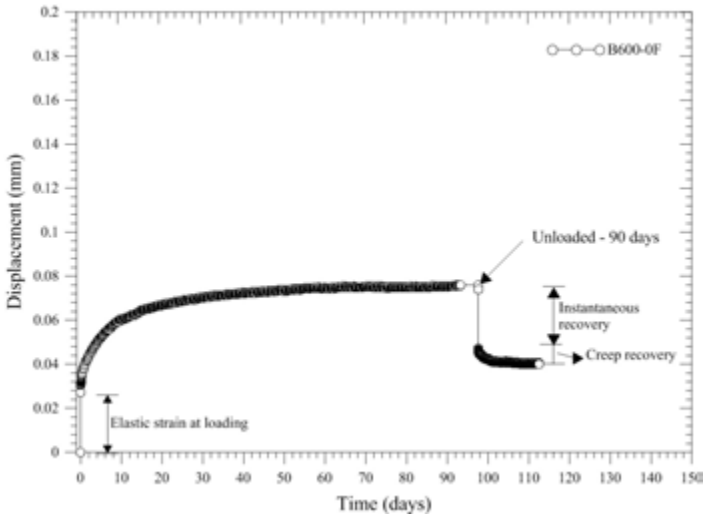

(b)

Figure 5.12: Flexure creep curves with elastic strain for matrix: a) subjected only to the drying process; b) subjected to the burning process at 600°C.

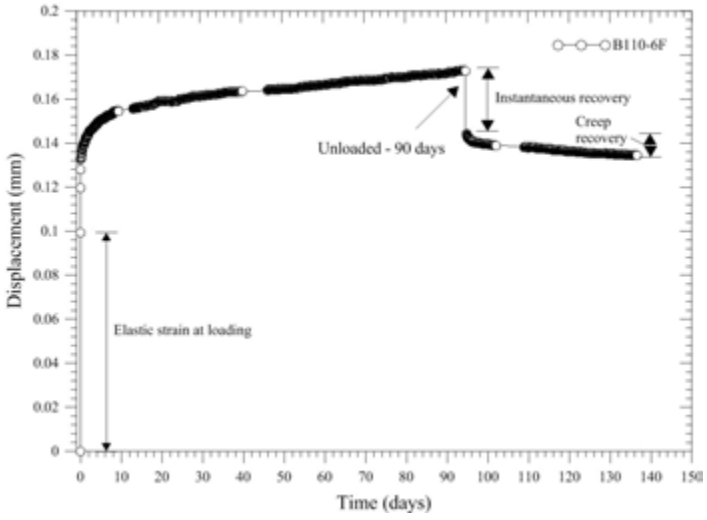

(a)

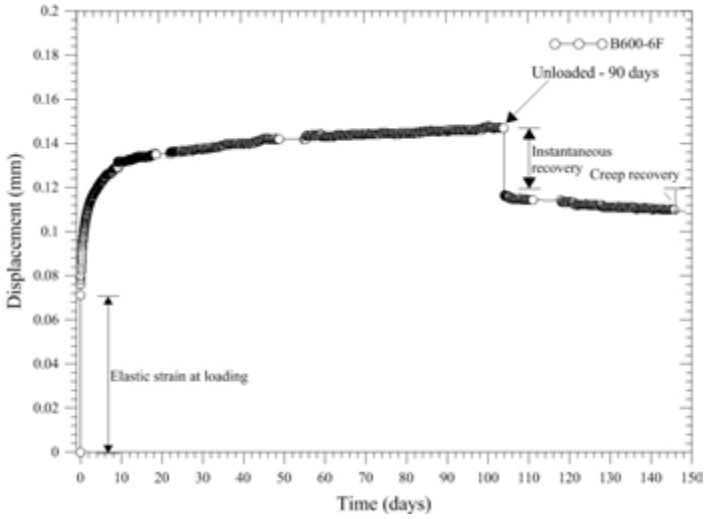

(b)

Figure 5.13: Flexure creep curves with elastic strain for matrix with reinforcement: a) subjected only to the drying process; b) subjected to the burning process at 600°C.

As shown in Figure 5.12, creep curves reached a steady state in 30 days for concretes without reinforcement. As Figure 5.13 showed that creep curves reached a steady state in 20 days for concretes with reinforcement. After reaching a steady state creep deformation was stable and had no significant increase. Concluding that flexure creep tests for this refractory concrete could be carried out for the period of only 30 days instead of 90 days.

As seen already in compression, the curves obtained in flexural tests presented the majority of creep displacement in the first days. The creep deformation was more pronounced in the first hours of the test.

Because of that and in order to compare results, specific creep curves using the

correspondence theorem were plotted for the first 24 hours. They are presented in Figure 5.14.

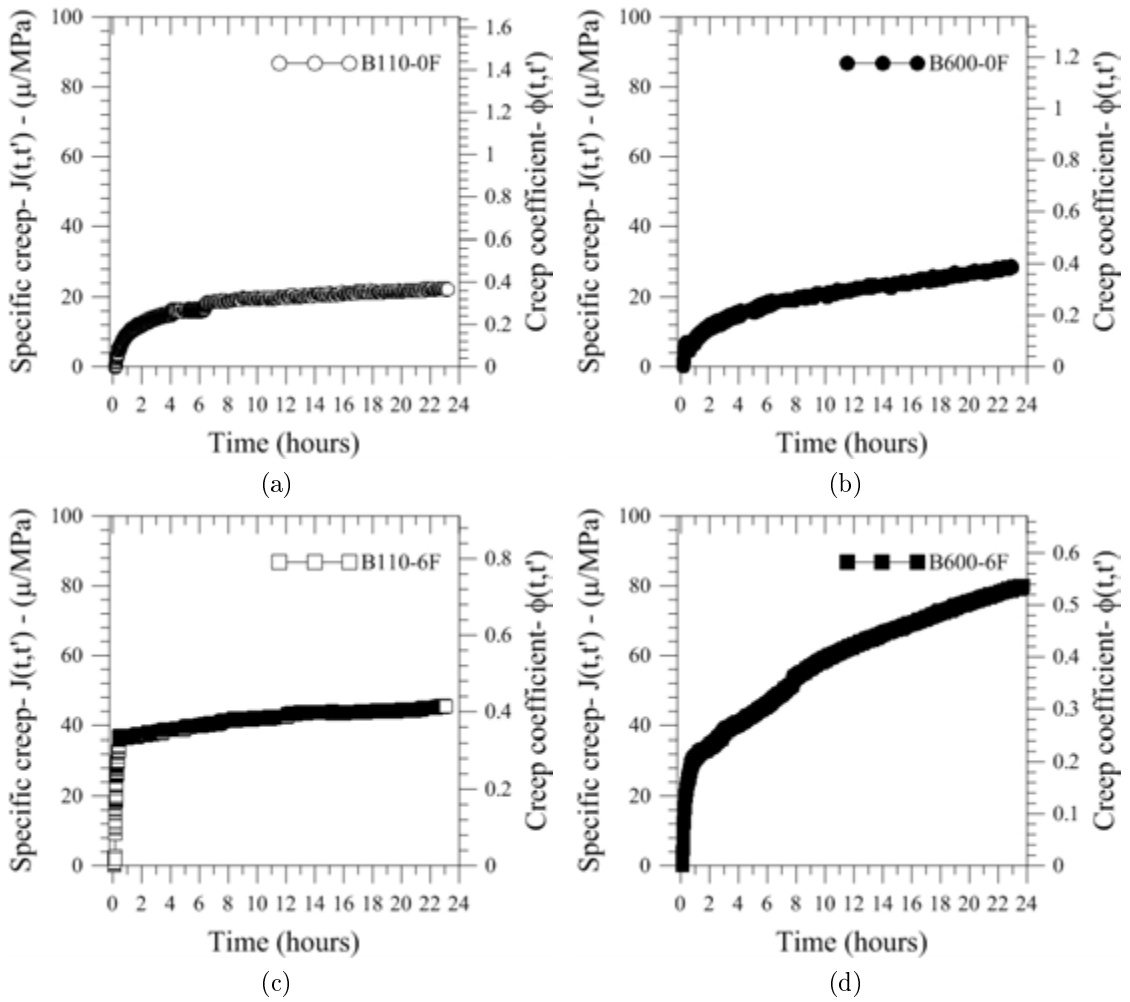

Figure 5.14: Specific flexure creep curves for matrix: a) subjected only to the drying process; b) subjected to the burning process at 600°C; c) with fibre reinforcement subjected only to the drying process; d) with fibre reinforcement subjected to the burning process at 600°C.

The specific elastic strain in loading, specific instantaneous recovery, specific creep, specific creep recovery and specific flow after 90 days were obtained from the flexure specific creep curves and presented in Table 5.2.

Table 5.2: Flexural specific creep main properties: specific elastic strain in loading, specific instantaneous recovery, specific creep, specific creep recovery and specific flow, after 90 days.

Type of concrete	Specific elastic strain at loading (μ/MPa)	Specific instantaneous recovery (μ/MPa)	Specific creep (μ/MPa)	Specific creep recovery (μ/MPa)	Specific Flow (μ/MPa)	Creep coefficient
B110-0F	60.60	14.49	48.05	13.30	79.86	0.8
B600-0F	73.78	13.33	122.57	78.86	104.17	1.7
B110-6F	109.73	23.32	80.43	19.96	147.43	0.7
B600-6F	149.37	38.36	177.46	43.76	244.56	1.2

The curves presented in 4.15 showed that creep occurred while loading. However, this portion of creep strain could not be separated from elastic displacement. In this analysis, creep while loading will not be considered, creep will be considered only after loading.

The tendency was confirmed,already observed in compression, for the burned concretes to present higher creep than that of the concretes only dried. It was also confirmed that the concrete burned with reinforcement presented the highest creep.

The burning for plain matrices increased slightly (15%) the creep deformation after 24 hours. However, the creep rate of the plain matrix burned was higher than the one that was only dried. After 90 days of creep tests, the specific creep of the plain matrix burned was 2.5 times higher than that the plain matrix only dried.

The plain matrix only dried had shown in 24 hours 55% of the total specific creep obtained after 90 days. As for the matrix burned with reinforcement in the first day around 45% of the total creep was obtained in 90 days.

The matrix only dried with reinforcement had shown in 24 hours 50% of the total specific creep obtained after 90 days. As for the plain matrix burned in the first day around 22% of the total creep was obtained for a total of 90 days.

All matrices in flexure reached a steady creep rate in 15 days, showing no significant creep deformation after this period.

The fibre reinforcement increased the creep deformation. For the dried matrix the increase was of 60% after 90 days. Specific creep deformation was even higher for the matrix burned. The fibre reinforcement increased around 185% at 24 hours, although the increase was of 45% at the end of the 90 days.

The concretes burned presented a higher creep coefficient in relation to the ones dried. The highest creep coefficient was of the burned matrix.

The results for flexure creep tests showed that the specific instantaneous recovery was significantly lower than the specific elastic strain at loading. They were 24%, 18%, 21%, 25% of the specific elastic strain at loading, for the concretes B110-0F, B600-0F, B110-6F and B600-6F respectively. This result showed that the instantaneous recovery for flexure is around 22% of the specific elastic strain at loading.

The specific creep recovery was 27%, 64%, 25% and 25% of the specific creep for the concretes B110-0F, B600-0F, B110-6F and B600-6F respectively. It indicates that creep of the refractory concrete in flexure does not recover fully, and recovers less than in compression. The highest percentage of recovery was of 64% in the case of the concrete burned and tested at room temperature without reinforcement. The same type of concrete presented also the highest recovery in compression creep tests. However, for all other types the recovery in flexure was about 25%.

The concrete that presented the highest flow or residual deformation was the one that was burned with fibre reinforcement and it also presented the highest creep deformation.

5.6 Tensile creep test

Tensile creep curve plotted using the average of two samples for each combination, are presented in Figure 5.15. Creep properties regarding these curves are also presented in Table A.3 of the Appendix.

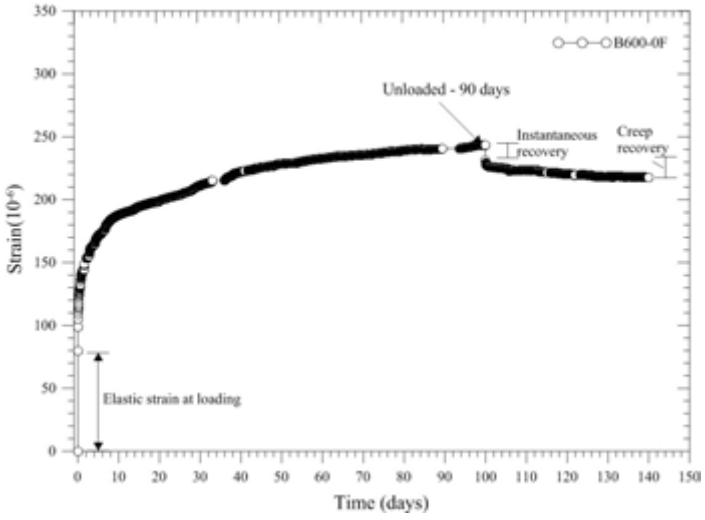

(a)

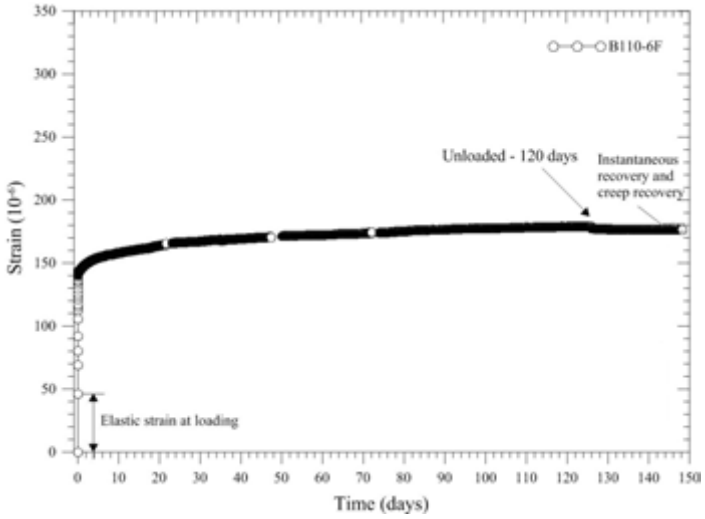

(b)

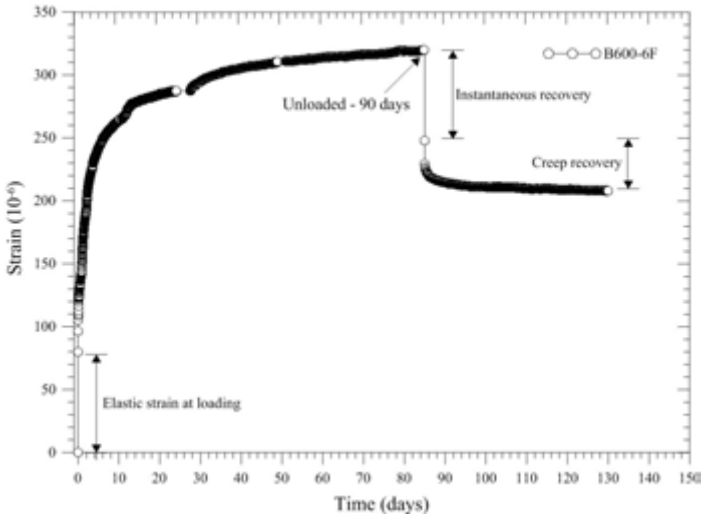

(c)

Figure 5.15: Specific creep curves with elastic strain for matrix: a) subjected only to the drying process; b) subjected to the burning process at 600°C and then tested at room temperature; c) tested at hot stage (600°C).

The curves presented in 4.17 showed that creep occurred while loading. However, this portion of creep strain could not be separated from elastic strain. In this analysis, the creep strain while loading will not be considered, creep strain will be considered only after loading.

As shown in Figure 5.15, creep curves reached a steady state in 30, 20 and 30 days for the concretes B600-0F, B110-6F and B600-6F respectively. After reaching a steady state creep deformation was stable and had lower increase. Concluding that tensile creep tests for this refractory concrete could be carried out for the period of only 30 days instead of 90 days.

As seen in compression and flexure, also the majority of tensile creep was obtained in the first days. The creep deformation was more pronounced in the first hours of the test. Specific creep curves were also plotted in the first 24 hours. They are presented in Figure 5.16.

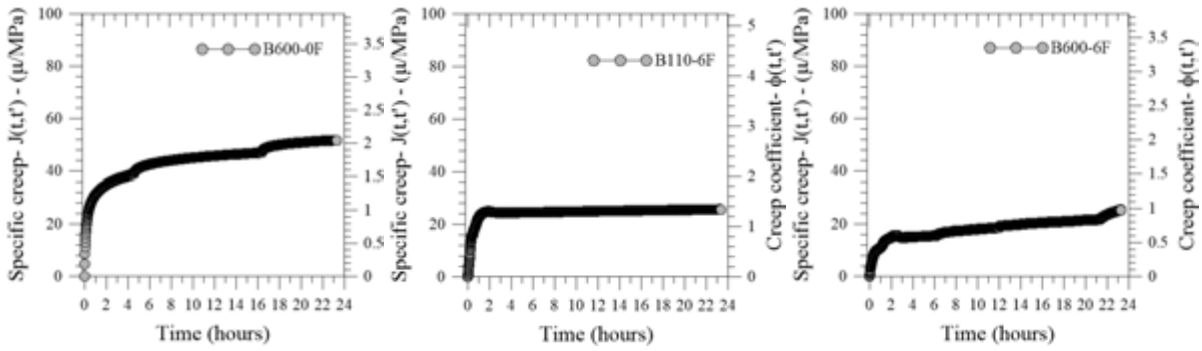

Figure 5.16: Specific creep curves without elastic strain for matrix: a) subjected to the burning process at 600°; b) with reinforcement subjected only to the drying process; c) with reinforcement subjected to the burning process at 600°C.

The specific elastic strain at loading, specific instantaneous recovery, specific creep, specific creep recovery and specific flow, after 90 days, were obtained from the tensile specific creep curves and presented in Table 5.3.

Table 5.3: Tensile specific creep main properties: specific elastic strain in loading, specific instantaneous recovery, specific creep, specific creep recovery and specific flow, after 90 days.

Type of concrete	Specific elastic strain at loading (μ/MPa)	Specific instantaneous recovery (μ/MPa)	Specific creep (μ/MPa)	Specific creep recovery (μ/MPa)	Specific Flow (μ/MPa)	Creep coefficient
B600-0F	25.3	5.6	106,4	8.4	118.5	4.2
B110-6F	19.1	0.3	36.7	0.6	54.9	1.9
B600-6F	26.0	20.9	80,0	16.3	68.9	3.1

The plain matrix burned presented in 24 hours 53% of the total specific creep obtained after 90 days. As shown in this curve creep reached a steady stage at 10 days. The matrix dried with fibre reinforcement presented 67% of the total specific creep obtained on the first day and reached a constant creep rate with no significant increase after 7 days. As for the matrix burned with fibre reinforcement presented less expressive creep in the first hours, presented only around 33% of the total strain presented in the total of 90 days, and reached a steady creep rate at 30 days.

For the tensile creep tests, the fibre reinforcement reduced the creep. The matrix that presented a higher specific basic creep after 90 days was the matrix without reinforcement burned at 600°C. For this case the fibre reinforcement reduced in about 25% the creep deformation.

The burning increased creep for concretes with fibre reinforcement showing a increase of 350% in the final creep deformation at 90 days.

The burning for plain matrices increased slightly by 15% of the creep deformation after 24 hours. However, the creep rate of the plain matrix burned was higher than the one that was only dried. After 90 days of creep tests, the specific creep of the plain matrix burned was 2.5 times higher than that of the plain matrix only dried.

The concretes burned presented a highest creep coefficient. Just as in flexure the mixture that presented highest creep coefficient was the matrix burned.

Tensile creep tests showed that the specific instantaneous recovery were insignificant for the concretes burned without reinforcement and for the concrete dried with reinforcement. However for the concrete with fibre reinforcement and burned the specific loading elastic strain was of 80% of the specific strain at loading.

The specific creep recovery was 8%, 2% and 20% of the specific creep for the concretes burned without reinforcement, dried with reinforcement, and burned with fibre reinforcement, respectively. Indicating that creep recovery in tensile is only relevant in the case of burned concrete with fibre reinforcement.

The concrete that presented the highest flow or residual deformation was the one that was burned without fibre reinforcement and it also presented the highest creep deformation at the end of 90 days. However, the concrete with fibre reinforcement and burned also presented substantial higher flow and creep deformation when compared to the one dried and with fibre reinforcement.

5.7 Comparisons with compression, tensile and flexural creep

Specific creep in compression, flexure and tensile were plotted together for each type of concrete and are presented in Figures A.1 to A.16 in the Appendix. It is possible to observe that flexure creeps more than tensile. Compression creep presented the lower creep deformation in all occasions. According to NEVILLE *et al.* (1983), creep in tensile as a general behaviour for concrete, presents an increasing creep rate, because there is a significant contribution to micro cracking in this kind of solicitation. Instead of creep in compression at the beginning of the test, it presented higher creep but stabilized faster.

It can also be noted that flexure and tensile creep presented similar behaviour, with flexure slightly more accentuated than tensile. According to NEVILLE *et al.* (1983), this could be attributed to the strain gradient as creep for a non uniform stress is larger.

The creep coefficient in tensile was in general 3 to 4 times higher than creep in compression and in flexure.

Also, there is a significant difference in instantaneous recovery and creep recovery. For these properties, compression presented higher results, flexure lower results and tensile the lowest. This indicates that the type of solicitation contributes to these properties and to the permanent creep strain.

Chapter 6

Conclusions

Some conclusions can be made for all combinations presented in this section.

- All creep tests reached a steady creep rate in less than 30 days, concluding that the duration of the tests, in any kind of solicitation, can be performed in this period, after which, no significant creep deformation was observed.
- Concretes reinforced with 6% of fibres submitted to the burning process showed the highest specific creep deformation for compression and flexure. However for tensile creep, the fibre reinforcement caused briefly creep to decrease.
- A tendency was observed that burned concrete showed a higher creep deformation than the ones only submitted to the drying process. This was explained by the conversion of the alumina cement, in the reaction of C_3AH_6 and AH_3 converting to $C_{12}A_7$ and CA, observed in the thermogravimetric and X-ray diffraction analysis, that increased the porosity of the concrete, shown in the performed porosity test. Porosity for plain matrix was increased by 25% and for the burned matrix with reinforcement it increased by around 33%.
- The increase of porosity in the burned matrix reduced the mechanical properties of the refractory concrete.
- Hot stage tests presented higher creep, about twice the creep deformation seen in tests performed at room temperature. This could be linked to the fact that the specimen had not been protected by sealing, being unsealed and exposed to the hot air from the kiln. Further studies need to be undertaken to investigate the cause of the drastic change.

- Metastable compounds convert to stable ones with time and temperature. As the concrete was subjected to high temperature and then cooled, creep was observed only in the first days, and then the creep rate was stabilized.

- Comparing the specific creep of this refractory concrete in compression, flexure and tensile. One can conclude that flexure creeps more then tensile. Further studies need to be undertaken to investigate this phenomenon.

- Instantaneous recovery and creep recovery presented higher results for compression in relation to flexure and tensile. And tensile instantaneous recovery and creep recovery presented the lowest results in relation to flexure and compression.

- The creep coefficient in tensile was in general 3 to 4 times higher than creep in compression and in flexure.

  For future studies it is proposed to find a creep numerical model that represents the creep behaviour obtained in these tests. In this way, it is possible to incorporate the relaxation stresses produced by creep deformation in the state of tensions, so that results can be taken into account in the design of structures for the Fluid Cracking Catalytic Units.

Chapter 7

Bibliography

ANTONOVIČ, V., KERIENĖ, J., BORIS, R., et al., 2013, "The effect of temperature on the formation of the hydrated calcium aluminate cement structure", *Procedia Engineering*, v. 57, pp. 99–106.

ASME SEC. II, P. D., 2010. "American Society of Mechanical Engineers Boiler and Pressure Vessel Code, Material Properties". AMERICAN SOCIETY OF MECHANICAL ENGINEERS (ASME), EUA.

BAZANT, Z. P., KAPLAN, M. F., 1996, *Concrete at high temperatures: material properties and mathematical models*. Longman Group Limited.

BRAULIO, M., MORBIOLI, G., MILANEZ, D., et al., 2011, "Calcium aluminate cement source evaluation for Al 2 O 3–MgO refractory castables", *Ceramics International*, v. 37, n. 1, pp. 215–221.

DÍAZ, L., TORRECILLAS, R., 2007, "Phase development and high temperature deformation in high alumina refractory castables with dolomite additions", *Journal of the European Ceramic Society*, v. 27, n. 1, pp. 67–72.

HEWLETT, P., 2003, *Lea's chemistry of cement and concrete*. Butterworth-Heinemann.

IBAR, 2010, "Folha de dados técnicos BRASILCAST 560", Indústria Brasileira de Artigos Refratários, 09.

KIM, G.-D., 1984, "Creep of refractory concretes", .

KUMAR, S., DAS, S. K., DASPODDAR, P. K., 2003, "Thermo-mechanical behaviour of low cement castables derived from mullite aggregates synthesised from beach sand sillimanite", *Ceramics international*, v. 29, n. 2, pp. 139–144.

LEE, W., VIEIRA, W., ZHANG, S., et al., 2001, "Castable refractory concretes", *International Materials Reviews*, v. 46, n. 3, pp. 145–167.

MARTINEZ, A. T., LUZ, A., BRAULIO, M., et al., 2012, "Creep behavior modeling of silica fume containing Al 2 O 3–MgO refractory castables", *Ceramics International*, v. 38, n. 1, pp. 327–332.

MEDEIROS, J., 2012, *Refratário de elevada tenacidade para uso em aplicações críticas na indústria do refino de petróleo.* Dissertação de mestrado, PEC/COPPE/UFRJ.

NBR-11222, 2010. "Materiais refratàrios densos não conformados - Determinação das resistências à flexão e à compressão à temperatura ambiente." ABNT - ASSOCIAÇÃO BRASILEIRAS DE NORMAS TÉCNICAS. Rio de Janeiro.

NBR-2142, 2012. "Concreto: determinação da resistência à tração na flexão em corpos-de-prova prismáticos". ABNT - ASSOCIAÇÃO BRASILEIRAS DE NORMAS TÉCNICAS. Rio de Janeiro.

NEVILLE, A. M., DILGER, W. H., BROOKS, J. J., 1983, *Creep of plain and structural concrete*. Construction press.

NTP-1728, P., 2005. "Concreto Refratário". PETRÓLEO BRASILEIRO S.A - Comissão de Normas Técnicas (PETROBRAS/CONTEC), Brasil.

NTP-1910, P., 2008. "Projeto de revestimentos de concretos Refratários". PETRÓLEO BRASILEIRO S.A - Comissão de Normas Técnicas (PETROBRAS/CONTEC), Brasil.

PARR, C., SIMONIN, F., TOUZO, B., et al., 2005, "IMPACT OF CALCIUM ALUMINATE CEMENT HYDRATION UPON THE PROPERTIES OF REFRACTORY CASTABLES", *Journal of Technical Association of Refractories Japan*, v. 25, n. 2, pp. 78–88.

PLAUT, R. L., HERRERA, C., ESCRIBA, D. M., et al., 2007, "A short review on wrought austenitic stainless steels at high temperatures: processing, microstructure, properties and performance", *Materials Research*, v. 10, n. 4, pp. 453–460.

RAMBO, D. A. S., 2012, *CONCRETOS AUTOADENSÁVEIS REFORÇADOS COM FIBRAS DE AÇO HÍBRIDAS: ASPECTOS MATERIAIS E ESTRUTURAIS*. Tese de Mestrado, PEC/COPPE/UFRJ.

SCRIVENER, K. L., CABIRON, J.-L., LETOURNEUX, R., 1999, "High-performance concretes from calcium aluminate cements", *Cement and concrete research*, v. 29, n. 8, pp. 1215–1223.

SHAMES, I. H., 1997, *Elastic and inelastic stress analysis*. CRC Press.

SILVA, E. F., 2007, *VARIAÇÕES DIMENSIONAIS EM CONCRETOS DE ALTO DESEMPENHO CONTENDO ADITIVO REDUTOR DE RETRAÇÃO*. Tese de Mestrado, PEC/COPPE/UFRJ.

TERZIĆ, A., PAVLOVIĆ, L., 2009, "Correlation among sintering process, porosity, and creep deformation of refractory concrete", *Journal of materials science*, v. 44, n. 11, pp. 2844–2850.

Appendix A

A.1 Compression creep

Table A.1: Compression creep main properties: value of elastic strain in loading and unloading, basic creep strain after 90 days, delayed elastic strain and flow.

Type of concrete in compression	Loading elastic Strain (μ)	Unloading elastic strain (μ)	Basic creep (μ)	Total creep (μ)	Delayed Elastic (μ)	Flow (μ)
B110-0F	649	645	780	1429	267	507
B600-0F	1002	986	569	1571	274	311
BQ600-0F	1400	905	1426	2826	508	1412
B110-6F	654	552	178	832	52	227
B600-6F	1638	1314	888	2520	156	1082
BQ600-6F	1059	883	1496	2555	66	1687

A.2 Flexural creep test

Table A.2: Flexural creep main properties: value of elastic displacement in loading and unloading, basic creep displacement after 90 days, delayed elastic displacement and flow.

Type of concrete	Loading elastic displacement (mm)	Unloading elastic displacement (mm)	Basic creep (mm)	Delayed Elastic (mm)	Flow (mm)
B110-0F	0.02468	0.00746	0.03129	0.00685	0.04114
B600-0F	0.02562	0.00517	0.05047	0.03056	0.04036
B110-6F	0.09992	0.02123	0.07324	0.01817	0.13425
B600-6F	0.06722	0.01726	0.07986	0.01969	0.11005

A.3 Tensile creep test

Table A.3: Tensile creep main properties: value of elastic strain in loading and unloading, basic creep strain after 90 days, delayed elastic strain and flow.

Type of concrete	Loading elastic Strain (μ)	Unloading elastic Strain (μ)	Basic creep (μ)	Delayed Elastic (μ)	Flow (μ)
B600-0F	46.49	10.35	196.87	15.44	217.52
B110-6F	61.40	0.83	117.78	2.06	176.24
B600-6F	78.46	63.02	241.29	49.06	207.66

A.4 Comparisons between compression, tensile and flexure creep behaviour

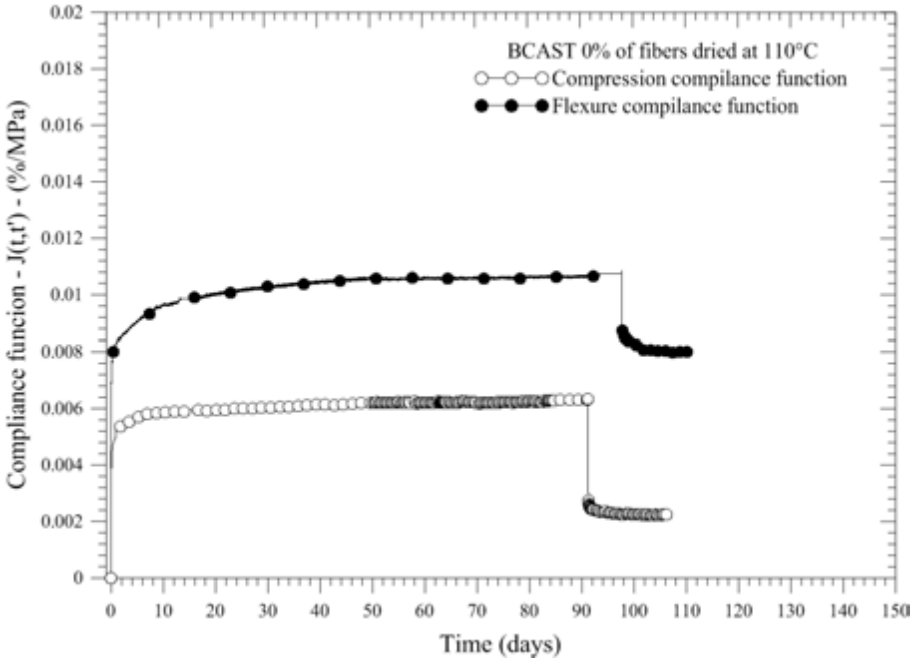

Figure A.1: Compliance functions of compression tensile and flexural creep with elastic strain, of the refractory concrete without reinforcement dried at 100°C

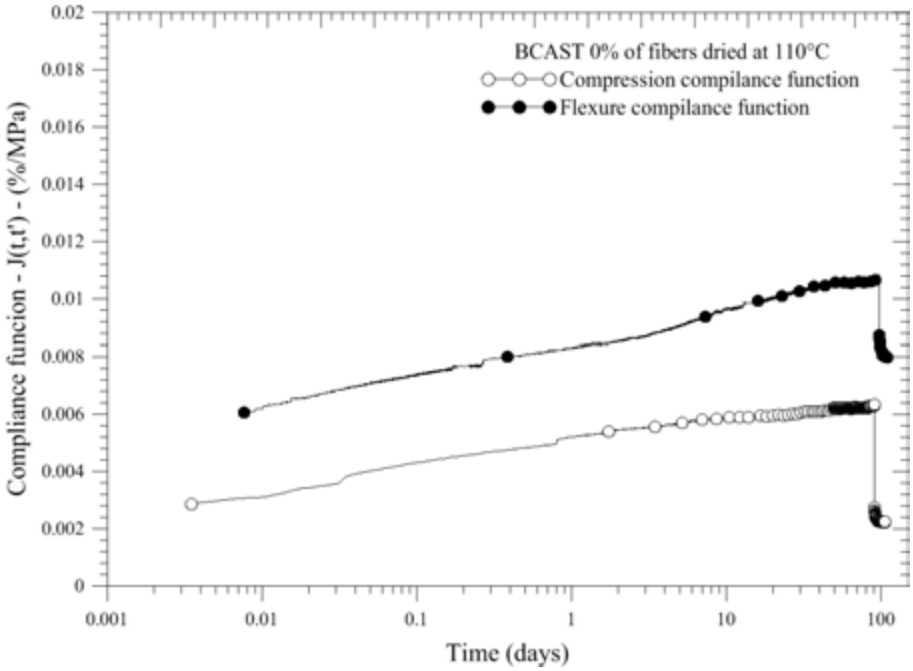

Figure A.2: Compliance functions of compression tensile and flexural creep with elastic strain, of the refractory concrete without reinforcement dried at 100°C, with log in time

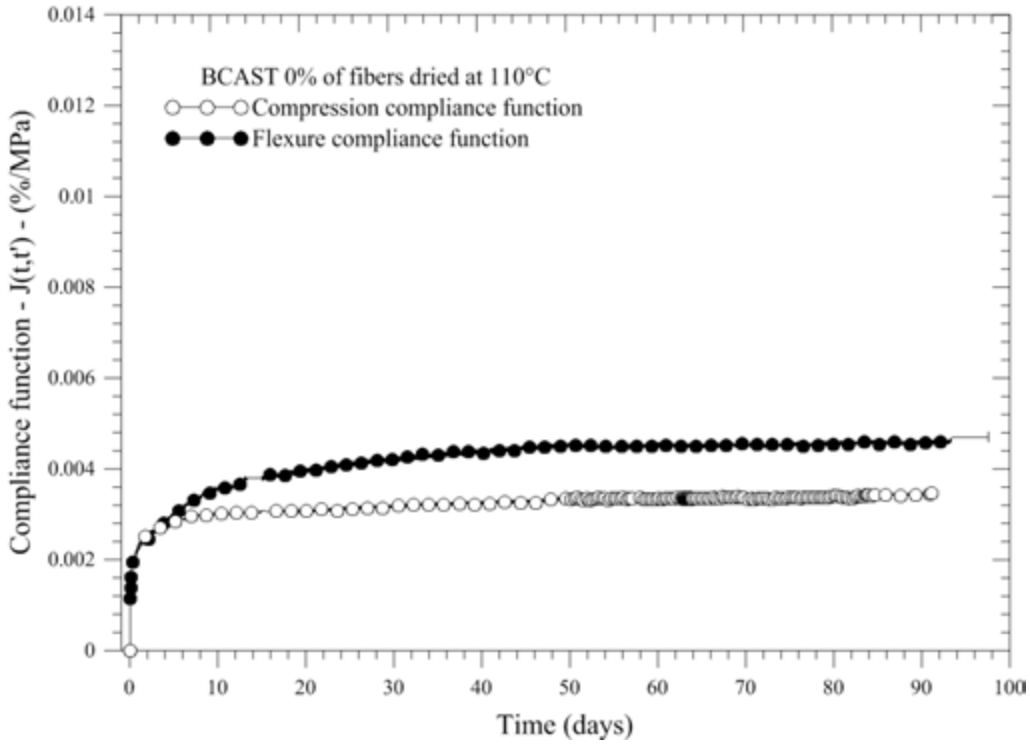

Figure A.3: Compliance functions of compression tensile and flexural creep without elastic strain, of the refractory concrete without reinforcement dried at 100°C

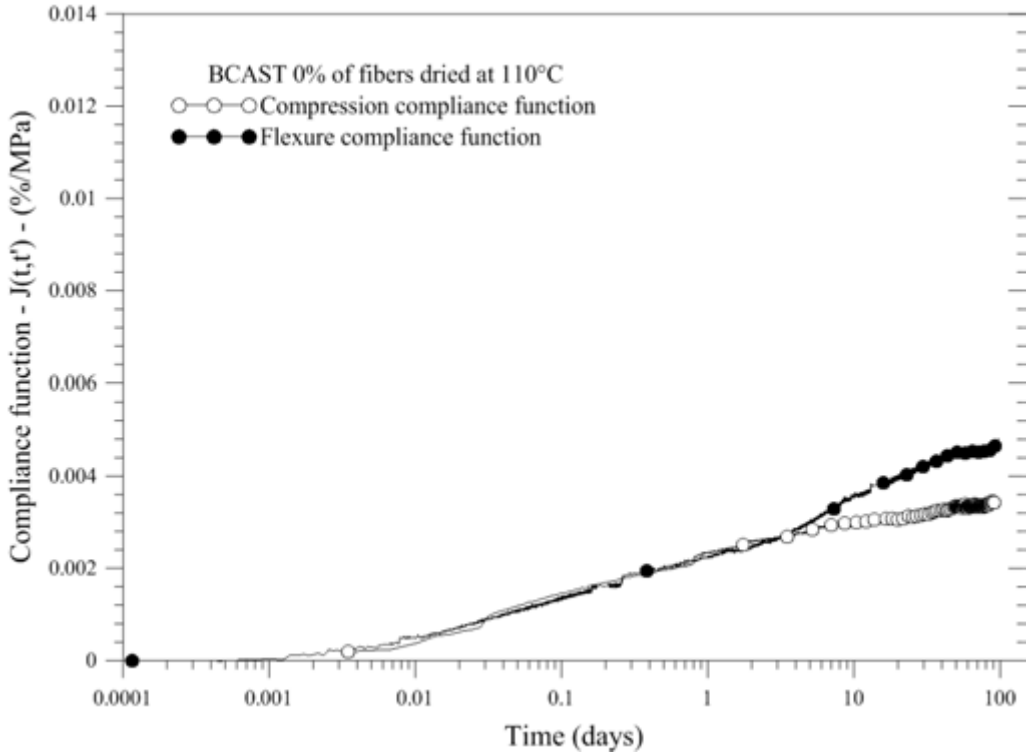

Figure A.4: Compliance functions of compression tensile and flexural creep without elastic strain, of the refractory concrete without reinforcement dried at 100°C, with log in time

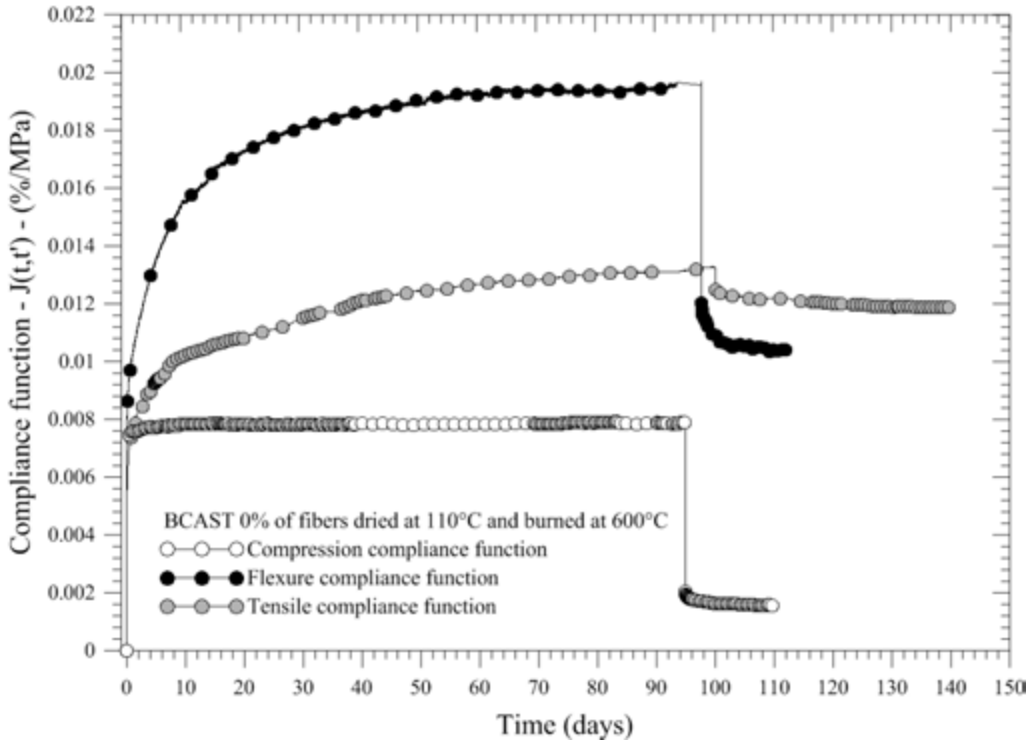

Figure A.5: Compliance functions of compression tensile and flexural creep with elastic strain, of the refractory concrete without reinforcement dried at 100°C and burned at 600°C

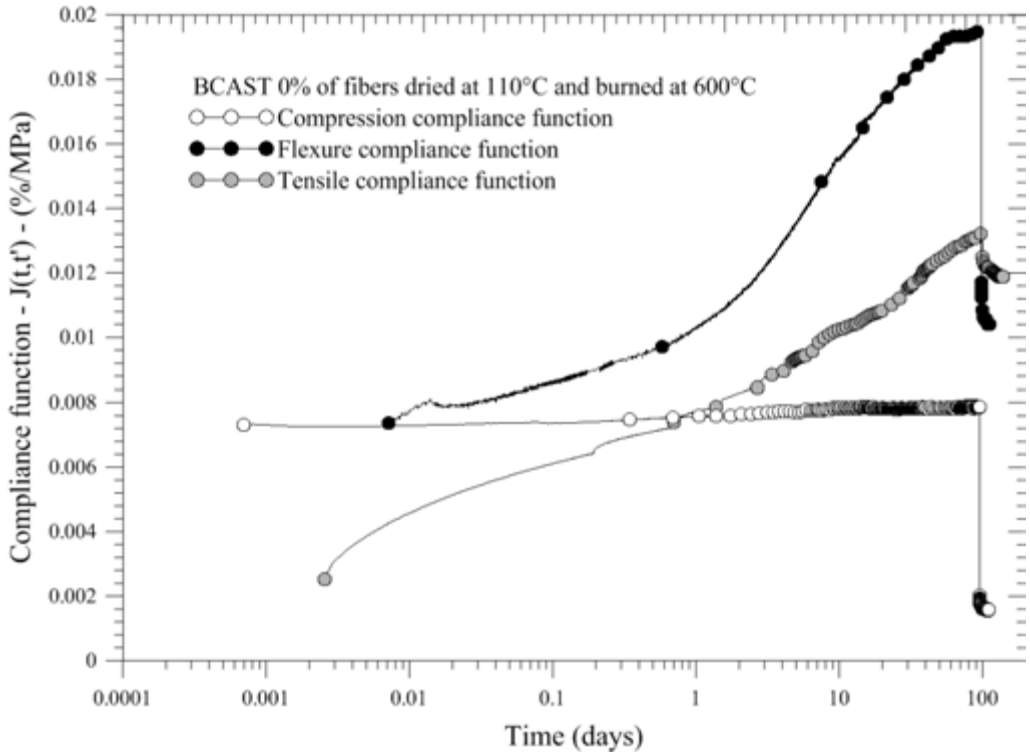

Figure A.6: Compliance functions of compression tensile and flexural creep with elastic strain, of the refractory concrete without reinforcement dried at 100°C and burned at 600°C, with log in time

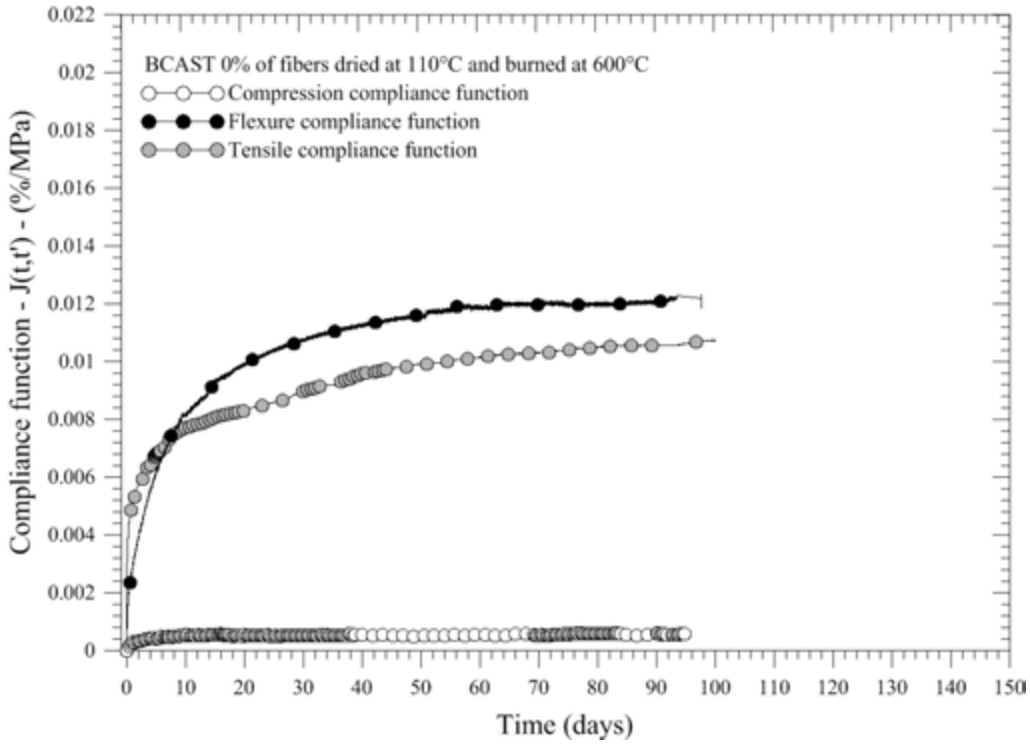

Figure A.7: Compliance functions of compression tensile and flexural creep without elastic strain, of the refractory concrete without reinforcement dried at 100°C and burned at 600°C

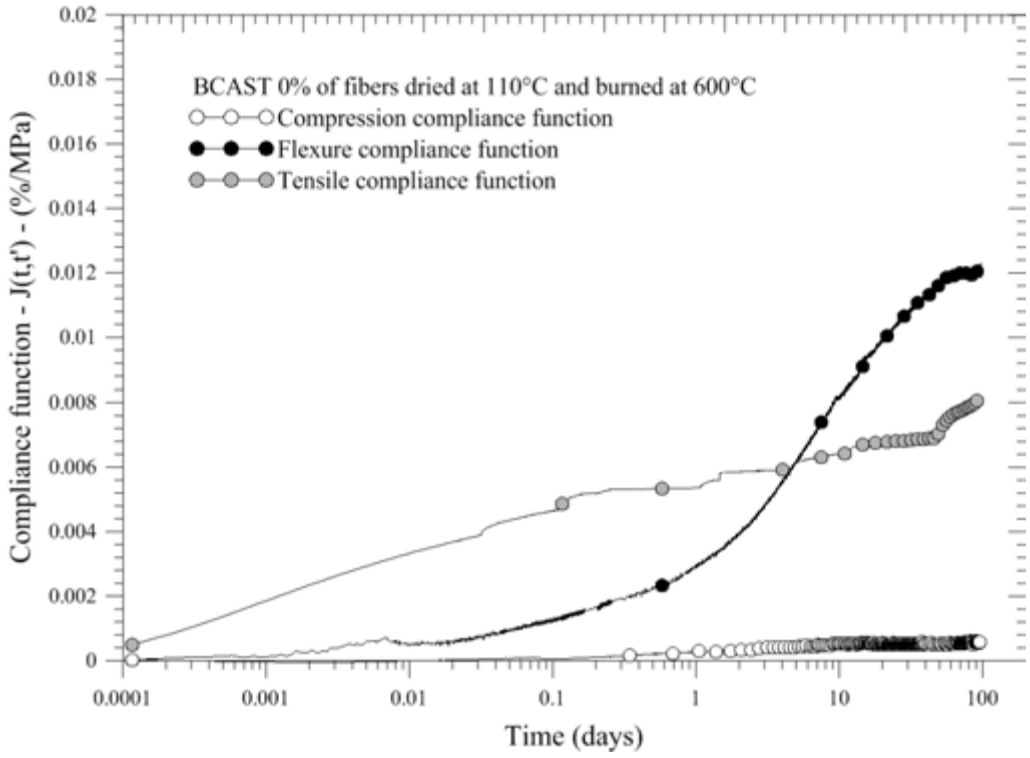

Figure A.8: Compliance functions of compression tensile and flexural creep without elastic strain, of the refractory concrete without reinforcement dried at 100°C and burned at 600°C, with log in time

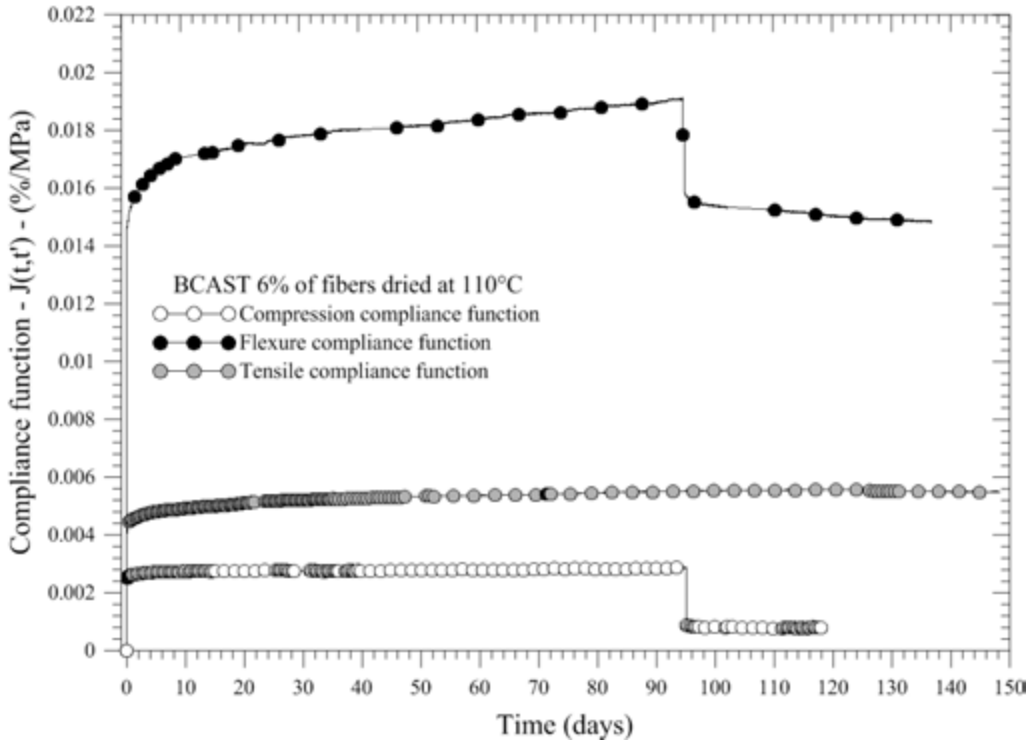

Figure A.9: Compliance functions of compression tensile and flexural creep with elastic strain, of the refractory concrete with 6% in mass of steel fibre reinforcement dried at 100°C

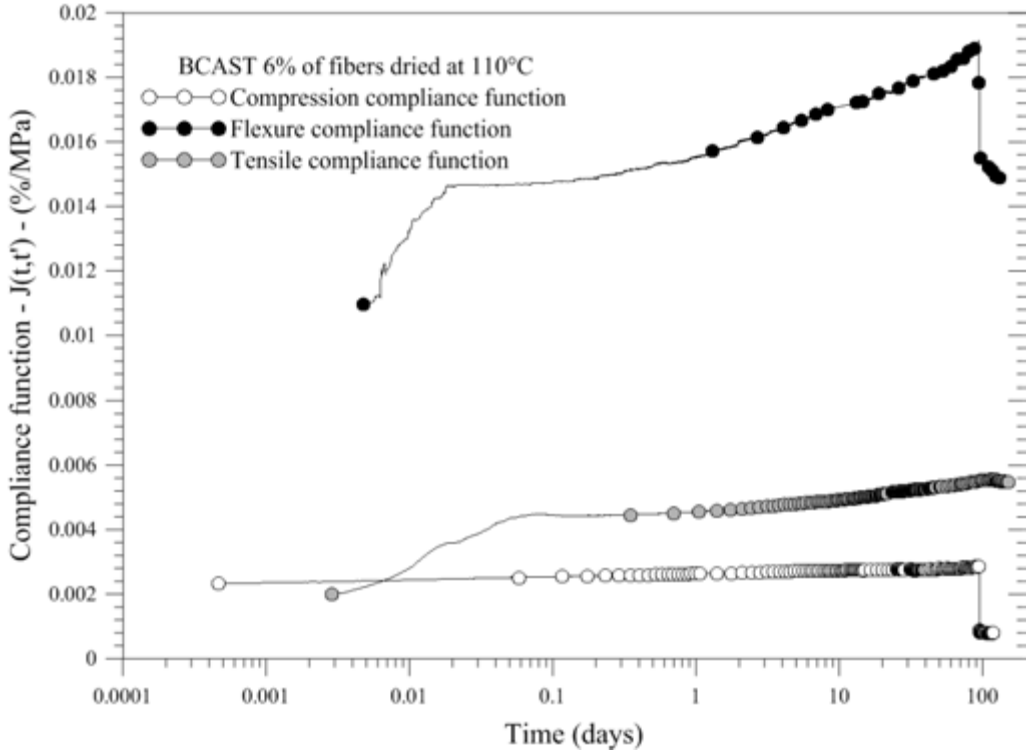

Figure A.10: Compliance functions of compression tensile and flexural creep with elastic strain, of the refractory concrete with 6% in mass of steel fibre reinforcement dried at 100°C, with log in time

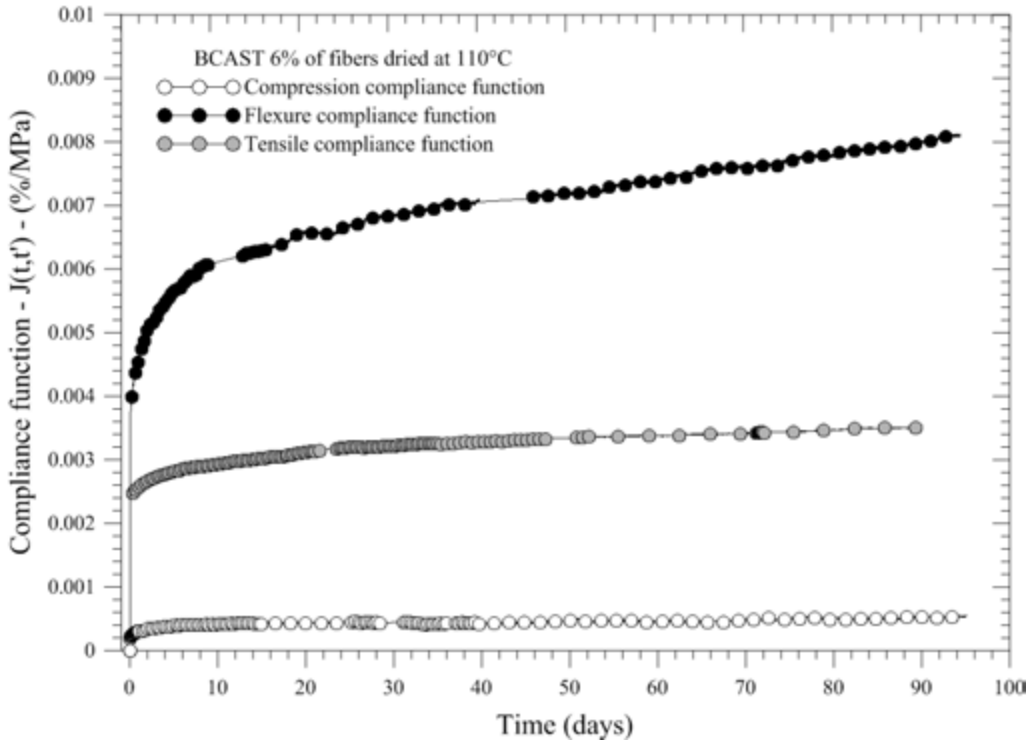

Figure A.11: Compliance functions of compression tensile and flexural creep without elastic strain, of the refractory concrete with 6% in mass of steel fibre reinforcement dried at 100°C

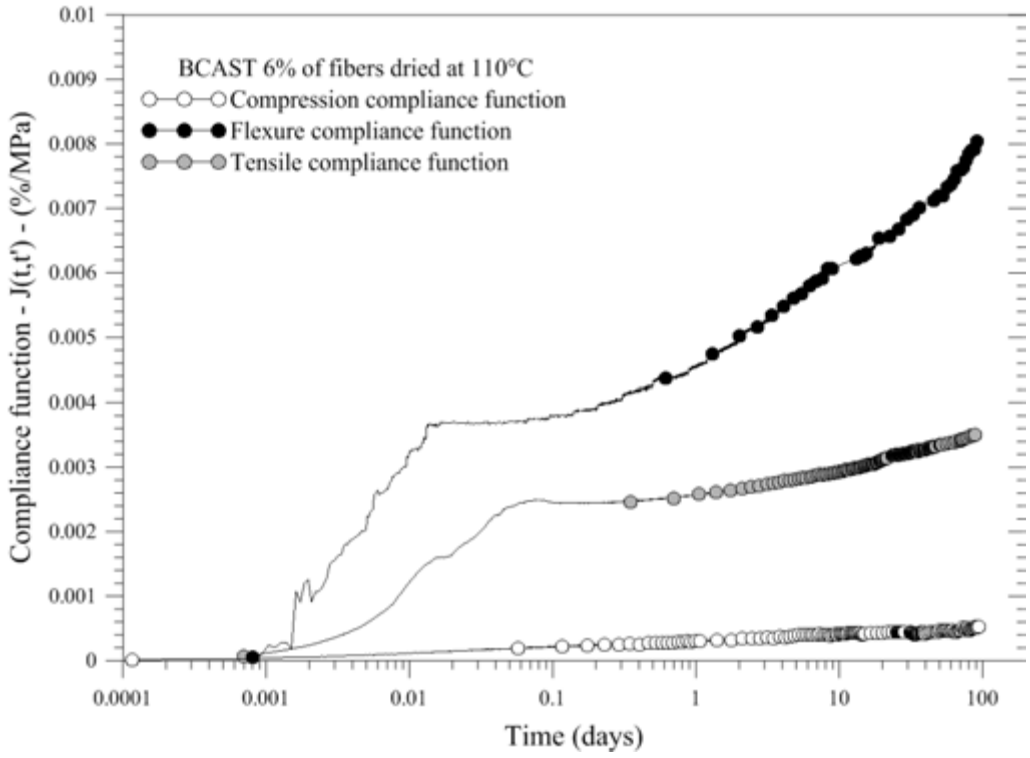

Figure A.12: Compliance functions of compression tensile and flexural creep without elastic strain, of the refractory concrete with 6% in mass of steel fibre reinforcement dried at 100°C, with log in time

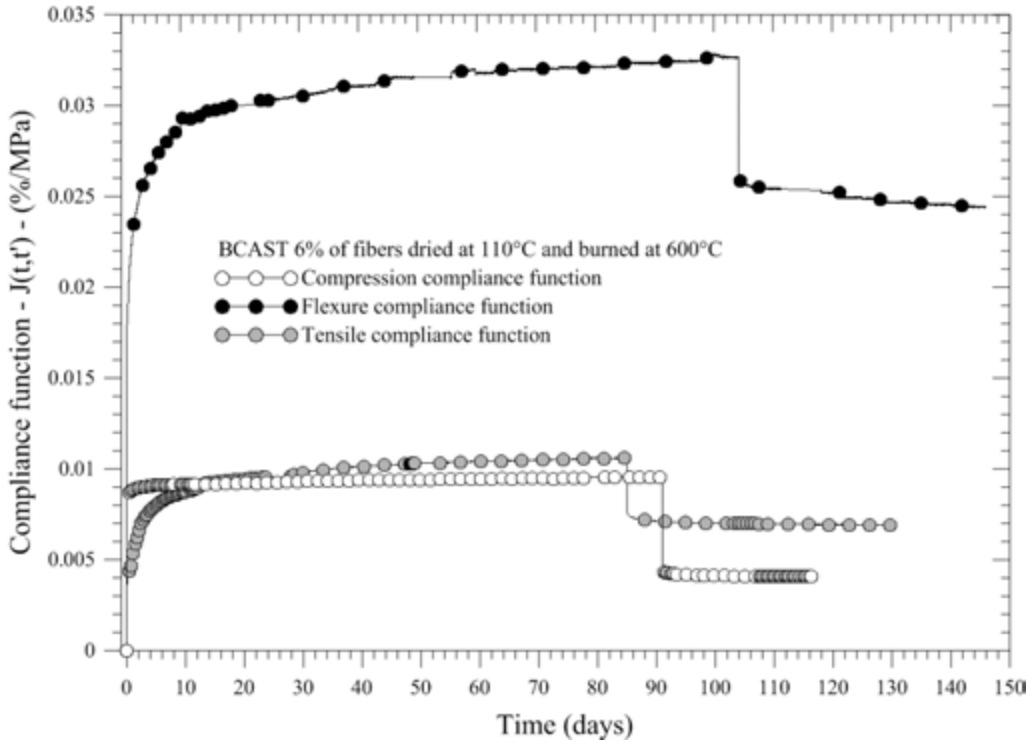

Figure A.13: Compliance functions of compression tensile and flexural creep with elastic strain, of the refractory concrete with 6% in mass of steel fibre reinforcement dried at 100°C and burned at 600°C

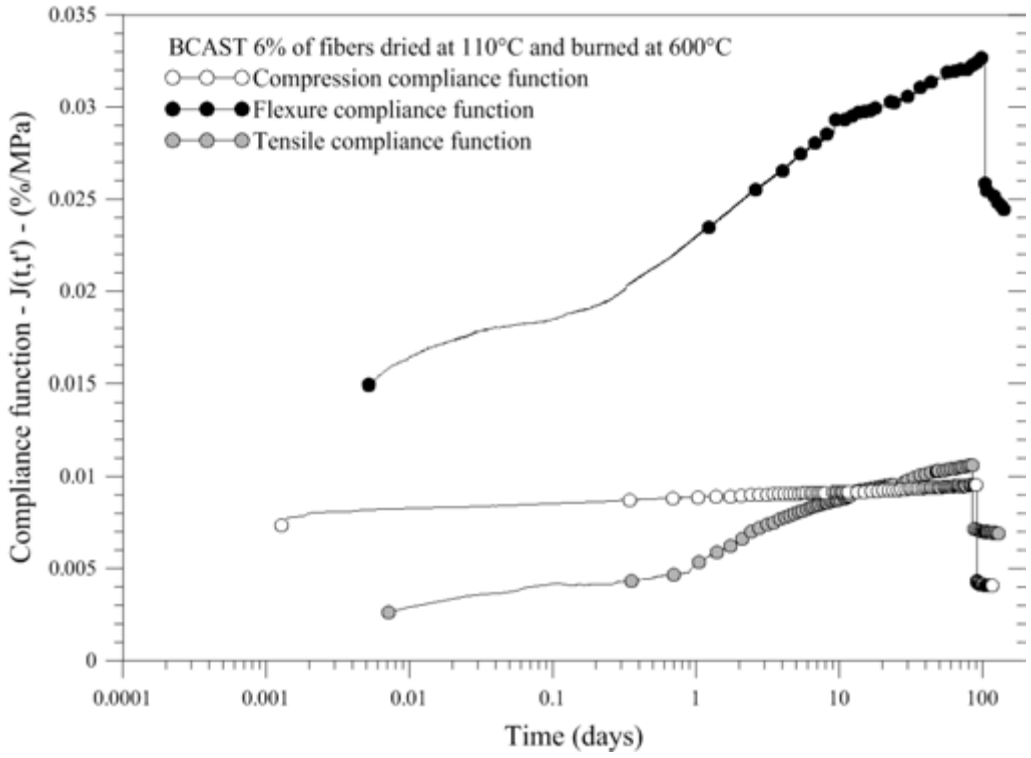

Figure A.14: Compliance functions of compression tensile and flexural creep with elastic strain, of the refractory concrete with 6% in mass of steel fibre reinforcement dried at 100°C and burned at 600°C, with log in time

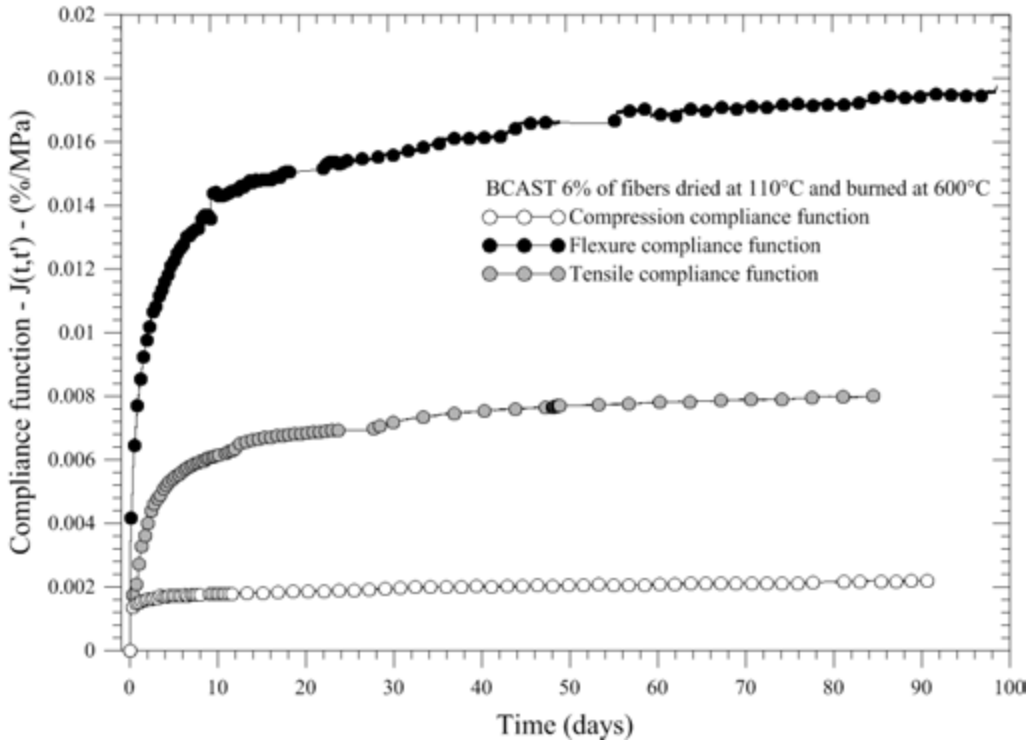

Figure A.15: Compliance functions of compression tensile and flexural creep without elastic strain, of the refractory concrete with 6% in mass of steel fibre reinforcement dried at 100°C and burned at 600°C

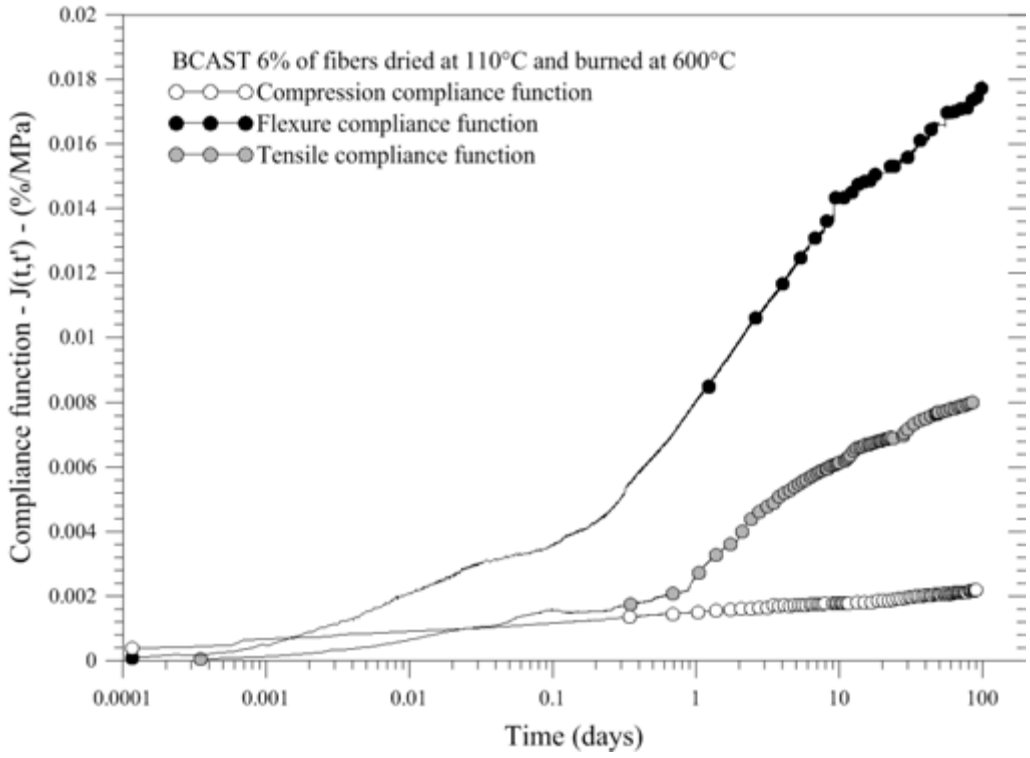

Figure A.16: Compliance functions of compression tensile and flexural creep without elastic strain, of the refractory concrete with 6% in mass of steel fibre reinforcement dried at 100°C and burned at 600°C, with log in time